Modeling of Erosion of Earth Structures Exposed to Overflowing

by

Miodrag B. JOVANOVIĆ

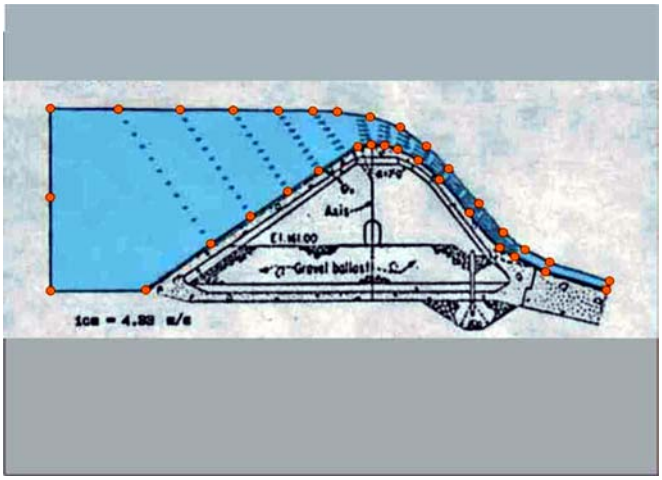

Belgrade, 1987.

Modeling of Erosion of Earth Structures Exposed to Overflowing

by

Miodrag B. JOVANOVIĆ

Belgrade, 1987.

This is an abridged version in English of the doctoral dissertation
submitted in partial fulfillment of the requirements for the degree of

Doctor of Technical Sciences

University of Belgrade
Faculty of Civil Engineering

January 1987.

Contents

Abstract

This dissertation presents the results of investigations undertaken in order to develop a mathematical model of erosion of earth structures, such as dams and embankments, in case of their overflowing.

The main assumptions are that the flow over the crest of the structure and the resulting erosion are two-dimensional phenomena (in vertical plane), and that the earth structure is formed of homogenous, moderately cohesive material. The first assumption implies that a structure is being entirely overtopped. The second assumption is applicable to small earth structures without seepage reducing elements, such as clay cores.

The proposed mathematical model consists of two components. The first component calculates curvilinear, accelerated flows over structures of arbitrary cross-sectional shape. The second component calculates quantity of the eroded material, and deformation of the structure. Assuming quasi-steady flow conditions, a two-step calculation procedure is proposed, so that the two components of the model are applied one after the other, in succession.

The flow over a deformable structure can be considered as the free-surface, accelerated, curvilinear flow, dominated by inertial effects and gravity, while effects of viscosity (friction) can be neglected. Thus, calculation of the flow field (water surface profiles, velocities, and pressures), can be based on the potential flow theory. This considerable simplification was justified by experiments.

The free-surface potential flow is calculated by the Boundary Element Method, chosen for its advantages over other numerical methods for solving moving boundary problems. Difficulties in the free-surface determination are due to the nonlinear nature of the problem, and simultaneous presence of subcritical and supercritical flow regimes.The proposed numerical model, based on the Newton-Raphson iterative procedure, is verified by several case studies.

Solution of the erosion problem is based on laboratory investigations, using scale models placed in a 22 m long, 1 m wide laboratory flume. The models, built of moderately cohesive, "equivalent material", are designed according to hydraulic and rheologic laws of similitude.

An exponential relationship between the flow rate of water and transport rate of the eroded material is established. A parameter, called the "erosion number", is introduced in order to quantify the instantaneous volume of the structure, relative to its initial volume. The obtained empirical relationship is used for calculation of the solid boundary changes (cross-sections of the overflown structure), assuming that the erosion depths are proportional to

the difference between the local depth-averaged velocity and the critical velocity for the given type of material.

Investigating scale effects, it is concluded that the experimental results cannot be considered reliable if scales are smaller than 1:15. This means that the experimental results in this dissertation can be extrapolated to relatively small prototype earth structures, built of homogenous, moderately cohesive material (cohesion 10-20 kPa). Their typical geometric characteristics are – height: 4-5 m, and side slopes: 1:1.5 or 1:2. Thus, application of the proposed numerical model is limited to small earth dams on micro-reservoirs, levees, embankments, emergency fuse plugs, and similar structures.

The proposed numerical model is calibrated and verified by experimental data. A rather good agreement between calculation and experiment is obtained. However, more general conclusions about model's performance would require additional laboratory investigations, preferably with bigger scale models, built of different equivalent materials. Data base for model calibration needs to be considerably extended, before the proposed numerical model can gain a wider application in practice.

The importance of numerical models such as the one proposed in this dissertation, lies in their capability to predict the failure mode, the maximum discharge, and the total failure time of overflown earth structures. These results represent the basic input data for calculation of flood zones, as well as for risk and damage assessment in the flooded region. In this respect the proposed model may be considered a step further in respect to some existing dam-break models which are based on geometrical schematizations and the broad-crested weir formula for evaluation of discharge.

1

Introduction

"When I turned back, I saw a huge wave of mud flooding the village .... As I struggled to save myself, the mud was rising all around me, and finally I was carried away .... This was Stava – the village that exists no more ...."

- Serbian newspaper "Politika", July, 21. 1985.

The testimonies of those who were lucky to survive the failure of the Stava dam near city of Trentno in the Northern Italy are moving and distressing, as is always the case when natural disasters devastate whole regions and take human lives[1].

This example of catastrophic consequences of dam-break incidents clearly points out the enormous responsibility of those who are involved in design, building, and maintenance of dams.

1.1 Relevance of the investigation

The statistics of the International Committee for Large Dams (ICOLD) register more than 500 such incidents up to 1965, practically in all countries where dams are built [13]. According to the same source, out of 92 dam-breaks from 1806 to 1969, 53 (almost 60%) pertain to earth dams.

This dissertation is concerned only with failure of earth structures, such as dams, dikes, and levees.

[1] On July 19, 1985, a fluorite tailings dam of Prealpi Mineraia failed at Stava, near Trento, Italy. A volume of 200,000 m^3 of water and tailings was released in 20 s, and flowed 4.2 km downstream at a speed of up to 90 km/h, killing 268 people and destroying 62 buildings. Aerial photographs of this catastrophic incident can be seen on: http://www.antenna.nl/wise/uranium/mdafst.html/.

The failure of an earth structure may happen due to one (or more than one) causes listed bellow:

- erosion of foundation or body of the structure;
- damage due to high pore pressures;
- cracks due to irregular consolidation;
- crest overtopping due to undersized, or damaged structure;
- seismic action;
- other natural or anthropogenic causes.

In most of the listed cases, the failure mechanism is characterized by formation of a *breach*, through which water is discharged from the reservoir (Fig.1.1). The breach evolution is the result of the erosion process which is investigated in this dissertation. Only the case when erosion is caused by dam *overtopping* is being considered.

Historical data confirm that this is one of the most frequent causes of dam failure. Almost 30% of dam failures in Switzerland, and 40% of dam failures in the USA up to 1966 occurred due to over topping [13, 50]. A survey of earth dam failures due to overtopping in the period 1800-1985 is given in Table 1.1.

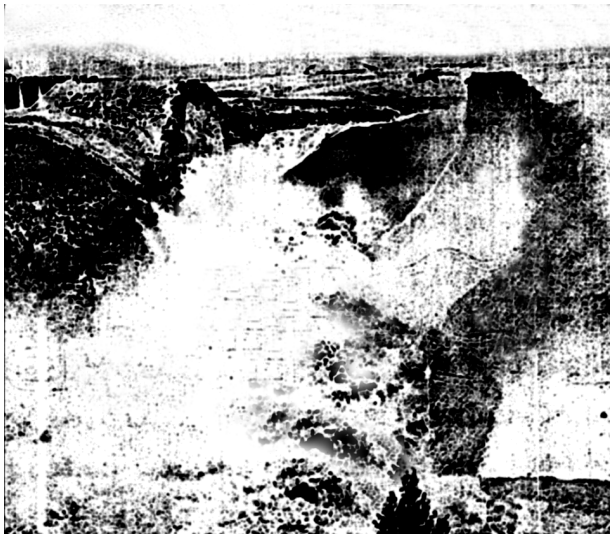

Figure 1.1: *Failure of the* 89 m *high Teton dam* (*USA*) *on June* 5*th,* 1976. *The photograph shows outflow through a breach* 15 *hours after the beginning of failure which was induced by excessive seepage. A volume of* 100×10^6 m^3 *of water was discharged from the reservoir, and* 3×10^6 m^3 *of material was washed away in a short period of time. Consequences:* 11 *dead,* 25 000 *homeless,* 400×10^3 ha *of farm land flooded, several thousand of cattle killed, the overall damage exceeding one billion dollars* [6].

Table 1.1: *Major earth dam failures due to overtopping* [9, 13, 50] ("const." - *failure under construction*)

Name of dam	Year of completion	Country	Height [m]	Volume [hm^3]	Year of failure	Failure time [h]	Reservoir volume [m^3]
Waghad	1883	India	32	17	1883	-	-
Johnstown	1881	USA	22	-	1889	2	20×10^6
Walnut Grove	1888	USA	34	11	1890	-	-
Altoona	1894	USA	11	-	1894	0.5	2.5×10^5
Oackford Park	1893	USA	6	-	1903	2-3	8×10^4
Red Rock	1910	USA	20	-	1910	-	-
Wisconsin Dells	1914	USA	18	25	1911	-	-
Sepulveda Canyon	1914	USA	20	-	1914	-	-
Lookout Shoals	1915	USA	25	49	1916	-	-
Lawer Otay	1897	USA	41	52	1916	-	-
Mammoth	1916	USA	23	14	1917	-	-
Tigra	1917	India	27	-	1917	-	-
Scott Falls	1921	Canada	15	-	1923	-	-
MacMahon Gulch	1924	USA	17	1	1926	-	-
Puddingstone	1928	USA	55	21	1926	const.	-
Briseis	1934	Austr.	27	-	1929	const.	-
Hebron	1934	USA	17	-	1942	-	-
Pagara	1927	India	30	166	1943	-	-
Heiwaike	1949	Japan	20	-	1951	-	-
Ashizawa	1912	Japan	15	-	1956	-	-
Serre-Ponçon	1943	France	-	-	1957	-	-
Kaddam	1957	India	41	215	1958	-	-
Oros	1962	Brazil	54	1000	1960	const.	700×10^6
Panshet	1961	India	49	212	1961	const.	-
Kharagpur	1956	India	24	56	1961	-	-
Ogayarindo Tameika	1944	Japan	19	1	1963	-	-
Lower Two Medicine	1913	USA	13	-	1964	-	2×10^4
Rot a.d.Rot	1958	Germany	5.5	-	1969	2	3×10^5
Dhuibara	1975	Indial	21	61	1976	-	-
Bolan	1961	Pakistan	19	89	1976	-	-
Salles de Oliveira	1966	Brazil	41	25	1977	-	2.5×10^4
Laurel Run	1970	USA	12	-	1977	-	-
Sandy Run	1972	USA	8.5	-	1977	-	-
Macchu 2	1973	Indial	26	101	1979	-	-

According to the U.S. Bureau of Reclamation, out of 8500 dams which were investigated in the course of the Dam Safety Program, over 3000 earth dams were classified as potentially unsafe [82]. About 85% of these dams are unsafe due to undersized discharge structures, or insufficient height. One explanation for this unfavorable situation is the fact that by extending hydrologic series over time, the maximum design discharges are likely to have higher values. Thus, some kind of dam rehabilitation is required[2].

The overtopping is unfortunately not the only cause of dam failure. Other causes are: seismic action, landslides, avalanches, failure of an upstream dam, etc. Anthropogenic factor, particularly in the field of dam operation and maintenance, is also present (Fig.1.2).

[2]In the case of old small earth structures, unconditional protection against overtopping is often either economically prohibitive, or physically not feasible. The rehabilitation of such structures presently consists of solutions enabling the structure to endure overflowing. Such constructive solutions, based on the roll concrete and vegetation protective covers, are intensively being investigated [75, 82].

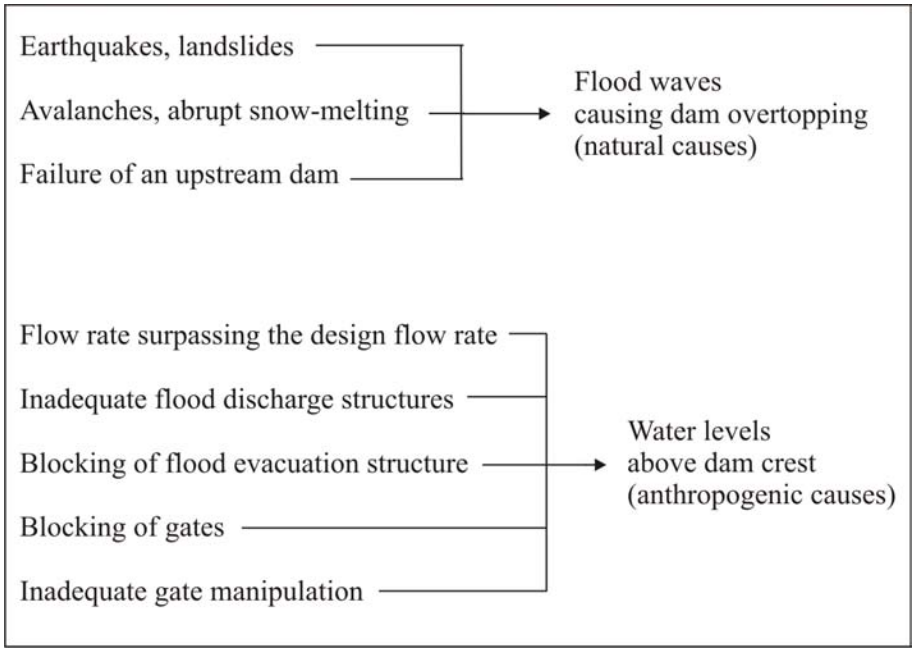

Figure 1.2: *Events causing dam failure*

Investigation of dam overflowing is especially important when *small earth structures* are concerned, as those structures are potentially more dangerous than high dams. Design of earth dams in the past was limited by insufficient hydrological data, and by modest technological possibilities. As overtopping prone, such dams are presently dangerous. Levees, and flood protection dikes inherently fall into the same category, as their height is designed in accordance to an acceptable level of risk.

An additional risk is due to scarcity or low quality of field investigation data. As prof. Nonveiller states in his book on earth dams [80]:

"Design and building of earth dams is sometimes assigned to companies without necessary experience and expertise for this kind of projects. Insufficient attention is payed to field investigations. They may be carried out more as a formality than as a real necessity, and as a result, only a few bore holes may be considered sufficient. Thus, design data are either incomplete, or are wrongly interpreted... If an earth dam does not fulfill safety requirements in all details, dangerous consequences will inevitably follow once it is fully loaded" .

The safety of small earth structures is especially important for Serbia, where a number of small dams are being built for water supply and flood detention purposes, and where a 3500 km long system of levees is maintained. Only in the province of Vojvodina, more than 50 levee failures are registered since 1859, with over 330 000 ha of farm land being flooded (Figs. 1.3, 1.4).

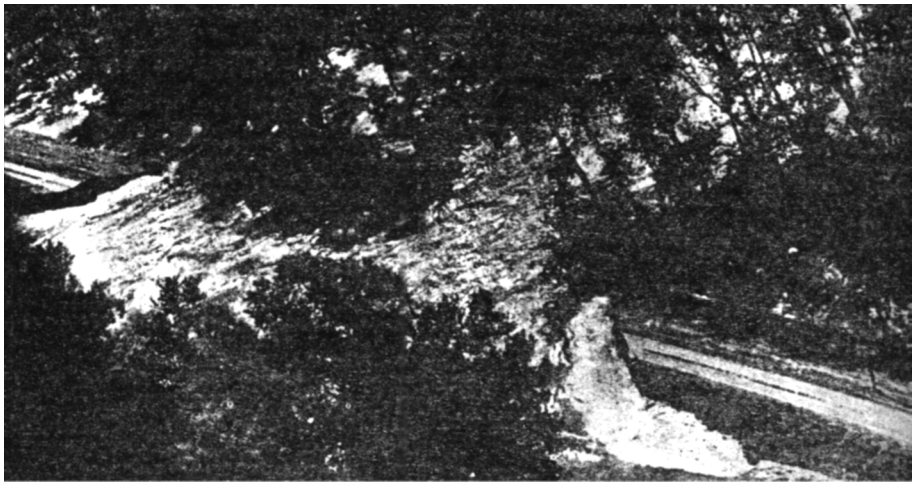

Figure 1.3: *Aerial photograph of a levee break on the Danube river near town Bogojevo, on June* 16*th,* 1965*, during one of the worst flooding events ever recorded on this river* [79]

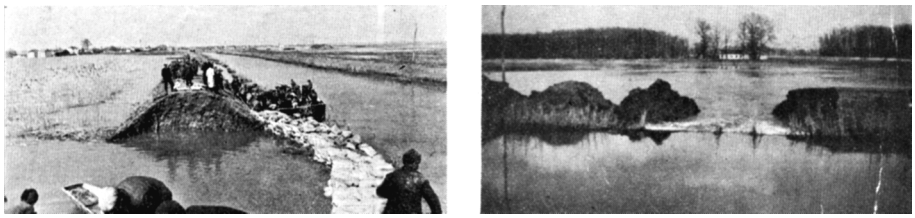

Figure 1.4: *Reparation of a Danubean levee near city of Novi Sad, and a breach formed in the course of levee failure in April,* 1940*.* [79]

More than 50% of farm land is potentially flooded in this region, with about 50% of the entire population, living in 173 villages.

Emergency earth structures, such as fuse plugs, also require investigation of erosion processes connected with overflowing. As is well known, these structures are built to be intentionally overtopped and washed away, providing way of excess water into retention basins used for flood management and control.

Investigations performed in this dissertation are to be a contribution to the prediction of hydraulic consequences of earth dam failures. There is a general feeling in the Serbian hydraulic engineering community that numerical modeling practices and tools should be upgraded in order to have more reliable forecasting of dam-break flows. The present legislature in Serbia requires that the early warning systems for potentially endangered regions should be designed according to the hypothesis of total, instantaneous dam failure [10].

Although on the safe side, this requirement is physically unrealistic, and practically inconvenient, since large earth volumes cannot be instantaneously removed, and an unnecessary computational effort is required, along with costly preparation of input geometric data and post-processing work. *Partial and progressive failure* of earth dams is not only physically more plausible, but allows quicker and financially more reasonable dam-break analyzes.

In order to investigate the hydraulic effects of partial, progressive dam failures, the author has performed a series of numerical experiments, assuming a schematized breach geometry (trapezoid/rectangular cross-section), breach evolution rates, and the downstream river channel geometry (rectangular cross-section, constant bed slope). The results are presented in Fig. 1.5.

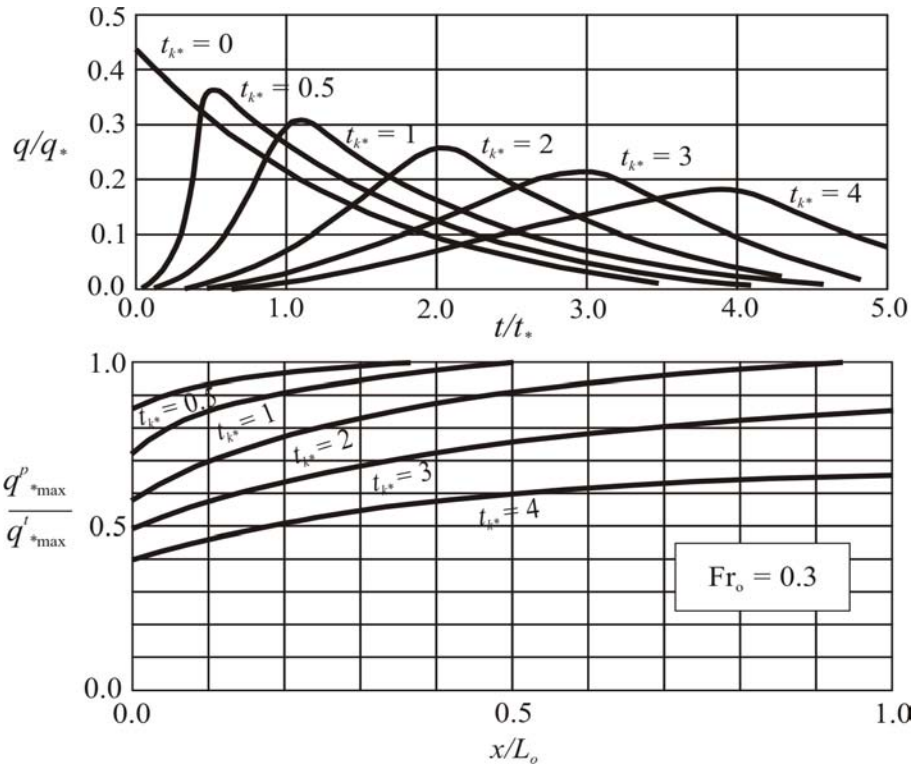

Figure 1.5: *The diagram on top shows dimensionless outflow hydrographs from a breached dam for various durations of breach evolution; the parameter t_{k*} represents the dimensionless breach evolution time (time in respect to the total failure time). Its zero value corresponds to the instantaneous dam failure. The diagram below shows the relationship between the maximum discharges for progressive and instantaneous dam failure, dimensionless breach evolution times, and dimensionless distance downstream from the dam. (More details can be found in reference* [14]).

The numerically simulated outflow hydrographs show that progressive dam failures yield (as can be expected), attenuated hydrographs. The degree of attenuation is proportional to the duration of dam failure. Such simple numerical experiments clearly underline the need for research of the erosion of earth structures exposed to overflowing, so that computations can be based on physically realistic, and not on assumed or schematized conditions. That was the principal motive for investigations initiated by this dissertation.

1.2 Objectives of the investigation

The failure of earth structures, such as dams and levees, due to their overtopping is not a sufficiently clarified phenomenon. This complex process is affected by numerous factors (Fig. 1.6).

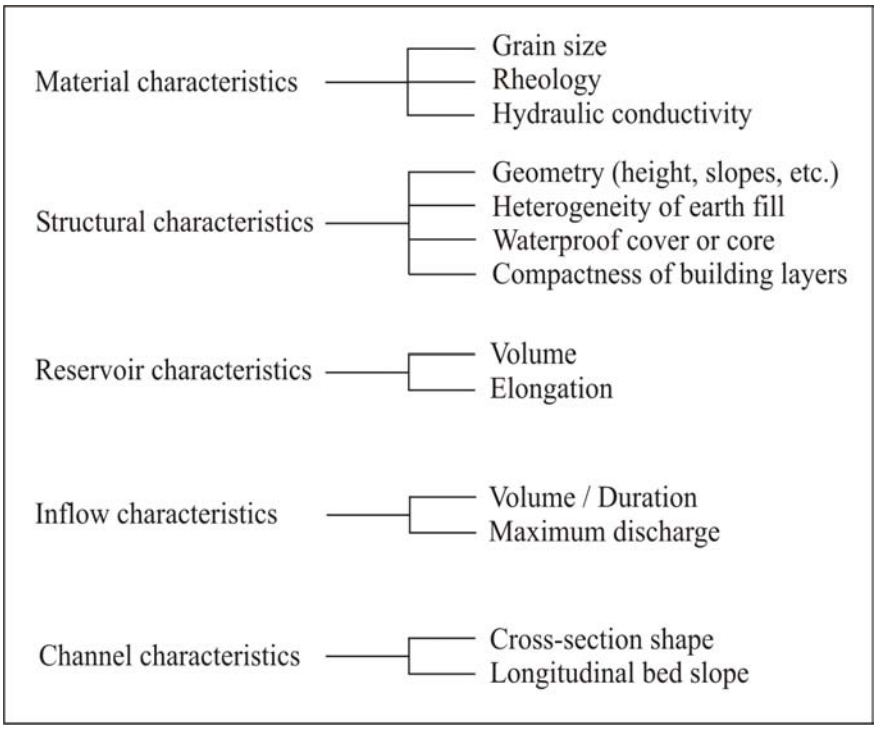

Figure 1.6: *Factors affecting the earth structure failure, and the resulting outflow hydrograph*

As it is impossible to fully investigate all these factors in one thesis, an objective to develop a general solution would certainly be too pretentious. Therefore, it is necessary from the start to assume certain limitations for experimental research, and thus to narrow down the problem to a reasonable level of complexity. However, it can be expected that, with more research in future, additional information on the subject will become available, and that more complex analytical tools will be developed.

The basic assumptions made in this dissertation are the following:

(i) *Material characteristics.* Experiments are limited to moderately cohesive materials.

(ii) *Structural characteristics.* Earth dams and levees are built of homogeneous, compactly layered material, without seepage preventing elements, such as clay cores.

(iii) *Reservoir characteristics.* The size of the laboratory flume is a limiting factor for investigations; in this particular case, the specific dam-to-reservoir volume ratio is typically 1:25.

(iv) *Inflow characteristics.* A constant reservoir inflow rate is assumed. Such boundary condition is convenient for experimental work and is physically justified by the fact that the failure time of overflown earth structures is, as experience shows [8], much shorter than duration of the flood event.

(v) *Topographic characteristics.* The experiments are carried out in a laboratory flume with rectangular cross-section and zero longitudinal slope. Thus, the valley immediately downstream from the dam is assumed to have a rectangular cross-section.

Considering the given limitations, the problem will be analytically treated as a quasi-steady 2D problem (in the vertical plane), whereby the erosion process is studied only in the *vertical* direction (3D effects are not considered).

The main objectives of this research can be summerized in four points.

1. Investigate possibilities of numerical modeling of the erosion process induced by overtopping of earth structures built of homogenous, moderately coherent materials.

2. Develop a reliable numerical procedure for calculation of 2D curvilinear gravity flow (water-surface profile, velocity and pressure distributions), for a given set of boundary conditions.

3. Study qualitatively and quantitatively the erosion of earth structures, treating this phenomenon as a 2D problem in the vertical plane (per unit length of the structure). Studies are to be based on laboratory experimental evidence, using pilot scale models built of homogeneous, moderately coherent materials. Theoretical and practical aspects of building such scale models need to be considered, as a number of similitude conditions are to be satisfied in order to ensure realistic and meaningful extrapolation of experimental results to actual (prototype) structures and field conditions.

4. Combine theoretical and experimental investigations and propose an original numerical model for calculating the failure of overtopped earth structures (dams, levees, embankments, etc.). This new model is to be more physically based than existing models, which treat the erosion process in a schematic way, by assuming the geometric characteristics of the breach, and the rate of its evolution.

1.3 Organization of the dissertation

A brief introduction and definition of objectives is given in the first chapter.

The numerical model of erosion of earth structures exposed to overflowing is conceptually decomposed in such a way that calculation of free-surface (gravity) flow over the structure is followed by calculation of erosion of this structure, based on the critical velocity concept.

Development of numerical model - part I, which refers to calculation of the free-surface curvilinear flows, is presented in the second chapter. A model based on the Boundary Element Method is proposed. In addition to theoretical considerations, practical aspects of the model application are discussed. A number of case studies are used for testing the performance of the model.

The third chapter is dedicated to original experimental investigations, which were undertaken in order to clarify some physical aspects of the phenomenon, and to provide experimental data base for deriving an empirical relationship between the water and sediment flow rates. Erosion resistance of moderately cohesive soils is investigated, and a number of similitude conditions for building pilot scale models are derived. Measuring equipment and techniques are described. Qualitative and quantitative analysis of experimental results are given, and scale effects are evaluated.

Development of numerical model - part II, which refers to calculation of erosion depths along the overflown structure, is presented in the fourth chapter. First, the critical velocity for incipient motion of cohesive materials is defined. Then, the empirical function derived from author's laboratory investigations, is used to calculate the total eroded volumes over time. A method for calculating deformable solid boundary (variable cross-sectional shapes of the earth structure during its failure), is proposed.

Chapter five is dedicated to validation of the numerical model. One of the laboratory experiments is chosen for this purpose. A complete set of results is presented, consisting of the water surface and erosion contours at specific time intervals. The quality of the calculated results is evaluated using photographs taken during experiments.

Finally, conclusions are formulated, and topics for further research are suggested in the sixth chapter. A comprehensive list of references, sorted according to topics, is given at the end.

2

Development of the Numerical Model - Part I

Erosion of earth structures exposed to overflowing is a very complex phenomenon, and its numerical simulation is coped with a number of problems. Some of these problems are of conceptual nature (governing equations), while others are linked with the model implementation.

This chapter starts with explanation how the mathematical model of this complex physical process may be decomposed into two, mutually connected, simpler component models. Then follows consideration of the first component which refers to calculation of the free-surface curvilinear flow over a structure of an arbitrary cross-sectional shape. Theoretical background is provided, and some practical aspects of the numerical model development and implementation are discussed.

The second component of the model, referring to erosion modeling, is presented in the fourth chapter.

2.1 Conceptual fundamentals

In order to develop a mathematical model of erosion of an overflown earth structure, several problems need to be considered, the most important ones being:

(i) *Unsteady flow regime.* Flow over deformable earth structures is variable in space and time. A concept of quasi-steady flow conditions is assumed, which means that the unsteady flow regime is analyzed as a succession of steady states within a number of very short time intervals Δt. This implies averaging the hydraulic and sedimentologic parameters in each time interval.

It must be stressed that numerical modeling of accelerated, curvilinear gravity flow is not simple even if the flow is assumed to be steady. Determination of the free-surface profile is a highly non-linear problem, imposing numerically sensitive iterative solutions.

(ii) *Liquid-solid interaction.* The mathematical model in this dissertation is based on the assumption that, under certain conditions, the hydraulic and sedimentologic computations may be uncoupled. As cohesion tends to slow down the erosion process, it can be assumed that the erosion-induced changes of the solid boundary are slower than changes of the free-surface boundary. Thus, if the problem is considered as two-dimensional in the vertical plane, computation of the free-surface profile and the corresponding velocity field may be done in the first step, and the computation of the deformed solid surface profile will follow in the second step. It means that erosion is calculated for the *known* flow field, representative for the time interval Δt. Then the new contour of the solid boundary is used for hydraulic computation in the next time period Δt, and the two-step procedure is repeated until the structure is completely washed away.

Theoretical justification for this approach is given by de Vries [72]. Starting from the basic conservation laws, and assuming that the sediment flow rate is proportional to the depth-averaged velocity, this author has formulated a dimensionless power relationship between propagation rates of disturbances on the water surface and the bed surface:

$$\phi^3 - 2\,\phi^2 + (1 - \mathrm{Fr}^{-2} - \psi \cdot \mathrm{Fr}^{-2})\,\psi + \psi \cdot \mathrm{Fr}^{-2} = 0, \tag{2.1}$$

where ϕ - the relative propagation rate of disturbances, $\mathrm{Fr} = \widetilde{u}/\sqrt{g \cdot h}$ - the local Froude number, defined in terms of the local depth-averaged velocity $\widetilde{u}$ and depth h, ψ - the sediment transport parameter reflecting sediment concentration.

The equation (2.1) has three real roots:

$$\left.\begin{aligned} \phi_1 &= 1 + \frac{1}{\mathrm{Fr}} \\ \phi_2 &= 1 - \frac{1}{\mathrm{Fr}} \\ \phi_3 &= \frac{\psi}{1 - \mathrm{Fr}^2} \end{aligned}\right\} \tag{2.2}$$

which are graphically depicted in Fig.2.1.

The roots ϕ_1 and ϕ_2 reflect the flow disturbance celerities, and the root ϕ_3, celerity of disturbances on the bed. From the given diagram it can be concluded that variables ϕ_1 and ϕ_2 are *independent* of bed mobility ϕ_3 in

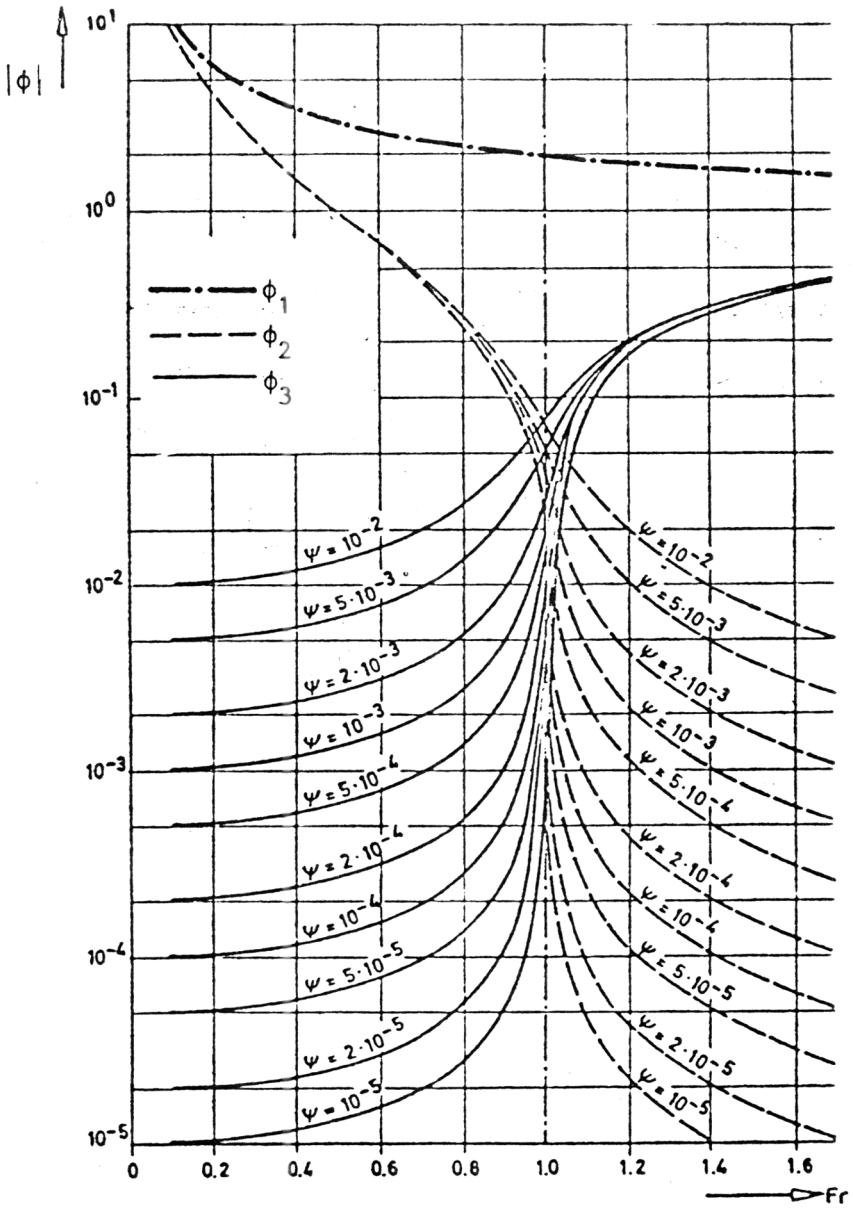

Figure 2.1: *Relative propagation rates of disturbances* [72]

either subcritical or supercritical flow regimes. It is only under the critical flow conditions (Fr $\approx$ 1) that the disturbance celerities become comparable in the absolute sense, in which case the concept of uncoupled hydraulic and sedimentologic calculations cannot be applied.

A schematic representation of an overflown earth structure is given in Fig.2.2. This diagram, showing the free surface profile at one particular instant, is based on author's laboratory experiments which will be later described.

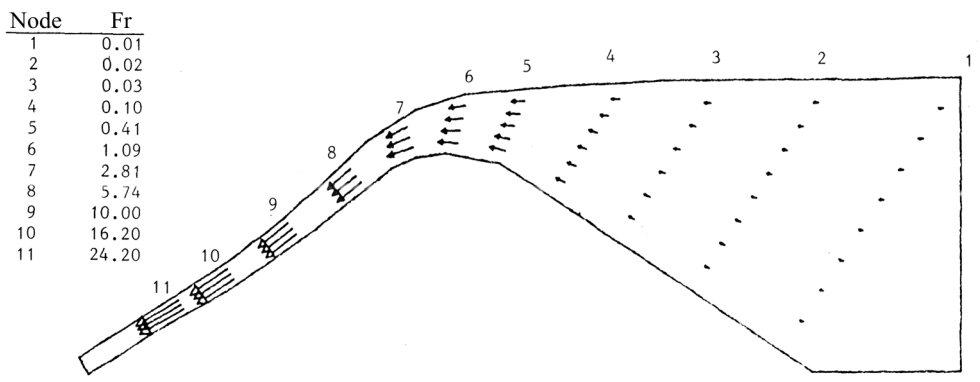

Figure 2.2: *The Froude number values along the flow*

Considering distribution of the Froude number values, the regions of subcritical (slow) and supercritical (accelerated) flows are clearly delineated, with a very short region of the critical flow at the crest of the structure. It is decided to apply the concept of uncoupled hydraulic and sedimentologic calculations, and to investigate whether in this particular case this concept can be justified.

(iii) *Erosion resistance of cohesive materials.* There is no general theoretical approach in defining the resistance of cohesive materials to flowing water. Answers may be found solely by the empirical research. For this reason, a program of laboratory experiments is proposed in order to determine an empirical relationship between water and solid discharges which could be subsequently incorporated in the numerical model.

2.2 Previous Work

A number of progressive dam-break numerical models have been developed in the past, some of which are more of theoretical than of practical significance. All of these models introduce some schematization which is the limiting factor for their general application.

One of the best known models is the model of Cristofano [5]. It is based on an assumed exponential relation between the water and solid flow rates,

formulated in terms of the breach size, water surface elevation in the reservoir, and the internal friction angle of the material. The trapezoidal breach cross-section is linearly increasing during an assumed period of breach development. The longitudinal breach slope is constant, and the flow through the breach is uniform. During the dam failure, the reservoir water surface elevation is invariable.

The model of Thiriot [12] treats the dam breach as rectangular broad crested weir with horizontal bottom. The material is cohesionless, and its transport rate is defined by the Meyer-Peter and Muller formula.

The US Bureau of Reclamation model [3] uses the Schoklitsch formula for sediment transport. The breach is schematized as a canal with longitudinal slope 5^o-20^o. Its cross-section has side slopes of 45^o and parabolic bottom, in accordance to the photographed Teton dam breach.

The model proposed by Fread, implemented in the National Weather Service (NWS) DAMBRK software [6, 8], also uses an assumed linear growth of the trapezoid breach in time. The reservoir outflow discharge is calculated by the broad crested weir formula. No parameters reflecting the physics of the erosion process are considered.

Contrary to the previous models, the approach of Sametz [11] is physically based. This author used scale models of dams made of homogenous, cohesionless material, and also models with waterproof cores. He found an exponential relationship between the breach flow rate and transport of the eroded material. Experiments showed that in case of the progressive dam failure, the maximum outflow can be up to 40% smaller than the maximum outflow when dam failure is instantaneous.

2.3 Solution methods for the free-surface accelerated flows

The mathematical model of flow over a deformable earth structure, developed in this dissertation, is based on the potential flow theory and the Boundary Element Method, for reasons which will be subsequently explained.

The problem of analytical treatment of curvilinear gravity flows is one of the classical problems in hydraulics. The solution methods are based either on the modified St. Venant equations ("Dressler equations"), or on the potential flow theory.

The first approach is physically more plausible than the second one, but numerically considerably more complicated (see for instance [70, 71, 73, 74]). On the other hand, application of the potential flow theory for the

curvilinear gravity flows is justified by the fact that effects of inertial and gravity forces on fluid particles are dominant in respect to effects of forces due to pressure and viscosity. Neglecting viscous effects (as secondary), the numerical flow model can be made relatively simple, but reliable and efficient for engineering application. In fact, one of the main objectives of this dissertation is development of such a simplified model and evaluation of its performance.

The numerical techniques for solution of free-surface potential flows can be generally classified into three groups: the Finite Difference Methods (F.D.M.), the Finite Element Methods (F.E.M.), and the Boundary Element Methods (B.E.M.).

After studying the comparative advantages and disadvantages of these methods, the Boundary Element Method is chosen, having the main advantage in the fact that a relatively small number of computational points on the boundary of the domain are sufficient to obtain solution. This is especially convenient for iterative determination of the free-surface, as there is no need for restructuring the computational mesh inside the domain in each iteration, as in other methods. This point will be later discussed in detail.

2.4 The Boundary Element Method

The Boundary Element Method (B.E.M.) is often erroneously considered as a variant of the Finite Element Method (F.E.M.). However, it has been used in Mechanics long before the F.E.M. under different names: The Method of Boundary Integrals, Treftz Method, The Panel Method, and Method of Green's Functions.

The basic idea of the B.E.M. is to replace, under certain conditions, a partial differential equation by a corresponding integral equation, and thus to solve the problem on the boundary of the domain. In this way a 2D problem is reduced to 1D problem. Solutions for chosen points inside the domain are obtained subsequently, from the known solution on the boundary.

The B.E.M. is an optimal method for analysis of potential flows, and free-surface flows which can be considered as potential flows (flow in porous media, small amplitude friction independent waves, and inertial dominated flows in vicinity of hydraulic structures – gates, orifices, spillways, etc.). The B.E.M. can efficiently provide the solution of a 2D free-surface problem, defined in the vertical plane. The free-surface is not known a priori, but has to be determined as a part of the overall solution, for the given set of boundary conditions.

As has been already pointed out, the main advantage of the Boundary Ele-

ment Method over the Finite Element Method (in the class of problems for which both are equally applicable) is the fact that the former method yields faster solutions, with considerably less input data. In addition to this, the B.E.M. gives not only the values of the dependent variable on the boundary, but also the values of its normal derivative.

The B.E.M. allows easier solution algorithms for determination of the free-surface, because only a small number of nodes on the free-surface are relocated at each iteration, while the F.E.M. requires regeneration of the complete mesh, including all interior points.

The main disadvantage of the B.E.M. is its limited applicability to the elliptic problems, defined by the Laplace equation, and the related equations.

Derivation of the basic integral equation of the B.E.M. starts from the Green's theorem specifying relation between the volume and surface integrals:

$$\int_{\forall} \nabla \cdot \boldsymbol{v} \, \mathrm{d}\forall = \int_{A} \boldsymbol{v} \cdot \boldsymbol{n} \, \mathrm{d}A, \tag{2.3}$$

where the Hamilton's operator ∇ represents vector:

$$\nabla = \frac{\partial}{\partial x}\boldsymbol{i} + \frac{\partial}{\partial y}\boldsymbol{j} + \frac{\partial}{\partial z}\boldsymbol{k},$$

$\boldsymbol{v}$ is an arbitrary vector, and $\boldsymbol{n}$ is the unit vector normal to the surface A.

The equation (2.3), used in Fluid Mechanics for formulating continuity laws, postulates that the flux of an arbitrary vector $\boldsymbol{v}$ through a closed surface A is equal to the integral of divergence of this vector ($\nabla \cdot \boldsymbol{v}$=div $\boldsymbol{v}$) over volume $\forall$, enclosed by the surface A.

In case of the 2D problems, the integral theorem (2.3) reads:

$$\int_{\Omega} (\nabla \cdot \boldsymbol{v}) \, \mathrm{d}\Omega = \int_{\Gamma} \boldsymbol{v} \cdot \boldsymbol{n} \, \mathrm{d}\Gamma, \tag{2.4}$$

where Γ is the closed curve enclosing the surface Ω (Fig. 2.3).

Let us assume now that the vector $\boldsymbol{v}$ can be expressed by two, twice differenciable scalar functions $U(x, y)$ i $V(x, y)$ in the following manner:

$$\boldsymbol{v} = U\nabla V \tag{2.5}$$

$$\boldsymbol{v} = V\nabla U. \tag{2.6}$$

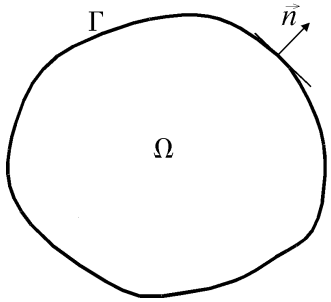

Figure 2.3: *Boundary of the solution domain*

In the first case, the following development is possible:

$$\begin{aligned}\nabla \cdot \boldsymbol{v} &= \nabla \cdot U\nabla V = \left(\frac{\partial}{\partial x}\boldsymbol{i} + \frac{\partial}{\partial y}\boldsymbol{j}\right)\left(U\frac{\partial V}{\partial x}\boldsymbol{i} + U\frac{\partial V}{\partial y}\boldsymbol{j}\right) = \\ &+ \frac{\partial U}{\partial x}\frac{\partial V}{\partial x} + \frac{\partial U}{\partial y}\frac{\partial V}{\partial y} + U\frac{\partial^2 V}{\partial x^2} + U\frac{\partial^2 V}{\partial y^2} = \\ &= \nabla U \cdot \nabla V + U \cdot \nabla^2 V, \end{aligned} \tag{2.7}$$

thus equation (2.4) becomes:

$$\int_\Omega \left(\nabla U \cdot \nabla V + U\nabla^2 V\right)\, \mathrm{d}\Omega = \int_\Gamma U\nabla V \cdot \boldsymbol{n}\, \mathrm{d}\Gamma, \tag{2.8}$$

where ∇^2 is the Laplace operator.

Similarly, in the second case:

$$\nabla \cdot \boldsymbol{v} = \nabla \cdot V\nabla U = \nabla V \cdot \nabla U + V \cdot \nabla^2 U, \tag{2.9}$$

and equation (2.4) becomes:

$$\int_\Omega \left(\nabla V \cdot \nabla U + V\nabla^2 U\right)\, \mathrm{d}\Omega = \int_\Gamma V\nabla U \cdot \boldsymbol{n}\, \mathrm{d}\Gamma. \tag{2.10}$$

Subtracting (2.10) from (2.8), an expression referred to as the "main", or the "second Green's formula" is obtained:

$$\int_\Omega (U\nabla^2 V - V\nabla^2 U)\, \mathrm{d}\Omega = \int_\Gamma (U\nabla V - V\nabla U) \cdot \boldsymbol{n}\, \mathrm{d}\Gamma. \tag{2.11}$$

Using the following notation for the normal derivatives:

$$\nabla V \cdot \boldsymbol{n} = \frac{\partial V}{\partial n} \quad \nabla U \cdot \boldsymbol{n} = \frac{\partial U}{\partial n}, \tag{2.12}$$

the basic equation (2.11) can be formulated in this way:

$$\int_{\Omega}(U\nabla^2 V - V\nabla^2 U)\,\mathrm{d}\Omega = \int_{\Gamma}\left(U\frac{\partial V}{\partial n} - V\frac{\partial U}{\partial n}\right)\,\mathrm{d}\Gamma. \tag{2.13}$$

If the functions U i V are chosen so to satisfy the Laplace equation:

$$\nabla^2 U = \nabla^2 V = 0, \tag{2.14}$$

the left side of equation (2.13) becomes zero, thus:

$$\int_{\Gamma}\left(U\frac{\partial V}{\partial n} - V\frac{\partial U}{\partial n}\right)\mathrm{d}\Gamma = 0. \tag{2.15}$$

The equation (2.15) is the basic integral equation of the B.E.M.[1].

Further transformation of this equation depends on the choice of functions U and V. Function U can be replaced by either the *velocity potential function* Φ or the *stream function* ψ. Both of these functions satisfy the Laplace equation defining potential flows.

Function V needs to be chosen in the form of the *fundamental solution* of the Laplace equation [28, 29], which means that it satisfies the Laplace equation everywhere in the domain, except at a singular point P (Fig. 2.4-(a)). This condition can be expressed as:

$$\nabla^2 V = \delta(P), \tag{2.16}$$

where the Dirac's function δ takes the value of one at point P (unit sink), and takes the zero value at all other points. Function V defined by (2.16) is also known as the "Green's function in the unbounded space" [41].

The solution of equation (2.16) for 2D problems takes this form [29, 41]:

$$V = \ln r, \tag{2.17}$$

where r represents distance between the singular point P and an arbitrary point Q on the boundary (Fig. 2.4-(a)). Near point P ($r \to 0$), function V tends toward infinity. In order for the basic equation (2.15) to be valid, it is necessary to exclude point P by circumventing it with a circle of small radius r_o, as is shown in Fig. 2.4-(a).

[1]The same integral equation can be derived following the residual methods approach in the F.E.M. theory.

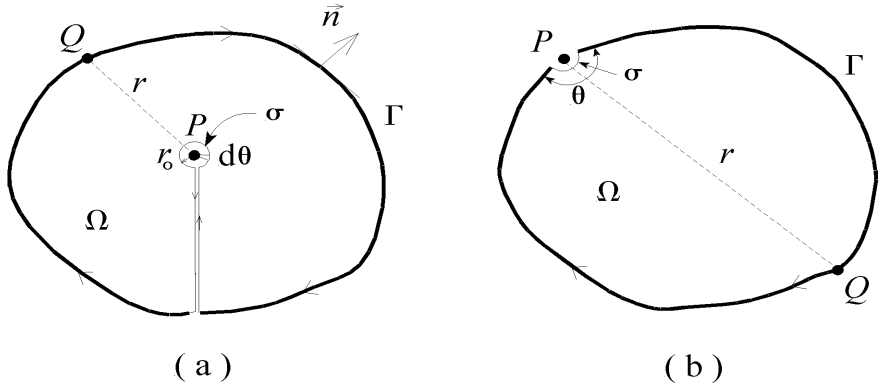

Figure 2.4: *Solution domain and boundary over which integration is performed:* (a) *singular point inside domain;* (b) *singular point on the boundary*

Substitute now function U in equation (2.15) with potential Φ, and assume that function V is defined according to (2.17):

$$\int_\Gamma \left[\Phi \frac{\partial(\ln r)}{\partial n} - \ln r \frac{\partial \Phi}{\partial n}\right] \mathrm{d}\Gamma + \lim_{r_o \to 0} \int_\sigma \left[\Phi \frac{\partial(\ln r)}{\partial n} - \ln r \frac{\partial \Phi}{\partial n}\right] \mathrm{d}\Gamma = 0. \tag{2.18}$$

The integrals along lines connecting the elementary circle with the boundary cancel each other due to the opposing directions of integration. Since the outside normal $\vec{n}$ to the domain Ω is on the circle σ directed toward point P, it follows for this part of the boundary:

$$\frac{\partial(\ln r)}{\partial n} = -\frac{1}{r} \cdot \frac{\partial r}{\partial n} = -\frac{1}{r}. \tag{2.19}$$

Considering that: $\mathrm{d}\Gamma = r_o \mathrm{d}\theta$ and that the function $\Phi(x, y)$ is independent of r_o, it can be shown for the integral around circle:

$$\lim_{r_o \to 0} \int_0^{2\pi} \left(\Phi \frac{1}{r_o} - \ln r_o \frac{\partial \Phi}{\partial r_o}\right) r_o \theta = \lim_{r_o \to 0} \int_0^{2\pi} (-\Phi) \mathrm{d}\theta = -2\pi \Phi(P). \tag{2.20}$$

Finally, equation (2.18) takes the form:

$$2\pi\ \Phi(P) = \int_\Gamma \left[\Phi(Q) \frac{1}{r} \frac{\partial r}{\partial n} - \ln r \frac{\partial \Phi(Q)}{\partial n}\right] \mathrm{d}\Gamma. \tag{2.21}$$

This equation shows that by integration along the boundary, the value of variable Φ can be determined for any point P *inside the domain*, once the

values of this variable and its normal derivative are known at any point Q *on the boundary of the domain.*

For the well-poised problem, the solution of equation (2.21) requires that values of either Φ or $\partial\Phi/\partial n$ are specified as the input data along certain parts of the boundary. Values of the other (missing) variable are calculated on the corresponding parts of the boundary. For this purpose, the singular (base) point is moved over to the boundary, where it is circumvented by a circular arch σ, with a characteristic angle θ (Fig. 2.4-(b)). Usually, $\theta \leq 2\pi$, but for straight boundary, $\theta = \pi$.

Ultimately, the integral equation used for solution of the unknown variables *on the boundary* has this general form:

$$\theta\ \Phi(P) = \int_\Gamma \left[\Phi(Q)\frac{1}{r}\frac{\partial r}{\partial n} - \ln r \frac{\partial \Phi}{\partial n}\right] \mathrm{d}\Gamma \quad (\theta \leq 2\pi). \tag{2.22}$$

2.4.1 Solution on the boundary of the flow domain

The numerical solution of equations (2.21) and (2.22) requires approximation of the boundary contour Γ by a polygon, whose sides represent *boundary elements*, and whose points are the *nodes* in which the solution is calculated (Fig. 2.5).

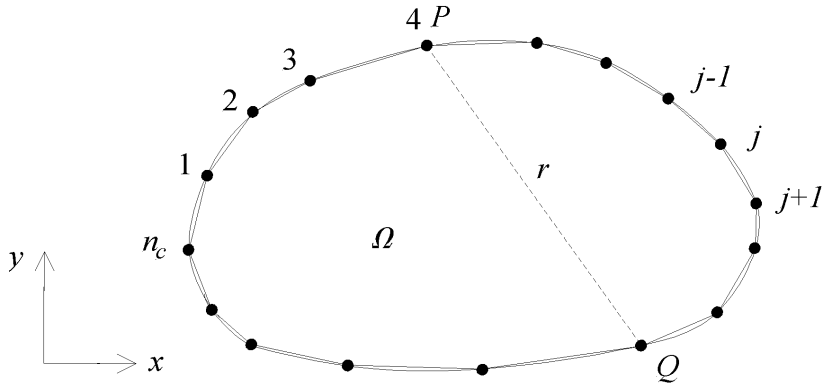

Figure 2.5: *Approximation of the solution domain by boundary elements*

Each nodal point P_i $(i = 1, 2, \ldots, n_c)$ becomes in turn, moving clockwise or counterclockwise, a singular point for which an equation of the type (2.22) can be applied. Thus, n_c equations, relating variables Φ and $\partial\Phi/\partial n$ on the boundary, are available.

The physics of the problem dictate on which parts of the boundary the values Φ are to be specified, and on which parts the values $\partial\Phi/\partial n$ are to

be specified[2]. In the former case the boundary condition is of the Dirichlet type, and in the latter case, it is of the Neumann type. At locations where the change of boundary condition type occurs, two nodes are set closely apart.

Following procedure which is similar to that in the F.E.M., the system of integral equations is, taking account of the boundary conditions, transformed to a system of linear algebraic equations to be solved for the boundary values Φ and $\partial\Phi/\partial n$. Those values are used for subsequent integration of equation (2.21), which gives the solution inside the computational domain.

Linear 1D elements. The simplest way to solve equation (2.22) is to assume linear variation of functions Φ and $\partial\Phi/\partial n$ along each element. In this case integration *in closed form* is possible over real elements (there is no need for introduction of referent unit elements, as when numerical integration is applied). The advantage of analytical integration is the accuracy and speed of calculation.

Consider an element defined by end nodes P_j and P_{j+1} (Fig. 2.6). The position of an arbitrary point along this element is defined by the distance to the singular point r_i, or by the local coordinates (ξ, η).

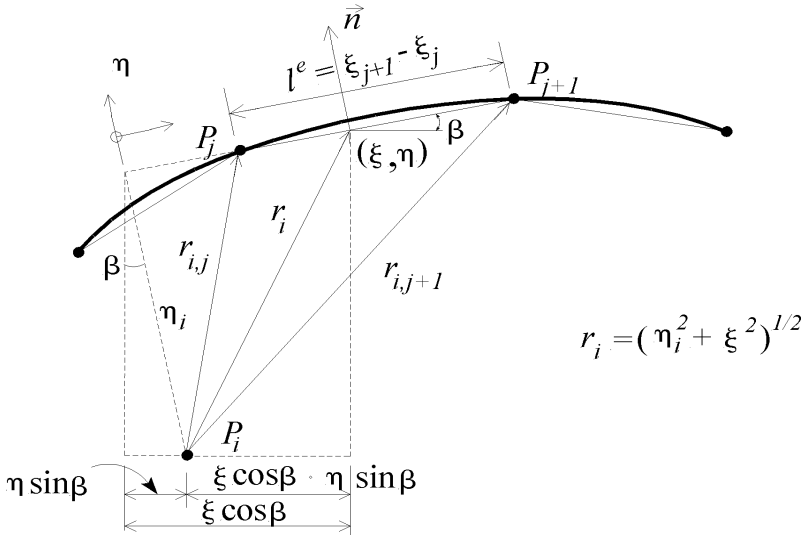

Figure 2.6: *Geometry of the boundary element*

[2]It is to be recalled from the elementary Fluid Mechanics that the derivative $\partial\Phi/\partial n$ represents the velocity component normal to the boundary. If alternatively, the stream function is chosen for the unknown variable, the derivative $\partial\psi/\partial n$ is the tangential velocity component in respect to the boundary.

The linear variation $\Phi = a + b \cdot \xi$ along the element implies that the values of the coefficients a and b are to be determined from the condition $\Phi(\xi_j) = \Phi_j$ and $\Phi(\xi_{j+1}) = \Phi_{j+1}$:

$$\left.\begin{array}{lcll} \Phi_j & = & a + b \cdot \xi_j & \\ \Phi_{j+1} & = & a + b \cdot \xi_{j+1} & \end{array}\right\}, \tag{2.23}$$

from where it follows that:

$$a = \frac{\xi_{j+1}\Phi_j - \xi_j\Phi_{j+1}}{\xi_{j+1} - \xi_j}; \qquad b = \frac{\Phi_{j+1} - \Phi_j}{\xi_{j+1} - \xi_j}. \tag{2.24}$$

If the length of the element is denoted by: $l^e = \xi_{j+1} - \xi_j$, where the superscript "e" stands for the element number, the linear variation can be formulated in this way:

$$\Phi = N_j^{(e)} \cdot \Phi_j + N_{j+1}^{(e)} \cdot \Phi_{j+1}, \tag{2.25}$$

$$\frac{\partial \Phi}{\partial n} = N_j^{(e)} \cdot \left(\frac{\partial \Phi}{\partial n}\right)_j + N_{j+1}^{(e)} \cdot \left(\frac{\partial \Phi}{\partial n}\right)_{j+1}, \tag{2.26}$$

where the linear interpolation functions are:

$$N_j^{(e)} = \frac{1}{l^e}(\xi_{j+1} - \xi); \quad N_{j+1}^{(e)} = \frac{1}{l^e}(\xi - \xi_j). \tag{2.27}$$

Consider now the same element and the singular point at the node "i". The unknown variables Φ and $\partial\Phi/\partial n$, appearing in the integral equation (2.22), can be defined according to expressions (2.25) and (2.26), and the following expression is obtained:

$$\begin{aligned} I_i^{(e)} &= \int_{\xi_j}^{\xi_{j+1}} \left(\frac{\Phi}{r_i} \cdot \frac{\partial r_i}{\partial n} - \ln r_i \frac{\partial \Phi}{\partial n}\right) \mathrm{d}\xi = \Phi_j \, (k_1^e)_{i,j} + \Phi_{j+1} \, (k_1^e)_{i,j+1} - \\ &- \left(\frac{\partial \Phi}{\partial n}\right)_j (k_2^e)_{i,j} - \left(\frac{\partial \Phi}{\partial n}\right)_{i,j+1} (k_2^e)_{i,j+1}. \end{aligned} \tag{2.28}$$

The equivalent matrix equation is:

$$I_i^{(e)} = \left[\begin{array}{cccc} (k_1^e)_{i,j} & (k_1^e)_{i,j+1} & 0 & 0 \\ 0 & 0 & -(k_2^e)_{i,j} & -(k_2^e)_{i,j+1} \end{array}\right] \left\{\begin{array}{c} \Phi_j \\ \Phi_{j+1} \\ \left(\frac{\partial \Phi}{\partial n}\right)_j \\ \left(\frac{\partial \Phi}{\partial n}\right)_{j+1} \end{array}\right\} =$$

$$
\begin{aligned}
&= \{(k_1^e)_{i,j} \quad (k_1^e)_{i,j+1}\} \left\{ \begin{array}{c} \Phi_j \\ \Phi_{j+1} \end{array} \right\} - \\
&- \{(k_2^e)_{i,j} \quad (k_2^e)_{i,j+1}\} \left\{ \begin{array}{c} \left(\dfrac{\partial \Phi}{\partial n}\right)_j \\ \left(\dfrac{\partial \Phi}{\partial n}\right)_{j+1} \end{array} \right\},
\end{aligned} \tag{2.29}
$$

where:

$$
\left.
\begin{aligned}
(k_1^e)_{i,j} &= \int_{\xi_j}^{\xi_{j+1}} N_j^{(e)}(\xi) \cdot \frac{1}{r_i} \frac{\partial r_i}{\partial n} \, \mathrm{d}\xi \\
(k_1^e)_{i,j+1} &= \int_{\xi_j}^{\xi_{j+1}} N_{j+1}^{(e)}(\xi) \cdot \frac{1}{r_i} \, \frac{\partial r_i}{\partial n} \, \mathrm{d}\xi \\
(k_2^e)_{i,j} &= \int_{\xi_j}^{\xi_{j+1}} N_j^{(e)}(\xi) \, \ln r_i (\xi_{j+1} - \xi) \, \mathrm{d}\xi \\
(k_2^e)_{i,j+1} &= \int_{\xi_j}^{\xi_{j+1}} N_{j+1}^{(e)}(\xi) \, \ln r_i (\xi - \xi_j) \, \mathrm{d}\xi.
\end{aligned}
\right\} \tag{2.30}
$$

Noting in Fig. 2.6 that the radial distance is:

$$
r_i = \sqrt{\eta_i^2 + \xi^2}, \tag{2.31}
$$

and that the corresponding normal derivative:

$$
\frac{\partial r_i}{\partial n} = \frac{\partial r_i}{\partial \eta_i} = \frac{\partial}{\partial \eta_i} \left(\eta_i^2 + \xi^2\right)^{1/2} = \frac{\eta_i}{r_i}, \tag{2.32}
$$

is equal to the cosine of the angle between the outward normal and the direction r_i, the matrix coefficients listed in (2.30), can be analytically defined in the following way [41]:

$$
\left.
\begin{aligned}
(k_1^e)_{i,j} &= - I_{11} + \xi_{j+1} \cdot I_{12} \\
(k_1^e)_{i,j+1} &= I_{11} - \xi_j \cdot I_{12} \\
(k_2^e)_{i,j} &= - I_{21} + \xi_{j+1} \cdot I_{22} \\
(k_2^e)_{i,j+1} &= I_{21} - \xi_j \cdot I_{22}.
\end{aligned}
\right\} \tag{2.33}
$$

where:

$$
I_{11} = \frac{1}{l^e} \int_{\xi_j}^{\xi_{j+1}} \frac{1}{r_i} \frac{\partial r_i}{\partial \eta} \xi \, \mathrm{d}\xi = \frac{\eta_i}{2l^e} \ln \left(\frac{\eta_i^2 + \xi_{j+1}^2}{\eta_i^2 + \xi_j^2} \right), \tag{2.34}
$$

$$\begin{aligned} I_{12} &= \frac{1}{l^e}\int_{\xi_j}^{\xi_{j+1}} \frac{1}{r_i}\frac{\partial r_i}{\partial \eta}\,\mathrm{d}\xi = \\ &= \frac{1}{l^e}\left[\tan^{-1}\left(\frac{\xi_{j+1}}{\eta_i}\right) - \tan^{-1}\left(\frac{\xi_j}{\eta_i}\right)\right], \end{aligned} \tag{2.35}$$

$$\begin{aligned} I_{21} &= \frac{1}{l^e}\int_{\xi_j}^{\xi_{j+1}} \ln r_i \cdot \xi\,\mathrm{d}\xi = \\ &= \frac{1}{4l^e}\Big\{(\eta_i^2+\xi_{j+1}^2)\left[\ln(\eta_i^2+\xi_{j+1}^2)-1\right] - \\ &- (\eta_i^2+\xi_j^2)\left[\ln(\eta_i^2+\xi_j^2)\right]\Big\}, \end{aligned} \tag{2.36}$$

$$\begin{aligned} I_{22} &= \frac{1}{l^e}\int_{\xi_j}^{\xi_{j+1}} \ln r_i\,\mathrm{d}\xi = \\ &= \frac{1}{2l^e}\Big\{\xi_{j+1}\ln(\eta_i^2+\xi_{j+1}^2) - \xi_j\ln(\eta_i^2+\xi_j^2) - 2l^e + \\ &+ 2\eta_i\left[\tan^{-1}\left(\frac{\xi_{j+1}}{\eta_i}\right) - \tan^{-1}\left(\frac{\xi_j}{\eta_i}\right)\right]\Big\}. \end{aligned} \tag{2.37}$$

It can be noticed that coefficients k_1^e and k_2^e depend solely on the geometry of the boundary[3].

The elementary matrix in equation (2.29) is nominally of size 2×2, since there are two degrees of freedom in each node (Φ and $\partial\Phi/\partial n$). However, there are four degrees of freedom per element, and in order to eliminate zero elements, the elementary matrix is, by splitting variables, replaced by two row-matrices, as is shown by the given equation.

[3]In derivation of expressions (2.34)-(2.37), the following relations are used:

$$\int \frac{\eta_i}{\xi^2+\eta_i^2}\xi\,\mathrm{d}\xi = \frac{\eta_i}{2}\ln(\xi^2+\eta_i^2);$$

$$\int \frac{\eta_i}{\xi^2+\eta_i^2}\mathrm{d}\xi = \tan^{-1}\frac{\xi}{\eta_i};$$

$$\int \frac{1}{2}\ln(\xi^2+\eta_i^2)\xi\,\mathrm{d}\xi \frac{1}{4}(\xi^2+\eta_i^2)\left[\ln(\xi^2+\eta_i^2)-1\right];$$

$$\int \frac{1}{2}\ln(\xi^2+\eta_i^2)\,\mathrm{d}\xi = \frac{1}{2}\left[\xi\ln(\xi^2+\eta_i^2) - 2\xi + 2\eta_i\tan^{-1}\frac{\xi}{\eta_i}\right].$$

By summing up the contribution of all elements along the boundary, and systematically moving the singular point P_i (i=1,2,...,n_c) over this boundary, it is possible to form a system of algebraic equations with unknowns Φ_j and $(\partial\Phi/\partial n)_j$:

$$\sum_{j=1}^{N_c} H_{i,j}\Phi_j = \sum_{j=1}^{N_c} G_{i,j}\left(\frac{\partial\Phi}{\partial n}\right)_j \qquad (i=1,2,\ldots,n_c), \tag{2.38}$$

where:

$$H_{i,j} = (k_1^e)_{i,j} - \delta_{i,j}\theta_i; \quad G_{i,j} = (k_2^e)_{i,j}. \tag{2.39}$$

The same system is in matrix notation:

$$[H]\{\Phi\} = [G]\{\frac{\partial\Phi}{\partial n}\}. \tag{2.40}$$

By introducing boundary conditions, the given system of linear equations (2.40), which has a full asymmetric coefficient matrix, can be solved by the direct Gauss method, with row exchange in case of zero diagonal element.

Higher order elements. As has been remarked, the advantages of linear elements is the accuracy and speed of the analytical integration. Therefore, the linear elements can be recommended for the majority of problems. Application of higher-order interpolation functions (which require numerical integration), does not necessarily warrant more accurate results. However, in some cases higher-order interpolation functions are necessary. Typical examples are local singularities which require *special interpolation functions*. Values of coefficients k_1^e and k_2^e in (2.30) need in such cases to be determined approximately, by some method of numerical integration.

The numerical integration is performed over a *referent element* of unit length: $0 \leq \xi \leq 1$, with the interpolation functions defined in form of complete or incomplete polynomials (Fig. 2.7):

$$\left.\begin{array}{ll} N_1 = 1-\xi^m; & N_2 = \xi^m \\ N_1 = (1-\xi)^m; & N_2 = \xi^m \\ N_1 = (1-\xi)^m; & N_2 = 1-(1-\xi)^m. \end{array}\right\} \tag{2.41}$$

The value of exponent $m \geq 1$ is problem dependent. For m=1, linear interpolation functions are obtained (2.27). The fundamental condition for interpolation is fulfilled; the value of function N_1 is equal to one at the first node (ξ=0), and is equal to zero at the second node (ξ=1). The opposite holds true for function N_2.

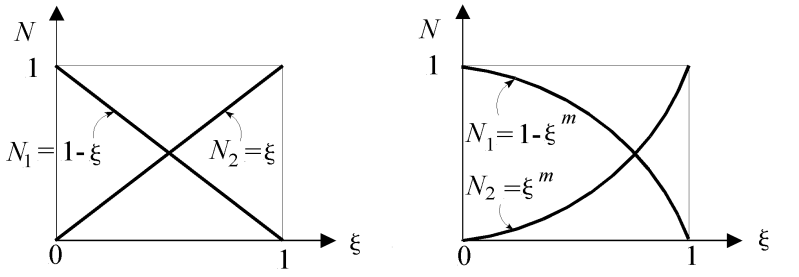

Figure 2.7: *Linear and non-linear interpolation functions over the referent element*

When special interpolation functions are used, their analytical form is chosen according to the type of singularity.

Here is an example. A flow region shown in Fig. 2.8 has one linear boundary, and one "broken" boundary, the elements e=11 and e =12 (with nodes 11, 12, and 12, 13 respectively) forming an angle of $3\pi/2$ (270^o). The vertex node no. 12 is a point of singularity in which the direction of the outward normal is not uniquely defined, and the velocity tends to infinity. This type of singularity is known as the "*boundary singularity*".

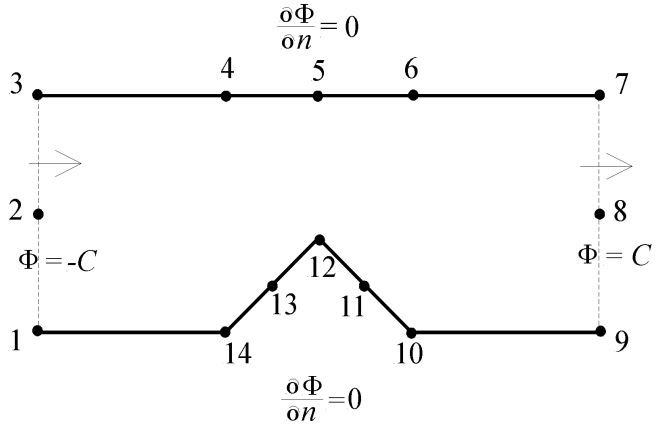

Figure 2.8: *Example of boundary singularity at node no.* 12

In order to get a solution more accurate than the one obtained by linear elements, special interpolation functions may be used over elements e=11 and e=12. These functions are based on the theoretical solution: $\Phi \propto s^{2/3}$, where s is distance measured from the point of singularity[4].

[4]In the theory of conformal transformations there is a relation between complex numbers $z = x + j\,y$ and $w(z) = \Phi(x, y) + j\,\psi(x, y)$ ("complex potential"), where j is the unit imaginary number. For flow near the boundary at an angle $\theta = \pi/m$: w=const$\cdot z^m$, the real flow being defined in the "z-plane", and the potential flow, in the "w-plane". Taking only the real parts of complex numbers, and setting θ=$3\pi/2$, and m=2/3, it follows that $w \propto z^{2/3}$=$s^{2/3}$, where s is the distance from the point of singularity [88].

New functions are introduced:

• element e=11:

$$N_1 = 1 - \xi^{2/3}; \qquad N_2 = \xi^{2/3}; \tag{2.42}$$

• element e=12:

$$N_1 = (1 - \xi)^{2/3}; \qquad N_2 = 1 - (1 - \xi)^{2/3}. \tag{2.43}$$

Integration is performed over the referent unit element with the origin at the left node (ξ=0). (When defining the interpolation functions, it is to be remarked that the coordinates ξ and s are oriented in the same direction in element no. 11, and in the opposite directions in element no. 12.)

The impact of singularities on the solution is variable. Some are "strong" singularities, causing unstable, oscillatory solutions for the normal derivative. Some are "weak" singularities, such as the boundary similarity in the previous example.

Generally, the problem of singularities can be solved either by locally increasing the number of nodes, or by introducing special elements. Local analytic solutions can be coupled efficiently with (linear or non-linear) standard interpolation functions, yielding results of remarkable quality.

Numerical integration. The well-known Gauss (or Gauss-Legendre) quadrature is standardly used in the F.E.M. [27, 29]. This type of numerical integration will not be discussed here.

In the B.E.M. integrals of the type:

$$I = \int_a^b f(x) \ln(x - a) \, \mathrm{d}x, \tag{2.44}$$

impose the problem of the logarithmic singularity: $\lim_{x \to a} \ln(x - a) = -\infty$, which can be solved only by the *special Gauss quadrature*.

The special quadrature is based on the change of variables:

$$\xi = \frac{x - a}{b - a}, \tag{2.45}$$

where ξ takes values from 0 ($x = a$) to 1 ($x = b$).

From (2.45) it is evident that: $\mathrm{d}\xi = \mathrm{d}x/(b-1)$ and $x = \xi(b-a) + a$, thus the integral (2.44) is replaced by the sum of two integrals:

$$I_1 \quad = \quad (b - a) \int_0^1 \ln \xi \cdot f[\xi(b - a) + a] \mathrm{d}\xi \tag{2.46}$$

$$I_2 \quad = \quad (b-a)\int_0^1 \ln(b-a)\cdot f[\xi(b-a)+a]\mathrm{d}\xi. \tag{2.47}$$

The second integral I_2 can be solved by the standard Gauss quadrature, while the first integral I_1 requires the special quadrature in the form [39]:

$$I_1 \approx (b-1)\sum_{i=1}^{r^s}\omega_i^s\cdot f(\xi_i^s), \tag{2.48}$$

where:

$$\xi_i^s = a+(b-a)\chi_i^s. \tag{2.49}$$

The values of weighting factors ω_i^s and corresponding zeroes χ_i^s are listed for r^s=4 in Table 2.1.

Table 2.1: *Values of the special weighting factors and zeroes*

χ_i^s	ω_i^s
0.0414484802	-0.3834640681
0.2452749143	-0.3868753177
0.5561654535	-0.1904351269
0.8489823945	-0.0392254871

2.4.2 Solution inside the flow domain

Once the values of variables Φ i $\partial\Phi/\partial n$ are determined over the boundary of the computational domain, the solution for a number of chosen interior points is sought by solving equation (2.21). Care must be taken that the interior point is not too close to the boundary, as it may affect the accuracy[5].

[5]Experience shows that the distance between the interior point and the closest boundary element should not be less than the length of the element itself.

The solution in the interior points consists of velocity components, obtained by differentiating (2.21)[6]:

$$u = \frac{\partial \Phi(P)}{\partial x} = \frac{1}{2\pi}\int_\Gamma \left[\frac{\Phi(Q)\sin\beta}{r_i^2} + \frac{2\Phi(Q)\eta_i(\xi\cos\beta - \eta_i\sin\beta)}{r_i^4} + \right. \\ \left. + \frac{\xi\cos\beta - \eta_i\sin\beta}{r_i^2}\cdot\frac{\partial\Phi}{\partial n}(Q)\right] \mathrm{d}\Gamma \tag{2.53}$$

$$v = \frac{\partial \Phi(P)}{\partial y} = \frac{1}{2\pi}\int_\Gamma \left[\frac{-\Phi(Q)\cos\beta}{r_i^2} + \frac{2\Phi(Q)\eta_i(\eta_i\cos\beta + \xi\sin\beta)}{r_i^4} + \right. \\ \left. + \frac{\eta_i\cos\beta + \xi\sin\beta}{r_i^2}\cdot\frac{\partial\Phi}{\partial n}(Q)\right] \mathrm{d}\Gamma, \tag{2.54}$$

Analytic solution of integrals (2.53) and (2.54) is possible[7].

Two important facts are to be acknowledged:

(a) Derivatives in respect to the x, y coordinates cannot be defined on the boundary, as coincidence of points P and Q leads to singular integrals.

[6] In derivation of the given expressions, the previously calculated values of the potential and its derivative in any point Q on the boundary are considered constants, and the following geometric relations, established in Fig. 2.6, were applied:

$$\frac{\partial\eta}{\partial x} = \sin\beta, \tag{2.50}$$

$$\frac{\partial r}{\partial n} = \frac{\eta}{r}, \tag{2.51}$$

$$\frac{\partial r}{\partial x} = -\frac{\xi\cos\beta - \eta\sin\beta}{r}, \tag{2.52}$$

[7] For this purpose, the following relations may be used:

$$\int \frac{\mathrm{d}\xi}{(\xi^2+\eta^2)^2} = \frac{\xi}{2\eta^2(\xi^2+\eta^2)} + \frac{1}{2\eta^3}\tan^{-1}\frac{\xi}{\eta};$$

$$\int \frac{\xi\mathrm{d}\xi}{(\xi^2+\eta^2)^2} = -\frac{1}{2(\xi^2+\eta^2)};$$

$$\int \frac{\xi^2\mathrm{d}\xi}{\xi^2+\eta^2} = \xi - \eta\tan^{-1}\frac{\xi}{\eta};$$

$$\int \frac{\xi^2\mathrm{d}\xi}{(\xi^2+\eta^2)^2} = -\frac{\xi}{2(\xi^2+\eta^2)} + \frac{1}{2\eta}\tan^{-1}\frac{\xi}{\eta}.$$

(b) Care must be taken of the sign of the coordinate η; if the location vector and the coordinate η are oriented in the same direction, as in Fig. 2.6, the sign is positive. It is negative when the location vector r_i connecting points P and Q "falls" outside the computational domain.

2.4.3 Iterative determination of the free-surface

As has been pointed out, the B.E.M. is very suitable for solution of the free-surface flows which can be considered as potential flows. This is the case with accelerated flows over weirs or spillways, where gravity and inertial effects are dominant over the viscous effects (friction).

Consider the problem defined in the vertical (x, y) plane (Fig. 2.9). Due to strong curvature of streamlines, the assumption of the hydrostatic pressure distribution over depth is invalid, and solution is based on the potential flow theory.

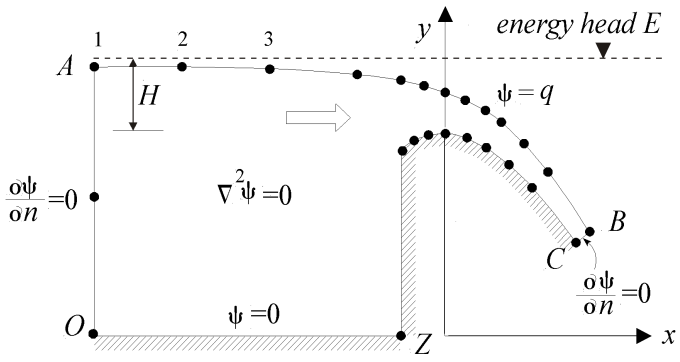

Figure 2.9: *Computational domain and the boundary conditions*

Assuming quasi-steady flow conditions, the problem can be defined in terms of the stream function ψ, by the Laplace equation:

$$\nabla^2 \psi = 0 \tag{2.55}$$

and the Bernoulli equation:

$$y + \frac{1}{2g}\left(\frac{\partial \psi}{\partial n}\right)^2 = E, \tag{2.56}$$

where the velocity in the flow direction is defined by the derivative $\partial\psi/\partial n$, and the energy head E is constant for the ideal fluid flow.

The stream function value on the free-surface is equal to the unit discharge.

The free-surface curve is defined by the vertical coordinates y of m nodes lying on the part of the boundary which represents the free-surface. Elevation of the free-surface nodes and the energy head E are to be determined iteratively for the given discharge, i.e. the given ψ value. (Alternatively, the discharge can be calculated for the given energy head E.)

The complexity of iterative solution for the free-surface is due to the fact that elevations of the free-surface nodes are mutually dependent, and that corrections of these elevations must be made *simultaneously* in each iteration. This non-linear problem can be efficiently solved by the Newton-Raphson method [41, 37].

The starting point is the fact that the energy head values in each of the m free-surface nodes depend on the vertical coordinates y of *all* such nodes, while their horizontal coordinates x are assumed unchanged:

$$\left.\begin{array}{lcl} E_1 &=& E_1(y_1, y_2, \ldots, y_m) \\ E_2 &=& E_2(y_1, y_2, \ldots, y_m) \\ \vdots &=& \vdots \\ E_m &=& E_m(y_1, y_2, \ldots, y_m). \end{array}\right\} \tag{2.57}$$

By expanding in Taylor series up to the first derivative:

$$\left.\begin{array}{lcl} \Delta E_1 &=& \dfrac{\partial E_1}{\partial y_1}\Delta y_1 + \dfrac{\partial E_2}{\partial y_2}\Delta y_2 + \ldots + \dfrac{\partial E_1}{\partial y_m}\Delta y_m \\ \Delta E_2 &=& \dfrac{\partial E_2}{\partial y_1}\Delta y_1 + \dfrac{\partial E_2}{\partial y_2}\Delta y_2 + \ldots + \dfrac{\partial E_2}{\partial y_m}\Delta y_m \\ \vdots &=& \vdots \\ \Delta E_m &=& \dfrac{\partial E_m}{\partial y_1}\Delta y_1 + \dfrac{\partial E_m}{\partial y_2}\Delta y_2 + \ldots + \dfrac{\partial E_m}{\partial y_m}\Delta y_m, \end{array}\right\} \tag{2.58}$$

a matrix equation is obtained:

$$\{\Delta E\} = \left[\frac{\mathrm{d}E}{\mathrm{d}y}\right]\{\Delta y\}. \tag{2.59}$$

The solution of this equation is a vector of corrections for the free-surface node elevations:

$$\{\Delta y\} = \left[\frac{\mathrm{d}E}{\mathrm{d}y}\right]^{-1}\{\Delta E\}. \tag{2.60}$$

The vector $\{\Delta E\}$ represents deviations of energy head values, calculated at the free-surface nodes, from the *mean* energy head, determined in the previous iteration.

The Jacobian matrix of derivatives $[\mathrm{d}E/\mathrm{d}y]$ is formed by numerical differentiation; an elementary vertical displacement is imposed on each free-surface node in turn, and then the energy head changes (in respect to values in the previous iteration) are calculated in *all* free-surface nodes.

After calculating the corrections, "new" position of the free-surface nodes is determined:

$$\{y\}_{it} = \{y\}_{it-1} + \{\Delta y\}_{it-1}, \tag{2.61}$$

where the subscript "it" denotes the iteration number[8]. The solution has converged when the calculated corrective values $\{\Delta y\}$ become smaller than a preset tolerance value.

2.5 Calibration and verification of the numerical model

In order to calibrate the numerical model based on the B.E.M. and test its predictive performance, three case studies from literature are considered.

2.5.1 The WES spillways

The first case study pertains to investigations, performed by the US Army Engineers Waterways Experiment Station ("WES") in order to prescribe the optimal spillway contour for any given design head [69]. The WES spillways have a vertical upstream face, a hydraulically shaped crest, and a downstream face at a slope of 45^o. The results of investigations consist of free-surface coordinates, defined for a number of ratio values H/H_d, where H is the *actual head*, and H_d is the *design head*. (Upstream velocity head is neglected.)

The proposed numerical model is evaluated considering a 7.55 m high WES spillway, hydraulically shaped for $H_d = 1.9$ m. The computational domain bounded by a system of linear elements is shown in Fig. 2.10.

[8]Experience shows that a certain amount of under-relaxation is necessary for the iterative process is to converge; this means that the second member on the right-hand side of the equation (2.61) is to be multiplied by a factor $\omega < 1$.

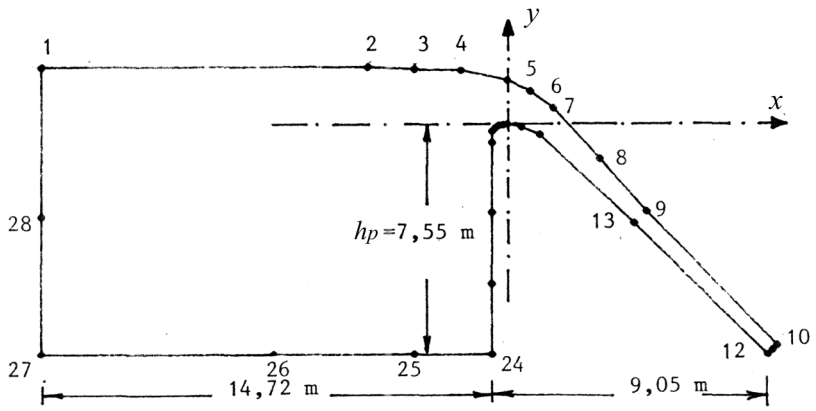

Figure 2.10: *The computational domain for the WES spillway*

The upper part of the boundary (nodes 1-10), representing the free-surface, is changing during computations, as the ultimate free-surface location is sought through the described iterative numerical procedure. It may be noted that only a small number of nodes is sufficient for numerical simulations.

For ratios $H/H_d = 1$, and $h_p/H_d = 1.33$, the discharge coefficient is equal to [69]:

$$C_q = \frac{q}{\sqrt{2g} \cdot H^{3/2}} = 0.49, \tag{2.62}$$

and the unit discharge is $q = 5.50$ m^3/(s m).

Comparison of the calculated and the measured free-surface profiles is given in Fig. 2.11. For $H/H_d = 1.0$, the calculated value of discharge coefficient is C_q=0.48. A rather good agreement between the calculated and measured results is evident.

Generally, the presented results are obtained in a small number of iterations (20–30). However, it is observed that there exists a region of instability immediately upstream from the spillway crest. It is the transition zone between the subcritical and the supercritical flow, and some convergence problems can be experienced in the vicinity of the critical depth. Depending on how much this problem affects the results, the following measures are at disposal: (i) increase the number of nodes in the region of instability, (ii) insert of a number of "pseudo" nodes in addition to the original set of the free-surface nodes, so that the perturbation matrix is calculated for all nodes, but based on elementary displacements of only original modes, and (iii) replace linear elements by cubic spline elements in the critical region. Further experimentation in this respect is to be done.

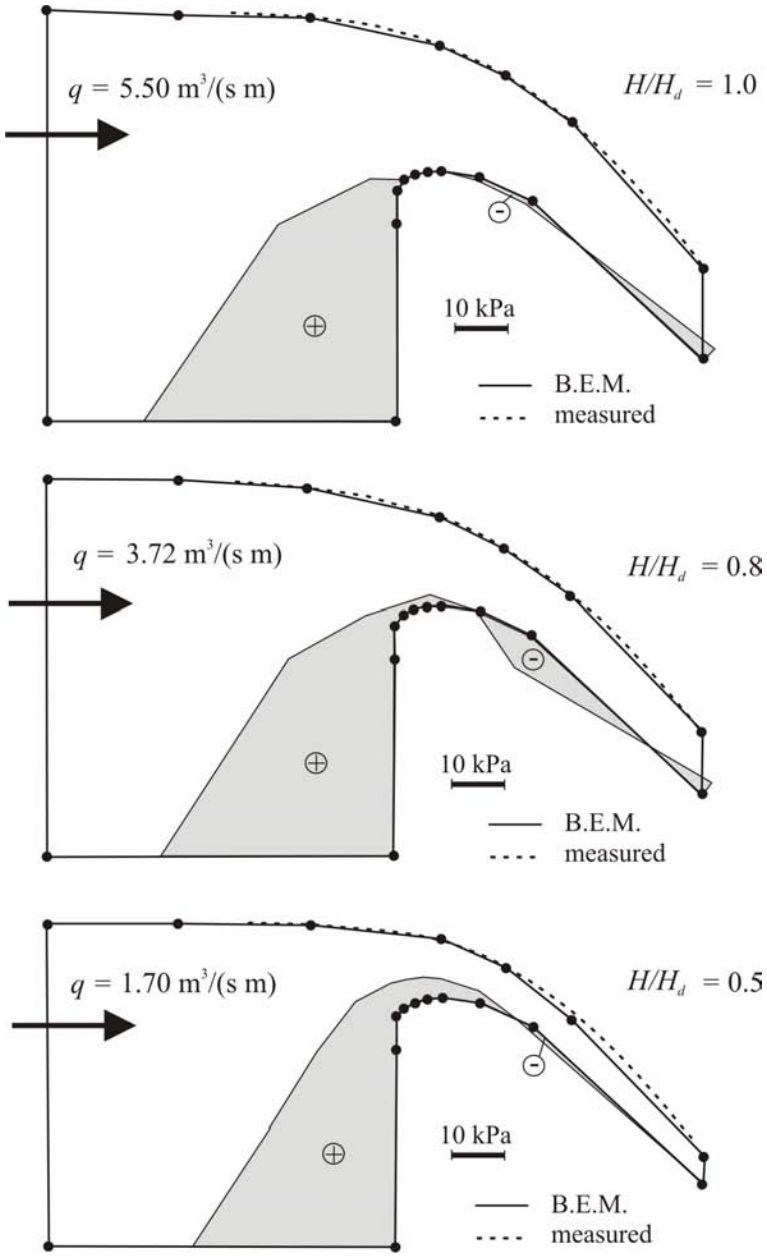

Figure 2.11: *Numerical simulation of the WES spillway flows for* H/H_d=1.0, 0.8, 0.5, *and corresponding unit discharges:* q=5.50, 3.72, 1.70 $\mathrm{m}^3/(\mathrm{s\ m})$. *(Only enlarged portions of the computational domain are shown)*

Some interesting results are obtained concerning the pressure distribution along the WES spillway. The hydraulic pressure at the free-surface nodes is zero (as can be expected), as well as along the spillway crest. Downstream, some small underpressures are calculated.

Generally, the calculated pressures are close to zero, as should be for the case H/H_d =1. In cases when $H/H_d \neq 1$, the pressure distribution along the spillway contour is not so favorable, as can be seen in Fig. 2.11. Although the obtained pressure diagrams could not be verified by data offered in literature [69], they illustrate the power of B.E.M. in practical applications.

The calculated velocity field for one of the studied cases is depicted in Fig. 2.12.

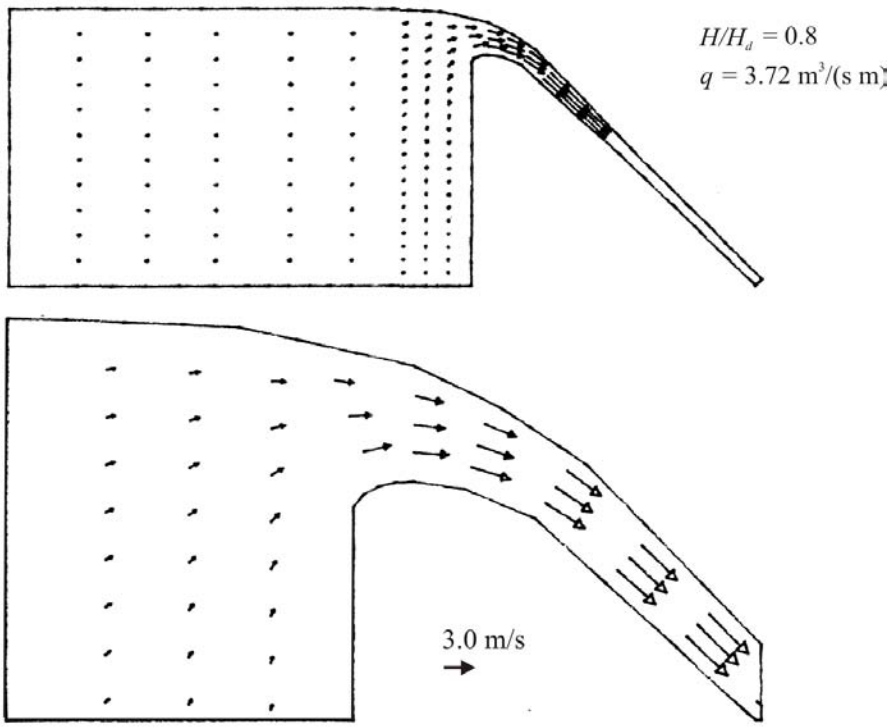

Figure 2.12: *The calculated velocity field shown for the entire computational domain (top) and an enlarged portion (bottom)*

2.5.2 The Imperial Dam spillway

The second example pertains to scale-model investigations of the Imperial Dam spillway, completed by the Bureau of Reclamation in 1949 [66]. The prototype is an Ambursen-type dam, with 8.2 m high spillway (Fig. 2.13).

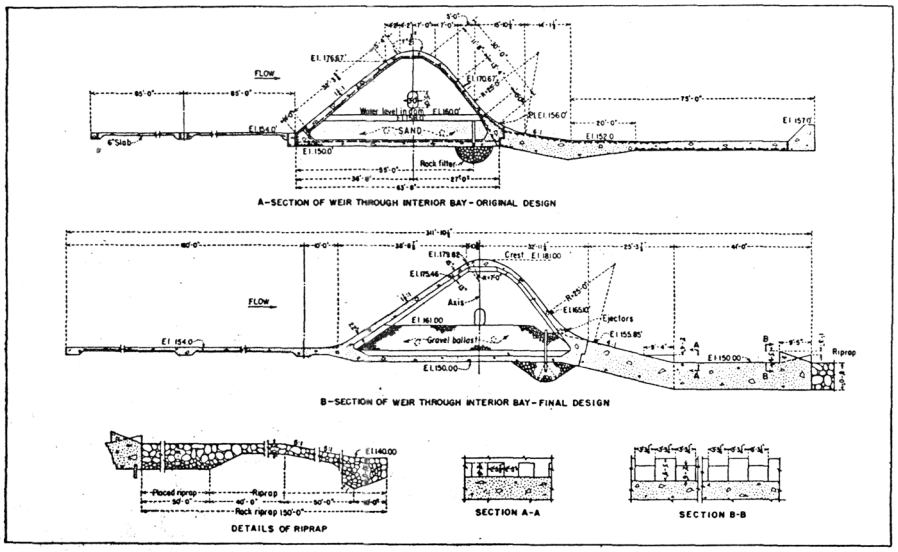

Figure 2.13: *Cross-section of the Imperial Dam spillway*

Extensive research using the spillway hydraulic model, built in scale 1:30, has been done in order to determine the optimal shape of the spillway crest. Free-surface profiles and pressure distributions, measured for a range of discharges 0.017–0.0635 $m^3/(s\ m)$, are valuable data for calibration and validation of numerical models for prediction of spillway flows.

The results obtained by the B.E.M. are given in Fig. 2.14. The calculated and measured free-surface profiles are in a good agreement. Comparison of calculated and measured pressure distributions shows also a very good agreement.

The calculated rating curve and the coefficient of discharge dependency on the upstream head, are presented in Fig. 2.15. The overall agreement is again acceptable. Deviations of calculated C_q values from the measured ones are within 3%.

The calculated velocity field for unit discharge of 0.038 $m^3/(s\ m)$ is presented in Fig. 2.16.

2.5.3 The Buk Bijela Dam spillway

The previously shown examples could not be used to verify the calculated velocity fields. This kind of verification is achieved using the experimental data of scale model investigations carried out in Serbia for the Buk Bijela Dam on the Drina river [86]. The cross-section of the prototype spillway is given in Fig. 2.17.

Velocities were measured on a hydraulic model built in scale 1:25.

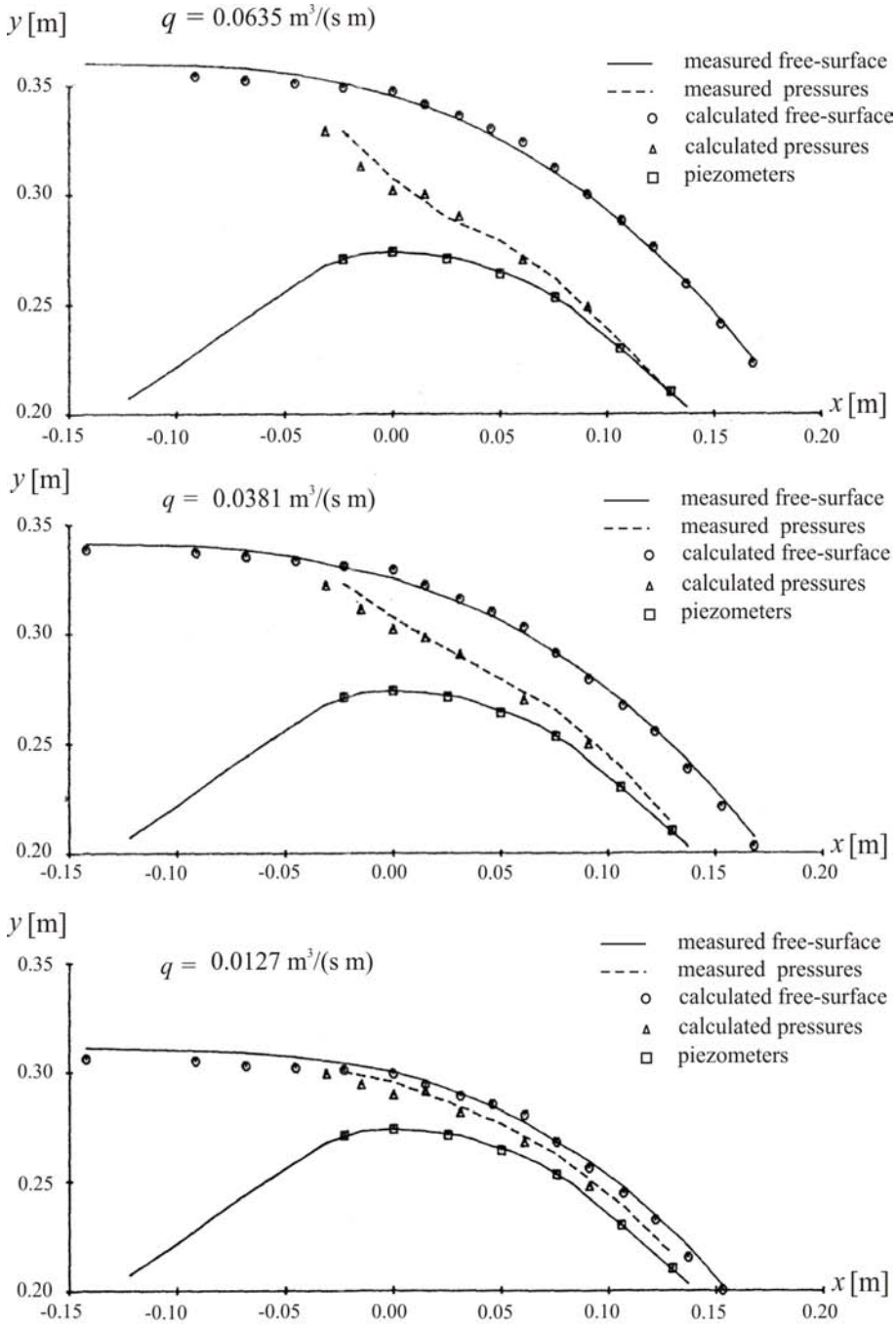

Figure 2.14: *Numerical simulation of flow over the scale model of the Imperial Dam spillway* [37]

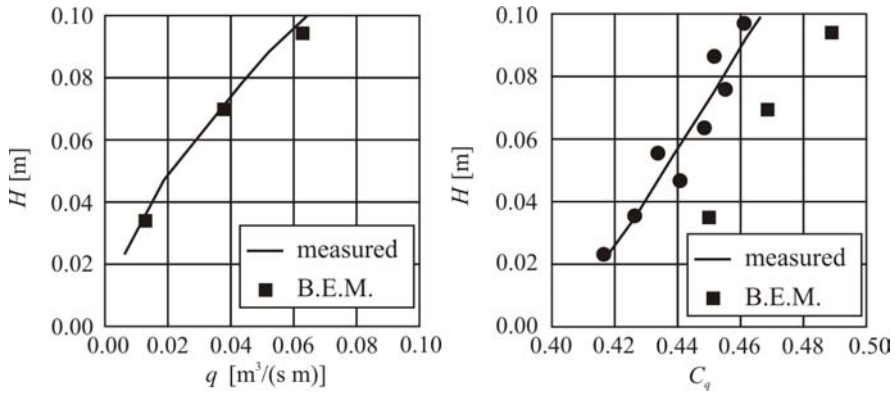

Figure 2.15: *Unit discharge and coefficient of discharge values pertaining to the scale model of the Imperial Dam spillway* [37]

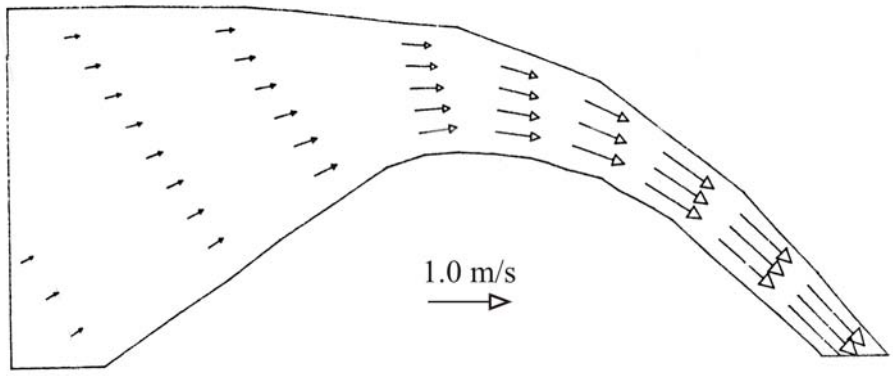

Figure 2.16: *The calculated velocity field for the scale model of the Imperial Dam spillway* ($q = 0.038$ m^3/(s m)) [37]

The comparison between the calculated and measured velocity fields for the prototype and the scale model unit discharges of 91.33 and 0.029 m^3/(s m) respectively, is given in Fig. 2.17.

The calculated free-surface profile is slightly below the measured one, thus the calculated velocities are slightly greater than the measured ones (10% on the average). It can be noted that although the viscous effects are neglected, the velocity distribution is generally acceptable, except near the solid surface. The calculated depth-averaged velocity can be accepted as sufficiently accurate for engineering purposes.

The results of calibration and validation of the B.E.M. presented in this dissertation clearly demonstrate that the potential flow theory is applicable for analysis of the curvilinear free-surface (gravity) flows, and that the B.E.M. has a remarkable applicability in engineering practice.

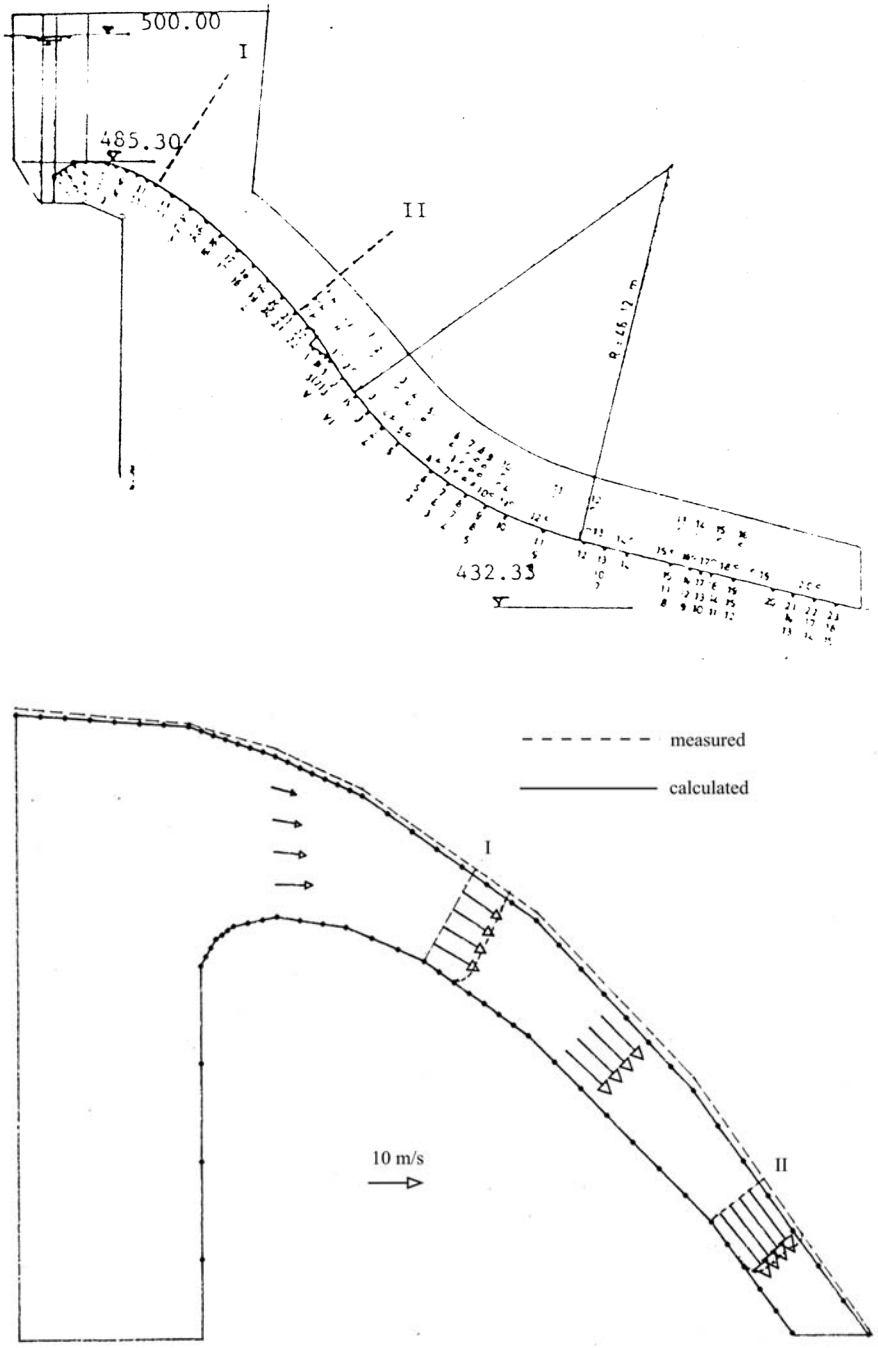

Figure 2.17: *A cross-section of the Buk Bijela Dam spillway and the calculated velocity field on the scale model for unit discharge* $q = 0.029\ \mathrm{m}^3/(\mathrm{s\ m})$)

Therefore, it is to be expected that the B.E.M. will gain a wider role in the open-channel hydraulics. However, further investigations are recommenced in order to: (i) improve the iterative procedure for free-surface determination, and (ii) achieve coupling of the potential flow region with the boundary layer near solid surface, where effects of friction are pronounced.

3

Experimental Investigations

In this chapter the results of experimental research are presented. Similitude conditions for building small scale models of earth structures exposed to overflowing are considered. The laboratory flume, the measuring equipment, and experimental procedures are described. The initial and boundary conditions are specified, and results of four characteristic experiments are presented. Empirical correlations defining the erosion rate of overflown model structures are established for subsequent numerical simulation of the process.

3.1 Erosion resistance of cohesive soils

The erosion of cohesive soils exposed to running water is a very complex phenomenon. Research in this field is interdisciplinary. Contrary to non cohesive soils, where the particle size and weight are the two main factors affecting the erosion process, the erosion resistance of the cohesive soils depends on a number of factors, the principal one being the electrochemical bond of the particles. This bond depends on electrolyte presence, mineral structure, temperature, pH, etc., [47, 61]. The mutual interaction of these factors, and specific ways in which they affect the erosion process, are not too clear, thus the erosion of cohesive soils is one of those topics which are predisposed for indefinite research.

Consequently, there is no general approach to the analytical treatment of this phenomenon. In spite of gros simplifications, equations defining the conservation laws of mass, momentum and energy for turbulent flows over cohesive materials cannot be solved in a satisfactory way [64]. For this reason, the engineering practice relies on semi-empirical research, including:

(a) laboratory investigations;
(b) investigations in situ for particular case studies;
(c) investigations for design of canals without revetment, and
(d) investigations for land use (particularly of farmland).

The experimental research carried out in laboratory flumes are of the main interest. Previous laboratory investigations have been aimed either toward better understanding of the physical and chemical processes (fundamental research on the microscopic level [59, 61]), or toward specifying criteria for the onset of erosion – the critical flow velocity [55], or the critical shear stress [52, 53, 58, 60]. Unfortunately, the published results of such investigations cannot be used for numerical modeling of overflown earth structures, because they refer to specific kinds of materials [49, 57], and are developed for steady, uniform flow conditions. Therefore, it was necessary to carry out a number of laboratory tests as a part of this dissertation, in order to establish a correlation between the hydraulic parameters of the accelerating flow and the quantity of the eroded material.

3.2 Physical factors affecting the erosion process

An overflown earth structure (dam, embankment, levee, etc.) is exposed to effects of gravity, flowing water, and pore pressures within the structure.

The overflowing water affects the erodible surface through shear stresses, which are proportional to the square of the local velocity and the absolute roughness. In addition to this, an overflown structure is exposed to hydrostatic pressures, forces of cohesion, and pore pressures which develop as saturation of the soil takes place[1]. As these physical factors affect the erosion resistance and structural stability, they all need to be considered when specifying the similitude conditions for the scale model investigations.

3.3 Similitude conditions

The choice of scales for physical (hydraulic) modeling of earth structures exposed to overflowing require a careful consideration of several similitude conditions, including weir flow, seepage, geomechanic and rheologic characteristics of the material. Each of these conditions is considered separately.

3.3.1 Weir flow

The polygon of forces acting on a fluid particle under the accelerating flow conditions is depicted in Fig.3.1. It is formed by forces of gravity $\vec{F}_g$, viscosity $\vec{F}_s$, pressure $\vec{F}_p$, and inertia $\vec{F}_i$.

If the forces are expressed relatively to the inertial force, the following dimensionless ratios: F_g/F_i, F_s/F_i, and F_p/F_i, known as the Froude number

[1] Water is being adsorbed on the particle surface, while the trapped air is being compressed, the overall pressure surpassing the hydrostatic one.

(Fr), the Reynolds number (Re) and the Euler number (Eu) respectively, are introduced. They quantify the impact of gravity, viscosity, and pressure, relatively to inertia.

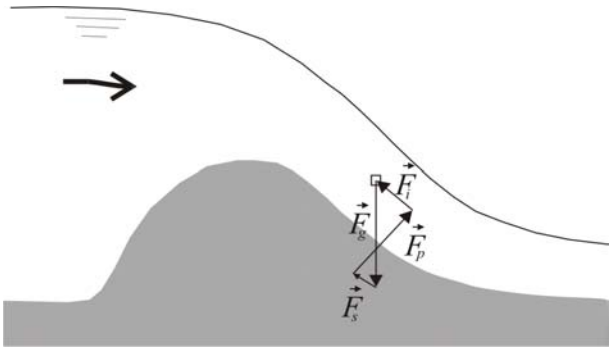

Figure 3.1: *Polygon of forces*

The complete ("dynamic") similitude between the model and the prototype is assured when the corresponding polygons of forces are geometrically similar, which implies the following equalities:

$$\frac{(F_i)_m}{(F_g)_m} = \frac{(F_i)_p}{(F_g)_p} \tag{3.1}$$

$$\frac{(F_i)_m}{(F_s)_m} = \frac{(F_i)_p}{(F_s)_p} \tag{3.2}$$

$$\frac{(F_i)_m}{(F_p)_m} = \frac{(F_i)_p}{(F_p)_p}, \tag{3.3}$$

where the subscript "m" refers to the model, and "p", to the prototype.

Another way to express the same conditions is to say that the complete similitude requires that the Froude, Reynolds, and the Euler number of the model must be equal to the Froude, Reynolds, and the Euler number of the prototype:

$$\mathrm{Fr}_m = \mathrm{Fr}_p, \tag{3.4}$$

$$\mathrm{Re}_m = \mathrm{Re}_p \tag{3.5}$$

$$\mathrm{Eu}_m = \mathrm{Eu}_p. \tag{3.6}$$

If two of the conditions (3.2) or (3.5) are satisfied (gravity and viscous forces), then the third equation (pressure forces) is dependent and automatically is satisfied.

As the sketch in Fig.3.1 shows, in an accelerated flow the viscous forces are much smaller than gravity, and can be neglected. Thus, only one condition

of similarity is required: Fr_m=Fr_p. This condition is referred to as the "Froude similitude". It can also be expressed in this way:

$$\mathrm{Fr}_* = \frac{\mathrm{Fr}_m}{\mathrm{Fr}_p} = 1, \tag{3.7}$$

where the subscript "$*$" denotes scale.

The Froude similitude is the imperative condition when the shape and position of a flow boundary – the free surface, is governed by gravity. In other words, the trajectory of fluid particles over a weir or spillway is predominantly determined by gravity. (If the Froude similitude is not ensured, and the approach Fr number on the model is too high, it might happen that the flow would simply shoot over the model spillway crest!)

If L_* is the chosen length scale, the Froude similitude yields scales for other variables, such as discharge, time, and velocity:

$$Q_* = L_*^{5/2} \tag{3.8}$$

$$t_* = L_*^{1/2} \tag{3.9}$$

$$V_* = L_*^{1/2}. \tag{3.10}$$

An additional similitude condition needs to be introduced, pertaining to the shear stresses, induced by water on the solid surface. This effect may be quantified by the friction coefficient:

$$C_\tau = f\left(\mathrm{Re}, \frac{k}{h}\right), \tag{3.11}$$

where Re is the Reynolds number, and the ratio between the absolute surface roughness k and water depth h is known as the relative roughness k/h.

As the effects of viscosity may be neglected in the fully developed turbulent flow, the friction coefficient (3.11) becomes independent of the Reynolds number, and depends solely on the relative roughness. Thus, the similitude condition for effects of friction may be expressed in this way:

$$\left(\frac{k}{h}\right)_* = 1, \text{ or } k_* = h_* = L_*. \tag{3.12}$$

If the absolute roughness k is represented by the so-called *"equivalent sand roughness"*, which is usually defined by the characteristic sand grain size d_{90} [50], the condition (3.12) can be replaced by:

$$(d_{90})_* = L_*. \tag{3.13}$$

The characteristic grain diameter d_{90} describes gradation of material, specifying that 90% grains have smaller diameters.

In addition to the above considerations, one has to keep in mind a practical recommendation that if fully turbulent flow conditions are to be ensured, water depths on scale models must not be too small (less than 1-2 cm).

3.3.2 Seepage

Although the surface shear on the water-solid interface is the dominant factor of the erosion process, similitude conditions for seepage and pore pressures must be considered as well, in order to reproduce the overall "behavior" of the overflown structure in a physically realistic way. The approach of Mandel and Weber [65] is adopted, according to which seepage is well reproduced on small scale models if the following conditions for density of the saturated material, porosity, and hydraulic conductivity are fulfilled:

$$\rho'_{s*} = 1 \tag{3.14}$$

$$n_* = 1 \tag{3.15}$$

$$K_* = L_*^{1/2}. \tag{3.16}$$

If the Hazen relation: $K \propto d_{10}^2$ is applied, the relation (3.16) becomes:

$$(d_{10})_* = L_*^{1/4}, \tag{3.17}$$

where d_{10} is the characteristic grain size (specifying that 10% grains have smaller diameters).

The scale for seepage velocities is, according to Darcy's law:

$$V_{f*} = K_* = L_*^{1/2}. \tag{3.18}$$

3.3.3 Geomechanics and rheology

The theory of geomechanic and rheological similitudes is important for experimental research of soil behavior, especially for studying stability limits. The basic postulate is that similarity of impact of gravity (weight) and the inertial force is only possible if the scale model and the prototype are made of the same material [54, 65]. If this is not feasible, the scale model has to be built of some material composed in such a way that its mechanic and rheologic characteristics are related to the prototype material through the scales for stresses, strain, and time. Material, carefully composed to be used

for scale models, is called the *"equivalent material"* [54]. Its composition should ensure that deformations of the model structure and the prototype structure are geometrically similar.

For a chosen length scale L_*, all other necessary scales for the equivalent material are derived, and the results are summarized in Table 3.1.

Table 3.1: *Scales for composition of the equivalent material*

.

Physical property	Scale
Density of saturated material	$\rho'_{s*} = 1$
Angle of internal friction	$\phi_* = 1$
Stresses/pore pressures	$\sigma_* = p_* = L_*$
Cohesion	$C_* = L_*$
Young's elasticity module	$E_* = 1$
Poisson's plasticity	$\nu_* = 1$

3.4 Composition of the equivalent material

Taking into account previously defined hydraulic and rheologic scales, the equivalent material is composed in such a way to simultaneously satisfy the following conditions:

- the grain size relevant for seepage (3.17):

$$(d_{10})_* = \frac{(d_{10})_m}{(d_{10})_p} = L_*^{1/4}$$

- the grain size relevant for surface roughness (3.13):

$$(d_{90})_* = \frac{(d_{90})_m}{(d_{90})_p} = L_*$$

- cohesion (3.1):

$$C_* = \frac{C_m}{C_p} = L_*$$

- hydraulic conductivity (3.18):

$$K_* = \frac{K_m}{K_p} = L_*^{1/2}.$$

The equivalent material is chosen to be a sand mixture. Its gradation is composed according to scales (3.17) and (3.13). A small amount of kaolin or bentonite additive is mixed with sand in order to provide some cohesion (3.1), and to ensure realistic hydraulic conductivity (3.18). The kaolin and bentonite bonding additives are minerals of kaolinite and montmorilonites with densities 1.8 – 1.9 t/m^3 and basic chemical components:

- S_iO_2 ..... 60 – 80% for kaolin; 50% for bentonite;
- Al_2O_3 ..... 33 – 40% for kaolin; 17 – 25% for bentonite;
- Fe_2O_3 ..... $\leq$ 3%;
- CaO ..... $<$ 5%.

The simultaneous fulfillment of conditions (3.17) and (3.13) requires fine sand of almost uniform gradation. This can be explained by an example. Assume that the characteristic grain sizes of material in the field are: $(d_{90})_p$=10 mm, and $(d_{10})_p$=1 mm. The corresponding characteristic grain sizes for the equivalent material are given in Table 3.2.

Table 3.2: *Analysis of gradation for the equivalent material*

	L_*	1:1	1:5	1:10	1:15	1:20	1:25	1:30	1:40
Scale	$(d_{90})_*$	1	0.200	0.100	0.067	0.050	0.040	0.033	0.025
	$(d_{10})_*$	1	0.669	0.562	0.509	0.473	0.447	0.426	0.398
Model	$(d_{90})_m$	10	2	1	0.67	0.50	0.40	0.33	0.25
[mm]	$(d_{10})_m$	1	0.67	0.56	0.51	**0.47**	**0.45**	**0.43**	**0.40**

From the given results it is clear that the hydraulic models in scales less than 1:15, must be made of more or less uniformly graded equivalent material.

As for the conditions imposed by seepage and cohesion, some practical problems may arise. Scale models require a relatively small amount of bonding additives, often insufficient for obtaining an adequate hydraulic conductivity. For this reason, addition of some hydrophobic substance may be required.

This aspect will be clarified by an example from practice[2]. The basic characteristics of the prototype are:

- dam height: $H_p = 15$ m;
- cohesion of material: $C_p = 12$ kPa;
- hydraulic conductivity: $K_p = 5 \times 10^{-9}$ m/s.

The corresponding model values depending on scale are given in Table 3.3.

[2]Design study of the Bela Reka earth dam, Hydroprojekt Co., 1986.

Table 3.3: *Cohesion and hydraulic conductivity of the equivalent material*

Scale	L_*	1:1	1:2	1:5	1:10	1:20	1:40	1:50
	C_*	1	0.500	0.200	0.100	0.050	0.025	0.020
	K_*	1	0.707	0.447	0.316	0.224	0.158	0.141
Model	H_m [m]	15	7.5	3.0	1.5	0.75	0.38	0.30
	C_m [kPa]	12	6.0	2.4	1.2	0.6	0.3	0.24
	$K_m \times 10^{-9}$ [m/s]	5.00	3.54	2.24	1.58	1.12	0.79	0.70

From the given results it can be concluded that the model values of cohesion and hydraulic conductivity decrease with reduction of the model scales. Eventually, the hydraulic conductivities become so small that addition of some hydrophobic substance becomes necessary.

After considering all described aspects, it was decided to use for the equivalent material a mixture of fine sand with 2 – 3% kaolin or bentonite additive.

The characteristic grain sizes of the sand mixture are:

$$d_{10} = 0.13 \text{ mm}$$
$$d_{50} = 0.20 \text{ mm}$$
$$d_{90} = 0.25 \text{ mm}.$$

The gradation curve[3] is given in Fig.3.2.

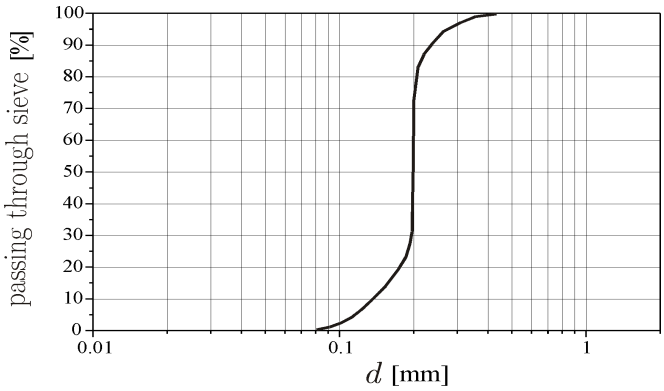

Figure 3.2: *Gradation curve of the equivalent material. It is almost uniform,* 90% *of grain sizes being* 0.1 – 0.3 mm.

The values of the coefficient of uniformity and the geometric standard deviation are: d_{60}/d_{10}=1.54 and $\sigma_g = \sqrt{d_{84}/d_{16}}$=1.22, respectively.

[3]Investigations were done at the Soil Mechanics Laboratory, Faculty of Civil Engineering, Belgrade.

The density of samples at about 20% degree of saturation is: $1.85 - 1.96$ t/m^3, and the cohesion: $1 - 5$ kPa. The hydraulic conductivity is, without addition of hydrophobic substances, of an order 10^{-8} m/s.

3.5 Laboratory installation and experimental conditions

Laboratory installation consists of a laboratory flume and the measuring equipment. After a short description, experimental conditions are specified, and the experimental procedure is explained.

3.5.1 Laboratory flume

Scale models of earth structures are built in the laboratory flume 22 m long, 1.0 m wide, and 1 m high. The flume has a concrete bottom and glass walls. It has its own recirculatory water supply system, with the maximum flow capacity of 180 L/s.

The erosion process is observed and photographed through the glass wall. For this purpose, a referent mesh is drawn on the glass wall. Qualitative and quantitative results are obtained using high-speed photography as the recording technique.

The flume inflow is regulated by a valve. The inflow discharge, measured by sharp-crested weir, is kept constant throughout each experiment at 4 L/s, which is $1/10 - 1/15$ of the maximum outflow discharge during the overflowing of the model structure. On the upstream end of the flume, the water passes through a system of stilling elements, placed immediately downstream from the sharp-crested weir.

The inflow is directed in such a way that the flow in the flume is parallel, and the velocity distribution is as much uniform over the cross section as possible. This is an important condition for uniform overtopping of the model structures. Only in this case the flow may be considered as two-dimensional, and analyzed in the vertical plane. In some experiments the width of the flume is reduced to 0.6 m in order to have more suitable flow conditions for overtopping of the model structures.

On the downstream end of the flume a 2 m long, 1 m wide, and 0.5 m high sediment trap is installed to hold the eroded material.

3.5.2 Measuring equipment

The measuring equipment consists of (a) electric gauges for continuous measurement of water levels, and (b) devices for recording the erosion process during overflowing of the model structures.

The electric gauges for continuous measurement and recording of water levels consists of power supply, gauges converting water level changes to electrical capacity changes, amplifying unit and an oscillograph (device used to output signal on screen and paper). The electrical gauges and the amplifying unit are combined in a single instrument called the "universal measuring Wheatstone bridge". The KWS Hottinger 6/T universal measuring bridge is used for continuous water level measuring, and the 14 channel data acquisition system is used for water level registration. All instruments are calibrated before each experiment. The accuracy of water level measurements is about $\pm$ 0.2 mm.

The erosion process is photographed directly through the glass wall of the flume by a high-speed camera. The average sampling interval was 5 s during experiments lasting several minutes. The recorded data are analyzed from enlarged photographs. The accuracy of reading photographs is about $\pm$ 0.5 mm. Time is measured by an electrical chronometer.

The measuring equipment set-up is schematically shown in Fig.3.3.

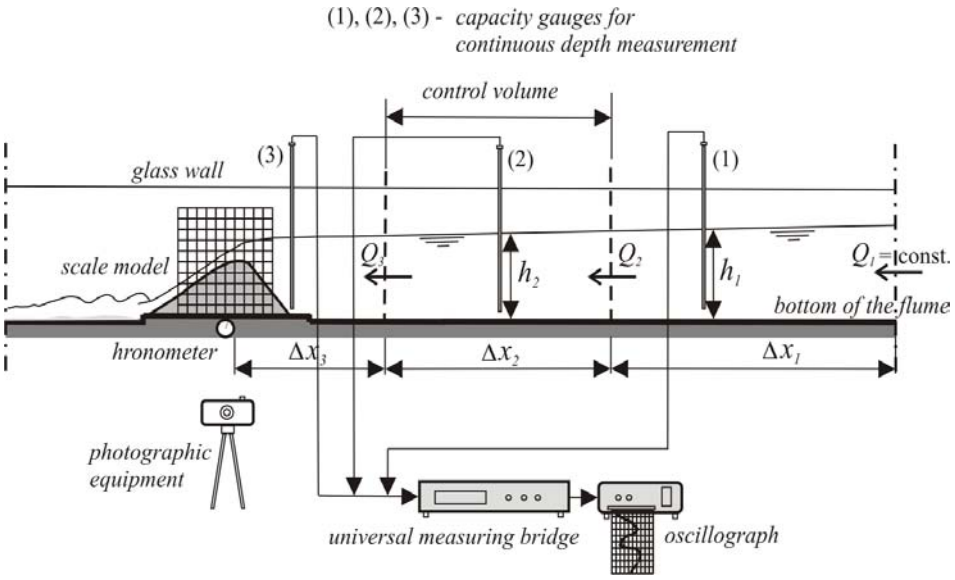

Figure 3.3: *Schematic presentation of the measuring equipment in the laboratory flume*

3.5.3 Measuring technique

Scale model structures are built in series of 3–4 cm thick horizontal layers of compacted equivalent material. The building procedure is carefully controlled, and special attention is payed that the crest of the structure is perfectly horizontal.

The experiment is started with filling the volume of the flume upstream of the structure, at an inflow rate of 4 L/s. At one point the water level reaches the crest of the structure, and the structure is overtopped. The erosion process that takes place after overtopping is photographed, as is illustrated in Figs. 3.4, 3.5, and 3.6.

It can be remarked that the erosion process takes place at once, its rate varying with the overflow discharge as the height (volume) of the structure progressively decreases.

It can also be noted that soon after the structure is overtopped, the overflow discharge becomes higher than the inflow at the upstream end of flume. The water level in the flume starts to decrease, and the storage is gradually depleted. One of the principal factors influencing the rate of this process is the ratio of the model volume to the storage volume. In most performed experiments this ratio is 1:25.

The flow hydrograph can be determined from the continuity equation, expressed in the the finite-difference form:

$$Q_{i+1} = Q_i - B\,\frac{\Delta h_i}{\Delta t}\,\Delta x_i \qquad (i = 1, 2, 3, ...) \tag{3.19}$$

where Q_i and Q_{i+1} are the inflow and outflow discharges for control volumes shown in Fig. 3.3; Δh_i are the depth variations in control volumes, recorded over the the time interval Δt; Δx_i are the control volume lengths, and B is the width of control volumes.

The quantity of the eroded material in each time interval can be calculated form the recorded change of the scale model volume which is equal to the change of cross-sectional area between two successive photographs.

Evolution of the erosion process can be presented either by changes of the scale model volume incrementally (for each time interval), or cumulatively, by integral curves. The mean transport rate of the eroded material is obtained by dividing the change of volume by the corresponding time interval.

3.6 Results of laboratory investigations

Eleven experiments are performed in this dissertation. Five of those experiments are used for improving scale model building methods, and adjusting measuring equipment. Out of six experiments which can be considered as completely valid, four are chosen to be presented in this section.

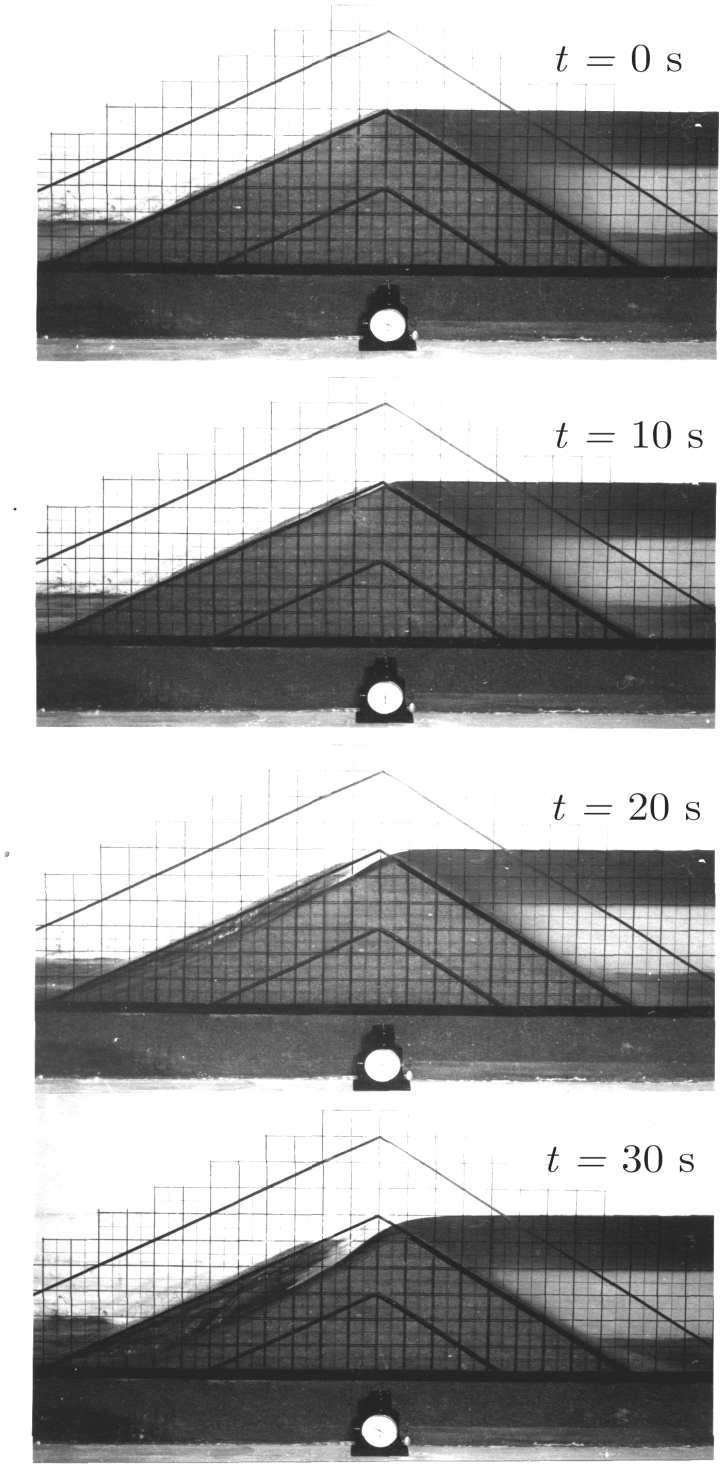

Figure 3.4: *Erosion of the scale model*

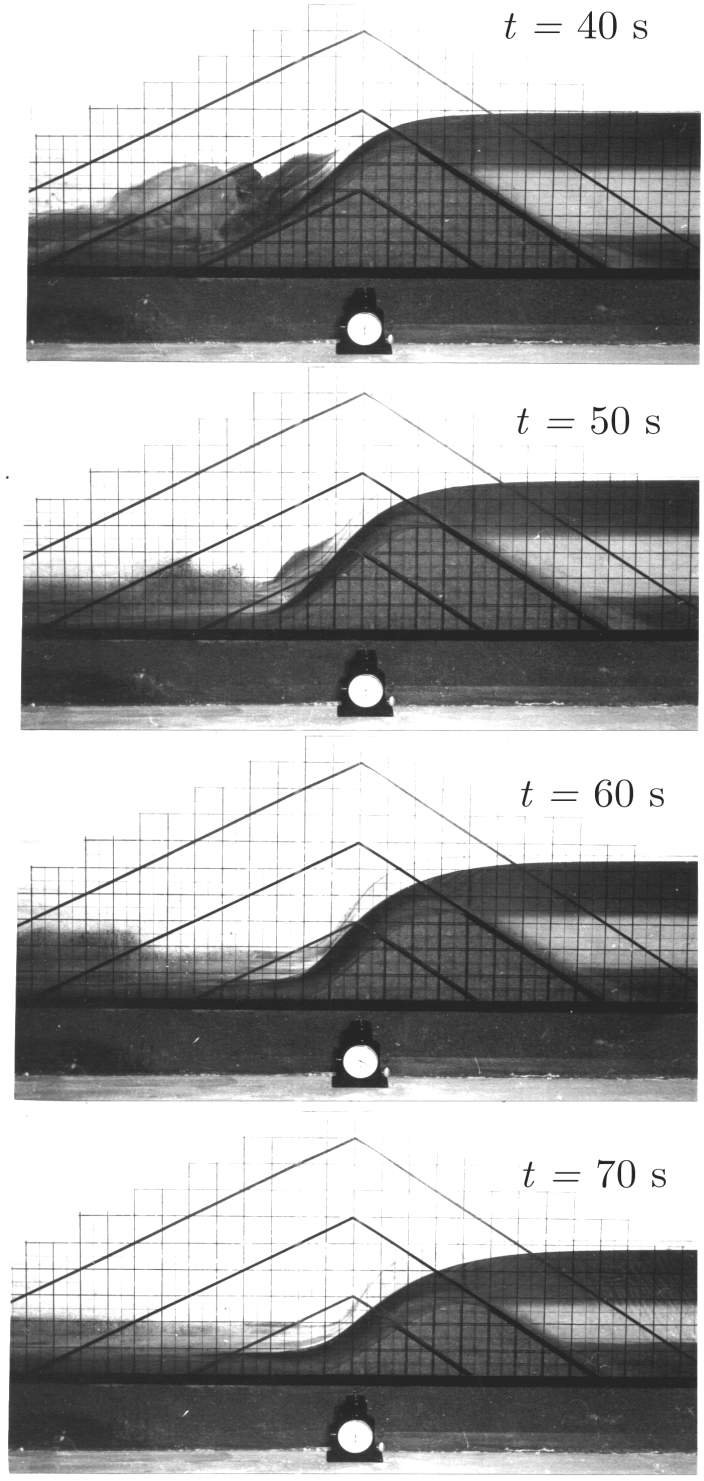

Figure 3.5: *Erosion of the scale model*

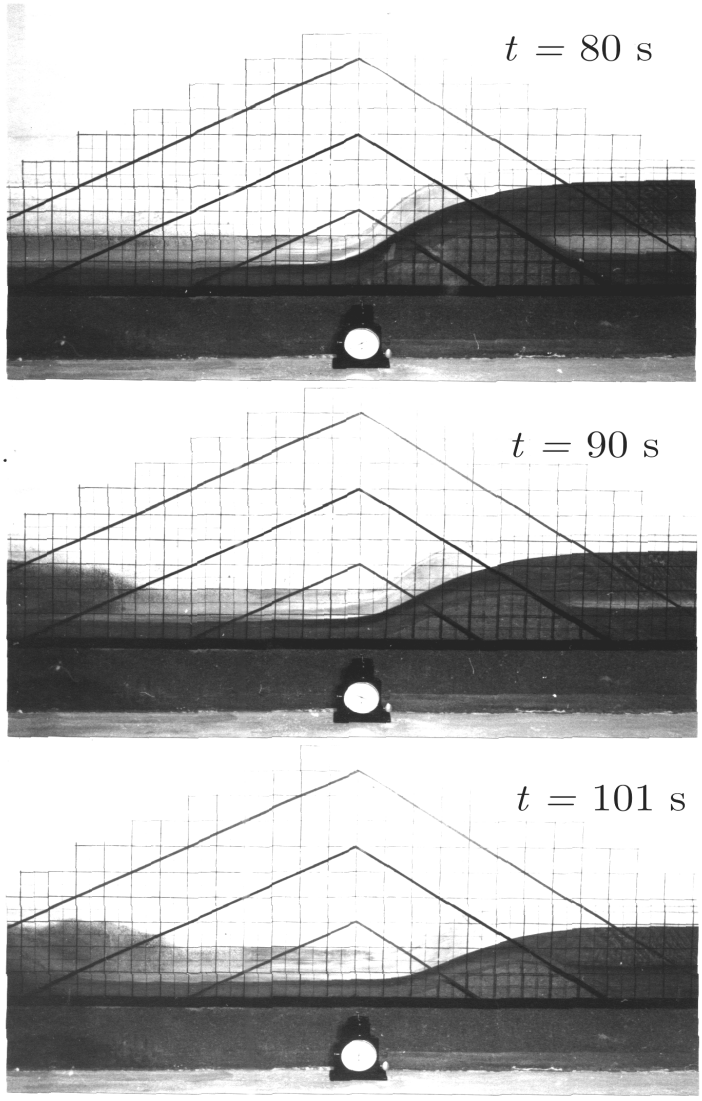

Figure 3.6: *Erosion of the scale model*

Three of the chosen experiments (numbers 1, 2, and 4) are performed under the following conditions:

1. Geometry of the scale model:

- shape of the cross-section: trapezoid;
- height: 0.3 m;
- upstream slope: 1:1.5;
- downstream slope: 1:2.

2. Building material:

- sand mixture: $d_{10} = 0.13$ mm; $d_{50} = 0.20$ mm; $d_{90} = 0.25$ mm;
- coefficient of uniformity: $d_{60}/d_{10} = 1.54$;
- geometric standard deviation: $\sigma_g = \sqrt{d_{84}/d_{16}} = 1.22$;
- angle of internal friction: $\phi = 32$ – 34^o;
- density in saturated state: $\rho'_s = 1.90$ – 1.93 t/m^3;
- wet content: $w = 19.6$ – 22.5%;
- cohesive additive: kaolin, 2%;
- cohesion: $C = 1$–2 kPa;
- hydraulic conductivity: $K = 10^{-8}$ m/s.

3. Experimental parameters:

- ratio of model volume to the upstream storage volume: 1:25;
- inflow rate: 4.0 L/s.

One experiment (no. 3) is performed under the same conditions as the other three experiments, except for the amount and type of the cohesive additive. In this case, a stronger, bentonite additive is used, its content being 3%. The cohesion is thus increased to $C = 5$ kPa, and hydraulic conductivity reduced to $K = 10^{-9}$. Density of the material in this case is: $\rho'_s = 1.94$ t/m^3, and the wet content $w = 23.1\%$.

3.6.1 Qualitative analysis

The contours of the overflown model structure, obtained from photographs, are shown in Fig. 3.7. These contours can be used to quantify the erosion process rate, and to study its evolution.

It is noticed that in the initial phase of the experiments (shortly after the model structures are overtopped), there is no major damage to the downstream slope of the structures. This period, lasting about 10-15% of the total failure time, is an "erosion time lag", due to small water depths. After this period, as depths of the overflowing current increase, the downstream surface of the model structures noticeably starts to erode.

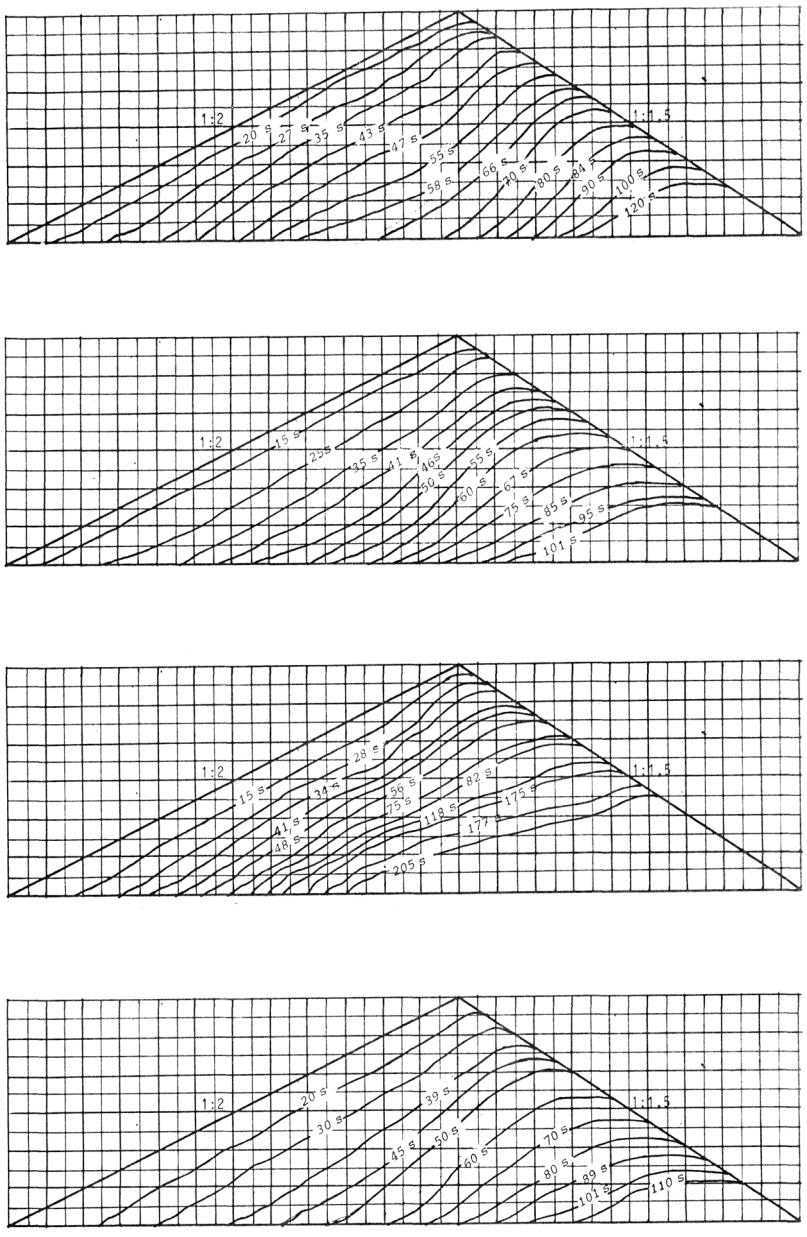

Figure 3.7: *Erosion contours in experiments* 1, 2, 3, *and* 4 *(top to bottom); drawing scale:* 1:10

In experiments with weaker cohesive additive (nos. 1, 2, and 4), the material is washed away continually, at an almost constant erosion rate. The erosion contours are smooth and streamlined. In the experiment with a stronger cohesive additive (no. 3), the process is evolving more slowly. In this case the material is being washed away in a "step-like" fashion (discontinuously), the erosion contours are not streamlined, and their downstream slope is milder than slopes in other experiments.

It is also observed that the scale model structures are never entirely washed away, and that a small volume of material remains long after the upstream storage is depleted. The height of this residual material is about 10-30% of the initial model height, depending on the type and amount of the cohesive additive.

3.6.2 Quantitative results

The overflow hydrographs, obtained by continuous measuring the water levels and application of the continuity equation (3.19), are presented in Fig. 3.8, as well as the corresponding unit discharge hydrographs. Even though the experiments 1, 2, and 4 are performed under the same initial and boundary conditions, the results are not the same. This is due to unavoidable differences in construction of the scale models, as homogeneity and compactness of the material can never be absolutely the same.

Comparing the overflow hydrographs in experiments nos. 1, 2, and 4 (all performed with the same equivalent material, and under the same conditions), and the experiment no. 3 (performed with more cohesive material), it is obvious that the maximum discharge decreases with the increase of cohesion.

The transport rate of the eroded material is presented in Fig. 3.9. It is expressed as volume of material washed away in unit of time. As may be recalled, since the problem is two-dimensional, the transport rate can be calculated from changes of the model cross-section, determined from photographs taken in regular time intervals.

From the overflow hydrographs and transport rates of the eroded material, cumulative volume curves for water and material can be determined (Fig. 3.10).

As expected, a slower process of erosion, with a less smooth cumulative curve, occurs in experiment no. 3 with more cohesive material. A trend of "step-like" curves reflecting non-uniform erosion rates is observed whenever a stronger bonding additive is used in experiments. Therefore, it can be concluded again, that the non-uniformity of the erosion rate increases with cohesion of the material.

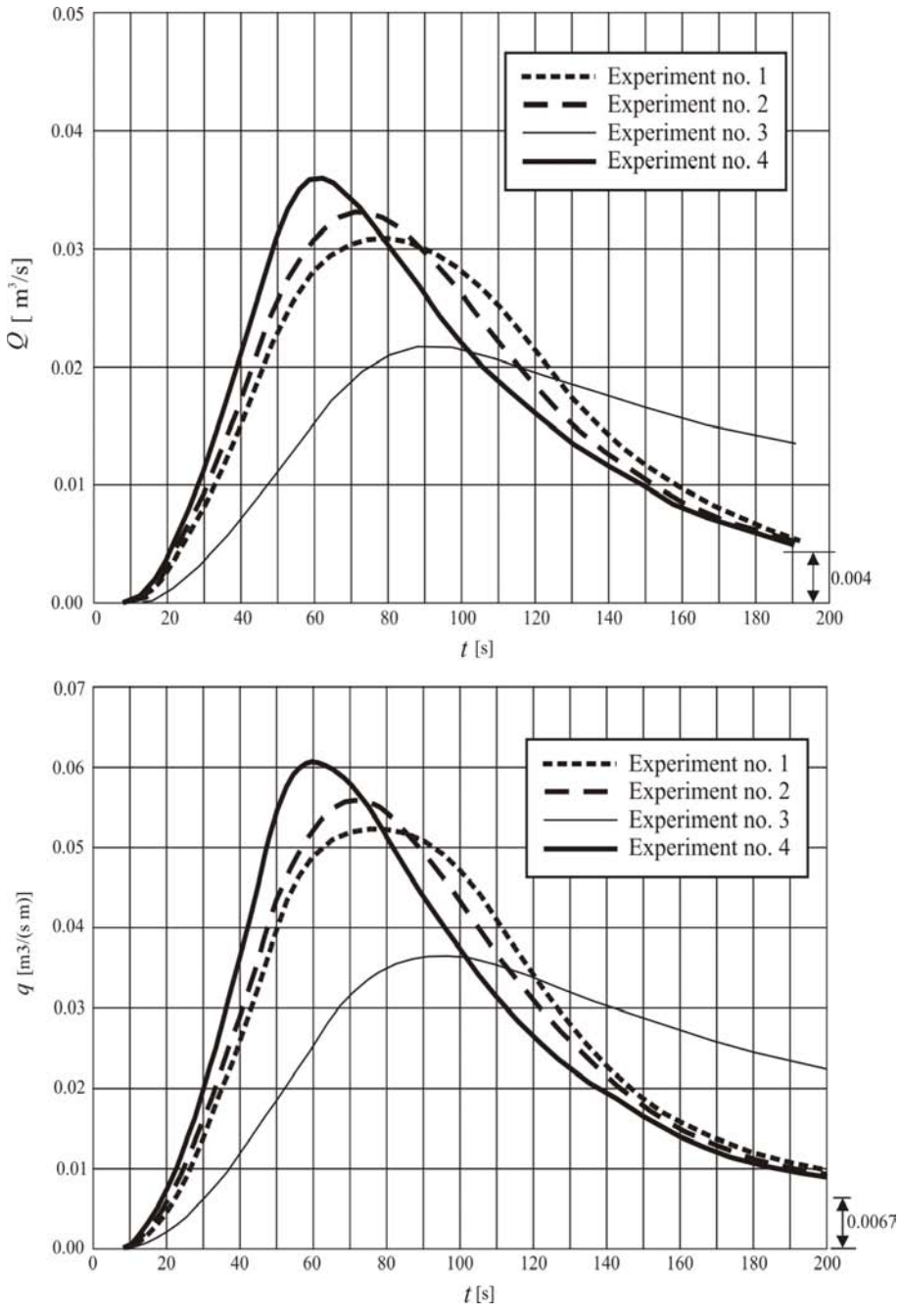

Figure 3.8: *Measured total and unit overflow discharges*

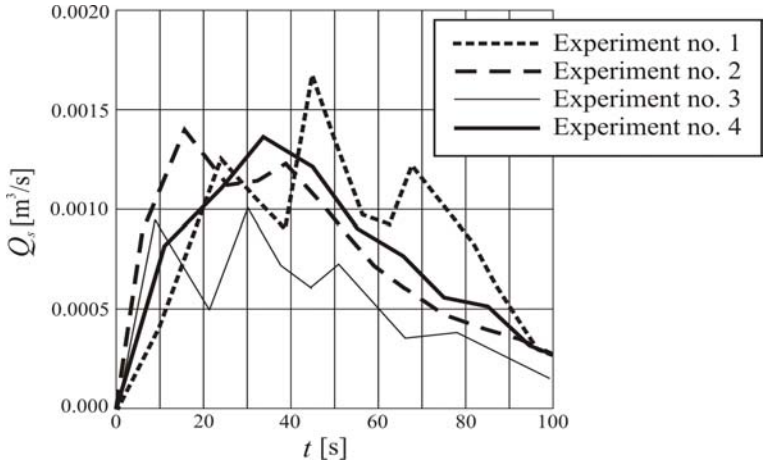

Figure 3.9: *Transport rate of the eroded material*

By combining the given cumulative curves, a dimensionless function $Q/Q_s = f(t/T)$ can be determined, where Q/Q_s is the ratio of water and material discharges, and t/T is the ratio of any instant of time and the total erosion time (Fig. 3.11). This relationship can be approximated by an exponential function. Values of the regression coefficients depend on the cohesion of the material.

Consider now the erosion rate in another way. The erosion rate in the vertical direction can be quantified from experimental data, and results are shown on two dimensionless diagrams in Fig. 3.12.

The first diagram depicts the reduction of the scale model height in time, where h and H are the instantaneous and the initial model heights respectively, and T is the total erosion time.

The second diagram is formed introducing the "*erosion number*" Er, instead of dimensionless time. The erosion number is a parameter which reflects the instantaneous degree of reduction of the structure volume, due to the erosion:

$$\mathrm{Er} = \frac{\forall_e}{\forall_o} = \frac{\forall_o - \forall}{\forall_o} = 1 - \frac{\forall}{\forall_o}, \tag{3.20}$$

where $\forall_o$ is the initial volume, $\forall$ is the instantaneous volume, and $\forall_e = \forall_o - \forall$ is volume of the eroded material.

The erosion number Er, which takes values between 0 and 1, reflects dynamics of the process. By its introduction, the instantaneous size of the structure and the duration of the erosion process can be combined in a convenient way for quantitative analyzes.

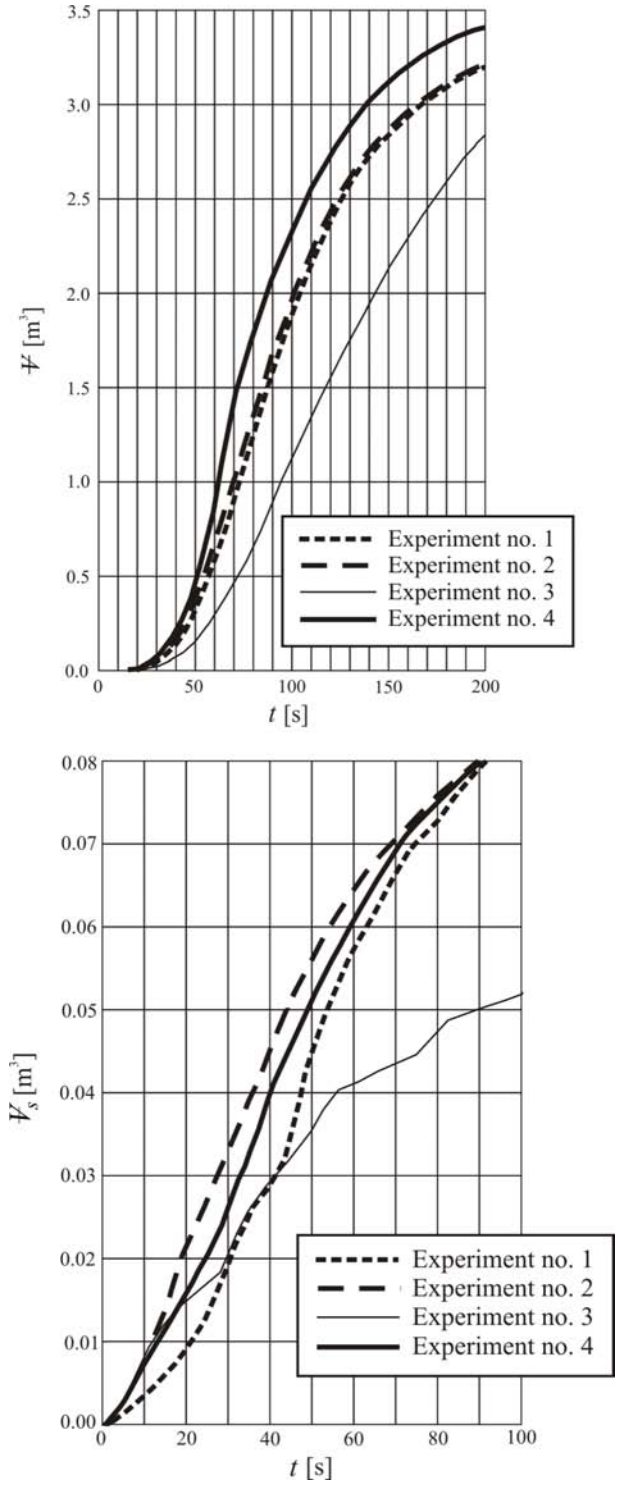

Figure 3.10: *Cumulative volume curves for water (top) and the eroded material (bottom)*

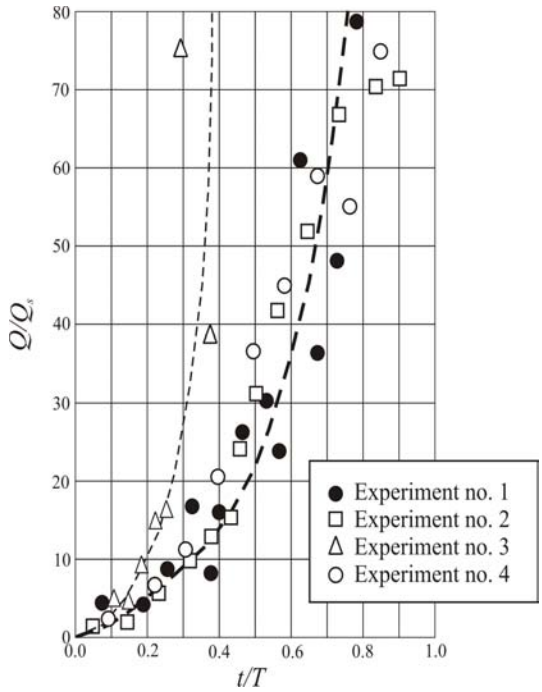

Figure 3.11: *Dimensionless water-to-solid discharge*

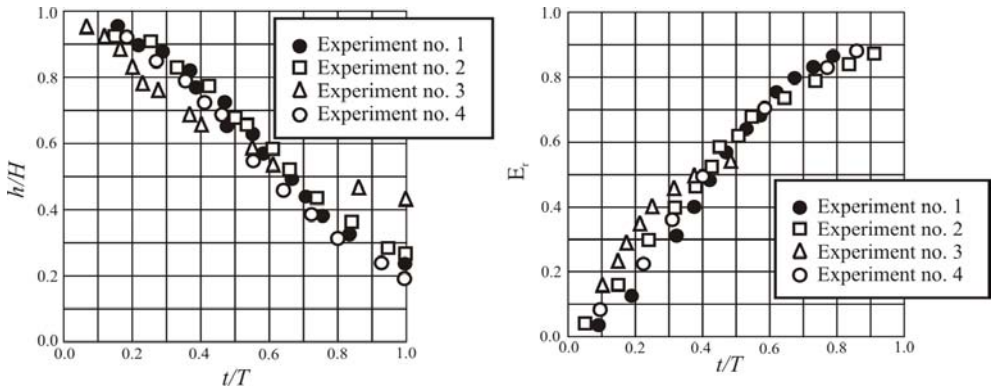

Figure 3.12: *Erosion rate in the vertical direction*

Diagrams in Fig. 3.12 show that in experiments nos. 1, 2, and 4, after a short initial period ($t/T > 0.15$), the erosion in the vertical direction is rather uniform – the erosion rate is constant[4]. In case of a more cohesive material (experiment no. 3), the erosion is not uniform, and the erosion rate is not linear.

[4]The linear regression is in the form: $h/H = 1.1 - 0.93(t/T)$, $r = 0.989$.

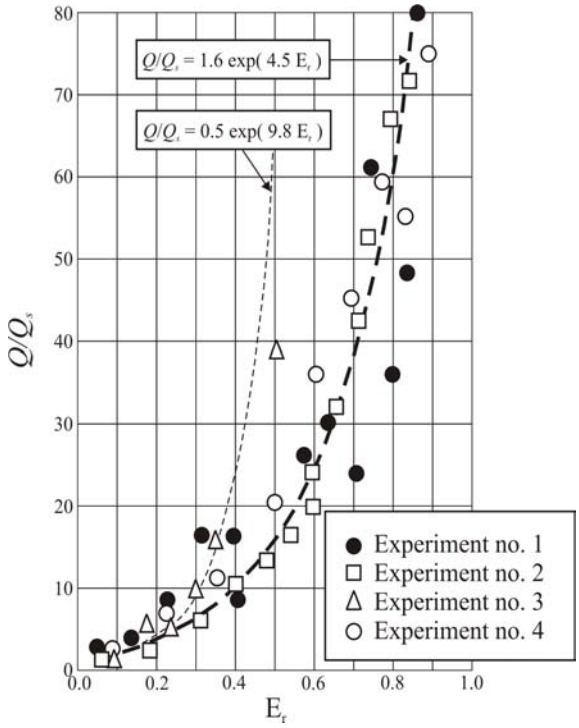

Figure 3.13: *Degree of erosion related to dimensionless discharge*

By combining the relationships $Q/Q_s(t/T)$ in Fig. 3.11, and $\mathrm{Er}(t/T)$ in Fig. 3.12, a relationship $Q/Q_s(\mathrm{Er})$ can be determined, as shown in Fig. 3.13.

Exponential approximations are possible for this relationship:

$$\frac{Q}{Q_s} = C_1 \, \exp(C_2 \cdot \mathrm{Er}). \tag{3.21}$$

Values of the regression coefficients C_1 and C_2 are experiment dependent (Table 3.4).

Table 3.4: *Regression coefficients*

Experiment no.	C_1	C_2	r
1, 2, 4	1.6540	4.4819	0.9473
3	0.4936	9.7770	0.9607

Generally, smaller values C_1 and higher values C_2 correspond to more cohesive materials. As the presented results are valid only for particular scale models built of particular materials, more research is needed for more general conclusions. However, the obtained results allow certain extrapolation to prototype structures, as is shown in the following section.

3.7 Scale Effects and Extrapolation of Experimental Results

The scale effects are manifested by discrepancies between the measured values and the values which are to be expected from the similarity laws. The discrepancies are larger as the model scale is smaller.

Investigating erosion of overflown earth dams on scale models of different heights (0.3 – 3 m), Dunglas and Fayoux [50] concluded that geometric similitude of model and prototype deformation can exist only if scales are not smaller than 1:10. Only in this case, the hydraulic and rheologic similitude laws, used for composition of the equivalent material, are valid. A similar conclusion can be drawn from experiments in this dissertation, the determined limiting scale being 1:15.

Considering these conclusions, the experimental results obtained in this dissertation are analyzed from the point of view of their extrapolation to field conditions. The averaged results of experiments nos. 1, 2, and 4, are used for estimation of their applicability to prototype earth structures of various sizes. The characteristics of these structures for a range of model scales 1:2 to 1:40, are presented in Table 3.5.

As can be seen from this table, the experimental results in this dissertation can be representative for relatively small earth structures, with heights up to about 4-5 m, and typical side slopes 1:1.5 or 1:2. These structures are made of homogenous materials with cohesion up to 20 kPa, and hydraulic conductivity in the order of 10^{-8} m/s.

The maximum unit discharge which can be expected in case of overflowing of such structures is about 20 $m^3/(s\ m)$, and the total failure time is 5–10 minutes.

Therefore, it can be concluded that the experimental results obtained in this dissertation can be extrapolated to small earth structures, such as dams on micro-reservoirs, levees along rivers, dikes, emergency fuse-plugs, and other similar structures.

Table 3.5: *Extrapolation of experimental results to field conditions in terms of model scales*

Ggeometric scale/ Prototype charact.	1:1 (model)	1:2	1:5	1:7	1:10	1:15	1:20	1:25	1:30	1:40
Height [m]	0.30	0.60	1.50	2.14	3.00	4.50	6.00	7.50	9.00	12.0
d_{10} [mm]	0.13	0.26	0.65	0.93	1.30	1.94	2.60	3.25	3.94	5.20
d_{50} [mm]	0.20	0.40	1..00	1.43	2.00	2.99	4.00	5.00	6.06	8.00
d_{90} [mm]	0.25	0.50	1.25	2.79	2.50	3.73	5.00	6.25	7.58	10.00
C [kPa]	1-2	2-4	5-10	7-14	10-20	15-30	20-40	25-50	30-60	40-80
K [m/s]	10^{-8}	10^{-8}	10^{-8}	10^{-8}	10^{-8}	10^{-8}	10^{-8}	10^{-8}	10^{-8}	10^{-8}
Max.unit discharge [m^3/(s m)]	0.06	0.3	3.5	8	19	52	107	188	303	607
Failure duration [min]	2	3	4	5	6	8	9	10	11	13

4

Development of the Numerical Model - Part II

After having developed the numerical procedures for calculating the curvilinear gravity flows, and an experimental relationship between the unit discharge of water and the corresponding transport rate of the eroded material, the numerical model is completed with a module for calculating the progressive failure of an overflown earth structure. Following the concept of two-stage calculation, the sediment transport and dam erosion is calculated for the *known* (previously calculated) flow field. The empirical relation $Q/Q_s = f(\mathrm{Er})$ is used for this purpose.

The onset of erosion is defined according to the critical velocity criterion. The main idea is to compare the calculated depth-averaged velocity along the flow path with the critical velocity for the given type of material. If the local depth-averaged velocity is greater than the critical velocity, the local erosion depth is calculated, as being proportional to the difference of the two velocities. In this way, a new contour of the solid boundary is obtained, providing geometry data for hydraulic calculation in the next step. Thus, no geometric schematizations are necessary, as is the case in earlier models, such as the one proposed in reference [5].

4.1 The critical velocity for incipient motion

The incipient motion of solid particles exposed to flowing water is defined by the critical velocity approach, rather than by the critical shear stress approach, because the bottom shear stresses cannot be accurately calculated by the potential flow model. On the other hand, it is demonstrated by the previous examples that, although the potential flow model cannot give an accurate velocity distribution over flow depth, it can yield quite an accurate

prediction of *depth-averaged velocities*, at least with an acceptable accuracy for engineering purposes.

For cohesionless materials, a class of critical velocity formulas has the general form:

$$v_c = a_1 \sqrt{2g \cdot \Delta \cdot d}, \tag{4.1}$$

where d is the mean grain diameter, $\Delta = (\rho_s - \rho)/\rho$ is the relative density of material (ρ_s, and ρ are densities of the solid and the liquid phase, respectively), g is the acceleration of gravity, and a_1 is an empirical factor, the value of which depends on the flow characteristics. According to Izbash et al. [77], $a_1 = 0.8$–1.2.

For cohesive materials, it is not easy to define conditions for incipient motion. A large number of references (some of the major ones are listed in Literature) clearly shows that no general approach is available. Some researches approach the problem on a "microscopic" level (see for instance [47, 59], while others look at the phenomenon from a simplistic, engineering point of view. The "engineering approach" is used in this dissertation, and a formula similar to the one suggested by Mirtskhulava [55] is assumed:

$$v_c = a_2 \sqrt{2g \cdot \Delta \cdot d + 2.5 \cdot C_f \cdot K_h/\rho}, \tag{4.2}$$

where C_f is the mean cohesion at the rupture "fatigue" limit, K_h is the homogeneity factor, and a_2 is an empirical constant, depending on the flow characteristics.

According to [55], the relationship between the cohesion C (determined from soil samples) and the cohesion at the rupture limit is: $C_f = 0.035 \cdot C$. The homogeneity factor K_h is equal to unity when the soil is homogeneous. The engineer is supposed to select the value of K_h in situ. Assuming the values of the given soil parameters are known, the formula (4.2) can be shortly written as:

$$v_c = a_2 \sqrt{2g \cdot \Delta \cdot d + c}, \tag{4.3}$$

where $c = 2.5 \cdot C_f \cdot K_h/\rho$ is a material constant.

It can be observed that the equation 4.3 is an extention of the equation 4.1, accounting for the effects of cohesion. In both cases, the critical velocities are defined as the time-averaged velocities at the "grain height" above the bed.

Assuming logarithmic velocity distribution over flow depth, the critical velocity formula (4.3) can be replaced by a similar expression formulated in

terms of the *critical depth-averaged velocity*:

$$V_c = a_3 \cdot \log\left(\frac{8.8h}{d}\right) \cdot \sqrt{2g \cdot \Delta \cdot d + c}. \tag{4.4}$$

The values of parameters a_3 and c are case-dependent, and are adjusted in order to match the results of calculation with measurements. Thus, a_3 and c are calibration parameters.

It is pointed out that the role of parameters a_1 in (4.1), a_2 in (4.2), and a_3 in (4.3) and (4.4) is to account for turbulence effects. As velocity fluctuations may be very strong, attaining up to 70% of the time-averaged velocity, the critical conditions for the grain detachment are to be defined by the local *instantaneous* velocity (including fluctuating component), rather than by the local time-averaged velocity. Values of parameters a_1, a_2, and a_3 quantify the impact of fluctuations.

The criterion for erosion is thus a simple one: if the local depth-averaged velocity ($\tilde{V}$) in a particular section along the flow path is greater than the critical velocity V_c, the erosion will take place. If this is not the case, the solid boundary will remain unchanged.

4.2 Calculation of erosion

Quantitative assessment of the erosion process is done by the following procedure:

(i) The flow rate over the earth structure is assumed to be constant during the time step Δt (quasi-steady flow conditions). From a calculated flow rate over the structure and the empirical relationship (3.21):

$$\frac{Q}{Q_s} = C_1 \exp C_2 \cdot \mathrm{Er}$$

the volumetric transport rate of the eroded material (Q_s) is calculated. It is the mean transport rate during the period Δt.

(ii) The volume of the material, eroded during the time interval Δt, is equal:

$$\Delta\forall = Q_s \cdot \Delta t. \tag{4.5}$$

The obtained value is at the same time equal to the change of the cross-sectional area of the structure (ΔA) as the problem is two-dimensional in the vertical plane, and the flow rates of water and sediment are the unit flow rates.

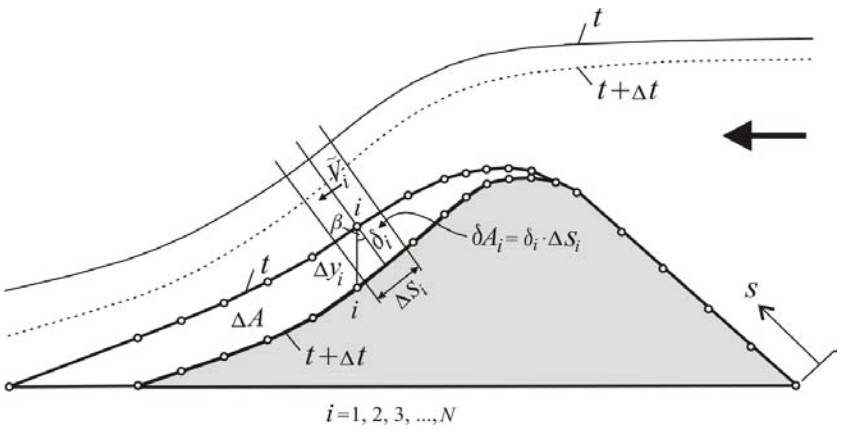

Figure 4.1: *Variables involved in calculation of the erosion contour*

(iii) Once the total eroded volume is known, it is necessary to define the new cross-section, or the new contour of the solid boundary over which water is flowing. This contour is defined by a number of coordinate points–nodes, and the corresponding segments–linear elements (Fig. 4.1). At each node, a normal to the boundary is defined, and its intersection with the calculated water surface yields the local depth. Then, 5-10 local velocities along each normal line are calculated by the B.E.M., giving the velocity distribution over depth. The depth-averaged velocity ($\tilde{V}_i$) is calculated by integrating over depth.

(iv) If the condition: $\tilde{V}_i > V_c$ is satisfied, the erosion will take place, and the normal displacement of the node (Fig. 4.1) is equal:

$$\delta_i = k \cdot \left(\tilde{V}_i - V_c \right), \tag{4.6}$$

where k is the factor of proportionality.

Since the total eroded area is:

$$\Delta A = \sum_{i=1}^{i=N} \delta A_i = \sum_{i=1}^{i=N} \delta_i \cdot \Delta s_i = \sum_{i=1}^{i=N} k \left(\tilde{V}_i - V_c \right) \Delta s_i, \tag{4.7}$$

the factor of proportionality is equal to:

$$k = \frac{\Delta A}{\sum_{i=1}^{i=N} \left(\tilde{V}_i - V_c \right) \Delta s_i}, \tag{4.8}$$

and equation (4.6) becomes:

$$\delta_i = \frac{\Delta A \left(\tilde{V}_i - V_c\right)}{\sum_{i=1}^{i=N} \left(\tilde{V}_i - V_c\right) \Delta s_i}. \tag{4.9}$$

The corresponding vertical displacement of each node is equal:

$$\Delta y_i = \frac{\delta_i}{\cos \beta_i}, \tag{4.10}$$

where β is the angle shown in Fig. 4.1.

(v) By relocating all nodes, a new profile of the solid boundary is obtained, and the new geometry is used for subsequent hydraulic computations, valid for the next period Δt.

The algorithmic structure of this module consists of the following steps at each time level:

1. Read the hydraulic data obtained by the "hydraulic module" (B.E.M): coordinates of the free-surface nodes and velocity distributions along generated normals.

2. Calculate the depth-averaged velocities.

3. From the unit discharge and the empirical relationship (3.21), calculate the unit transport rate of eroded material for the current time.

4. Calculate the volume of the eroded material per unit length of the earth structure, using (4.5). This volume is equal to the change of cross-sectional area of the structure multiplied by 1 m.

5. Using (4.6)-(4.10) calculate displacement of all nodes along the solid boundary.

6. Correct the coordinates of nodes along the solid boundary and define the erosion contour, i.e. the new cross-sectional geometry of the overflown earth structure.

7. Export the new cross-sectional geometry to the "hydraulic module" and proceed with flow calculation on the next time level.

Results of application of the suggested algorithm are presented in the next section.

5

Verification of the Numerical Model

The verification phase generally consists of evaluation of the mathematical model applicability (reliability with which the basic equations describe the given physical phenomenon), as well as performance of the numerical model (convergence and accuracy of solutions).

The model proposed in this dissertation is verified using data obtained in experiment no. 2. A 60 s long period of erosion is numerically simulated, and compared with photographs taken through the glass wall of the laboratory flume. The time step for numerical simulation is equal to the time interval between two successive photograph shots ($\Delta t = 5$ s). The cross-sectional contour computed after each time step is taken as the input geometric data for the next computational step.

The figures that follow depict the calculated water surface levels and the velocity field. The results of calculation are compared with experimental evidence in a visual manner, by overlapping photographs with diagrams pertaining to the same instant. No attempt is made to quantify the differences between calculated and measured data.

During the given numerical simulation, the number of iterations for the water surface varied from 18 to 66. The results of hydraulic calculation were used to calculate volumes of the eroded material, and erosion contours, as explained in the previous chapter. The calculated erosion contours are compared with the ones recorded on the model. As in the case of free-surface, the comparison is purely visual, and is presented on separate diagrams, given for all computational steps.

This verification case shows that calculation is in a rather good agreement with experiment. It can be concluded that the proposed numerical model is capable of simulating experiments. However, its predictive capabilities are yet to be investigated.

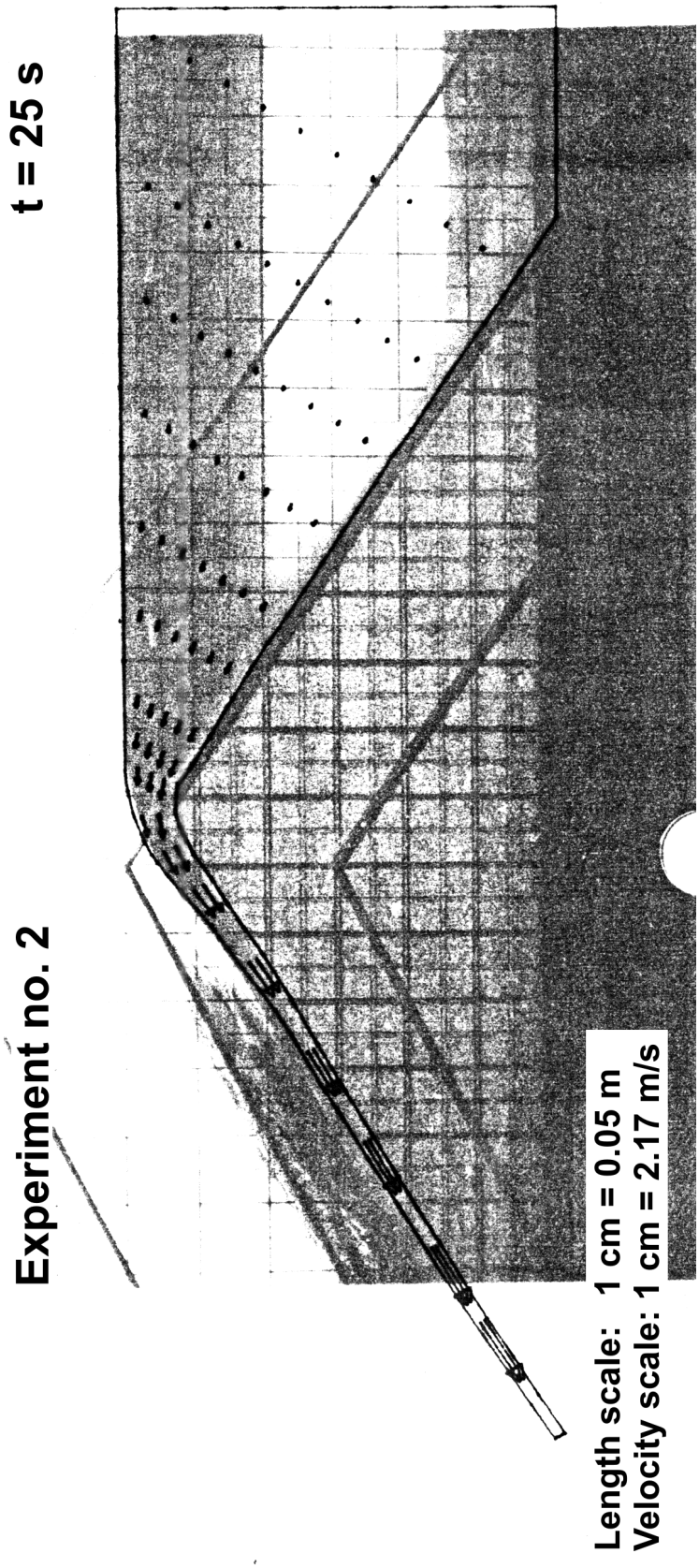
Experiment no. 2
t = 25 s
Length scale: 1 cm = 0.05 m
Velocity scale: 1 cm = 2.17 m/s

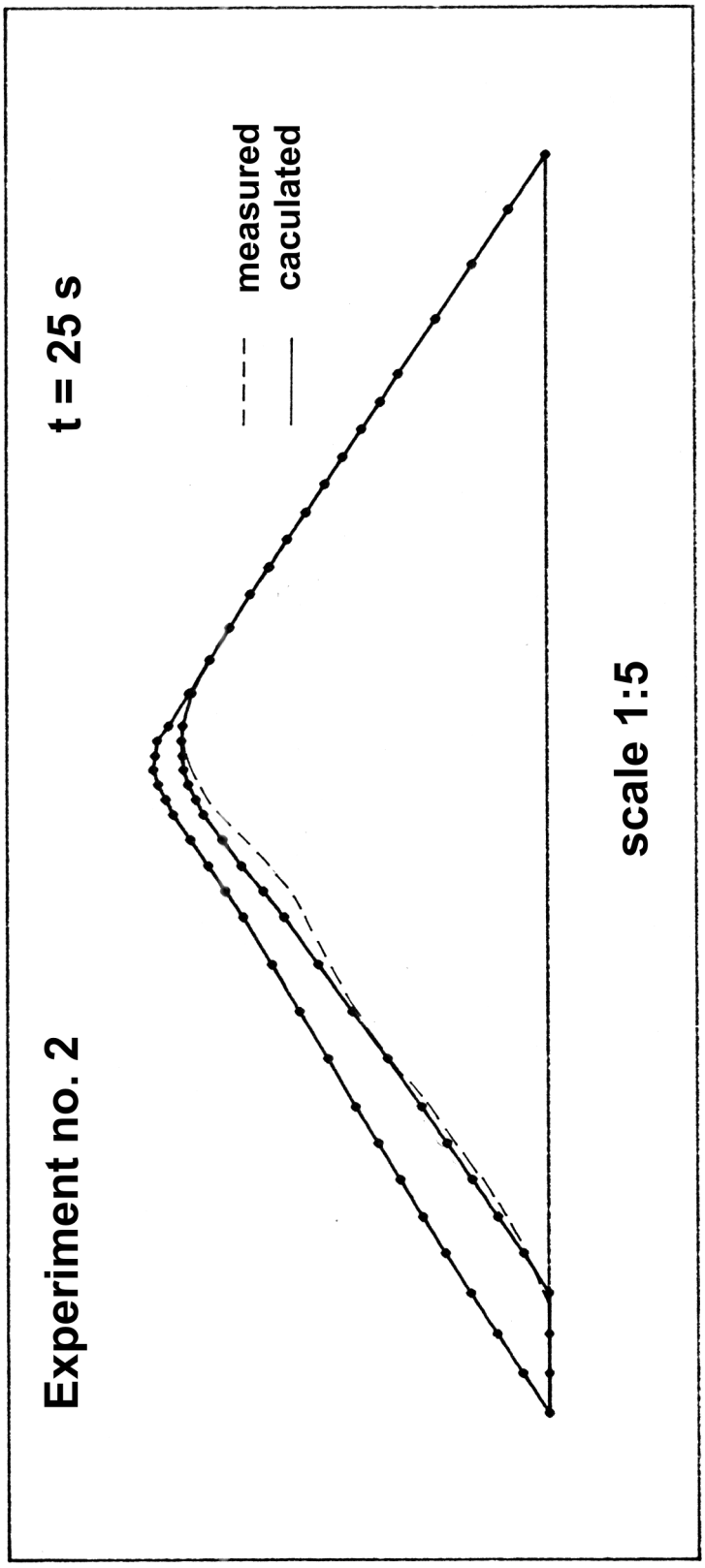
Experiment no. 2
t = 25 s
measured
caculated
scale 1:5

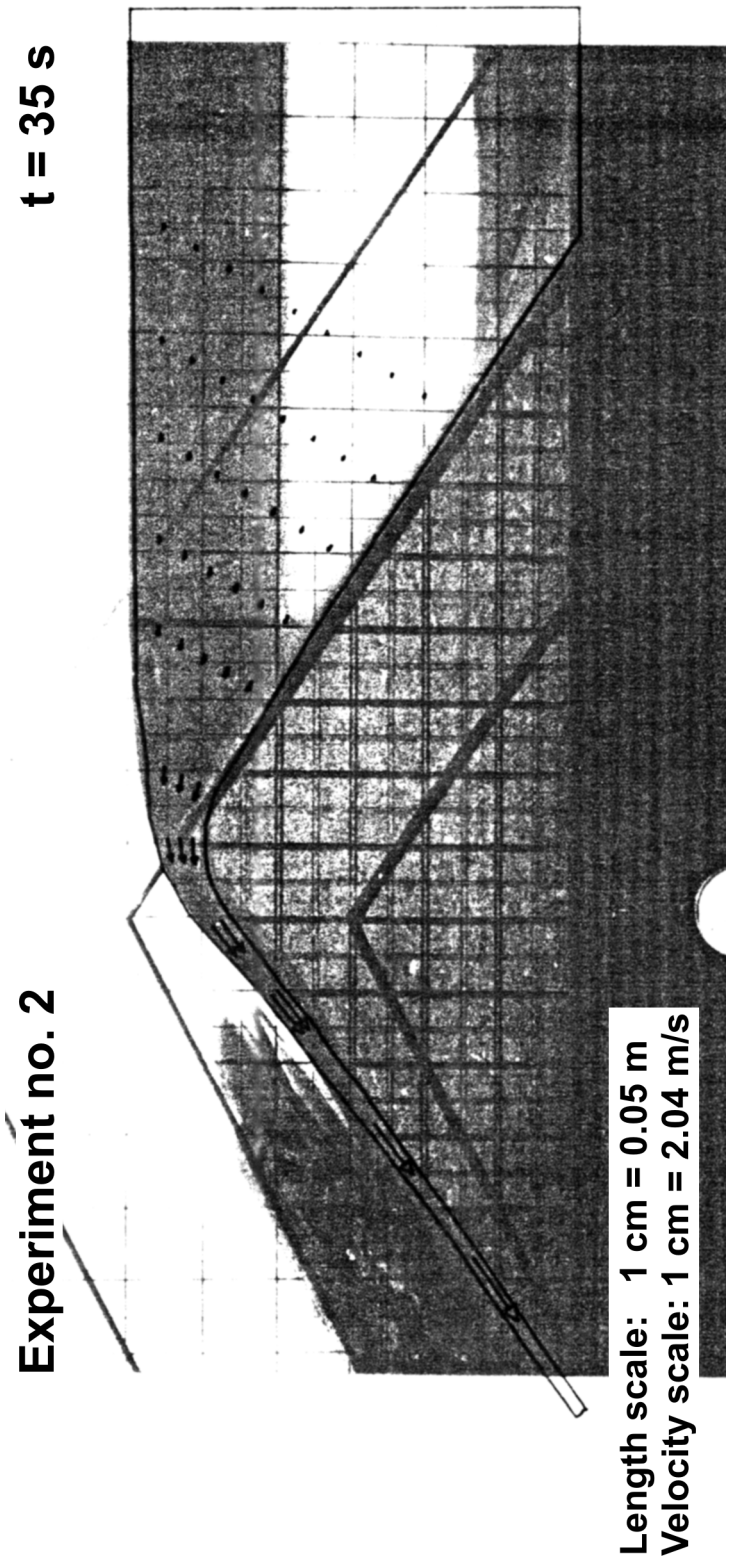
Experiment no. 2
t = 35 s
Length scale: 1 cm = 0.05 m
Velocity scale: 1 cm = 2.04 m/s

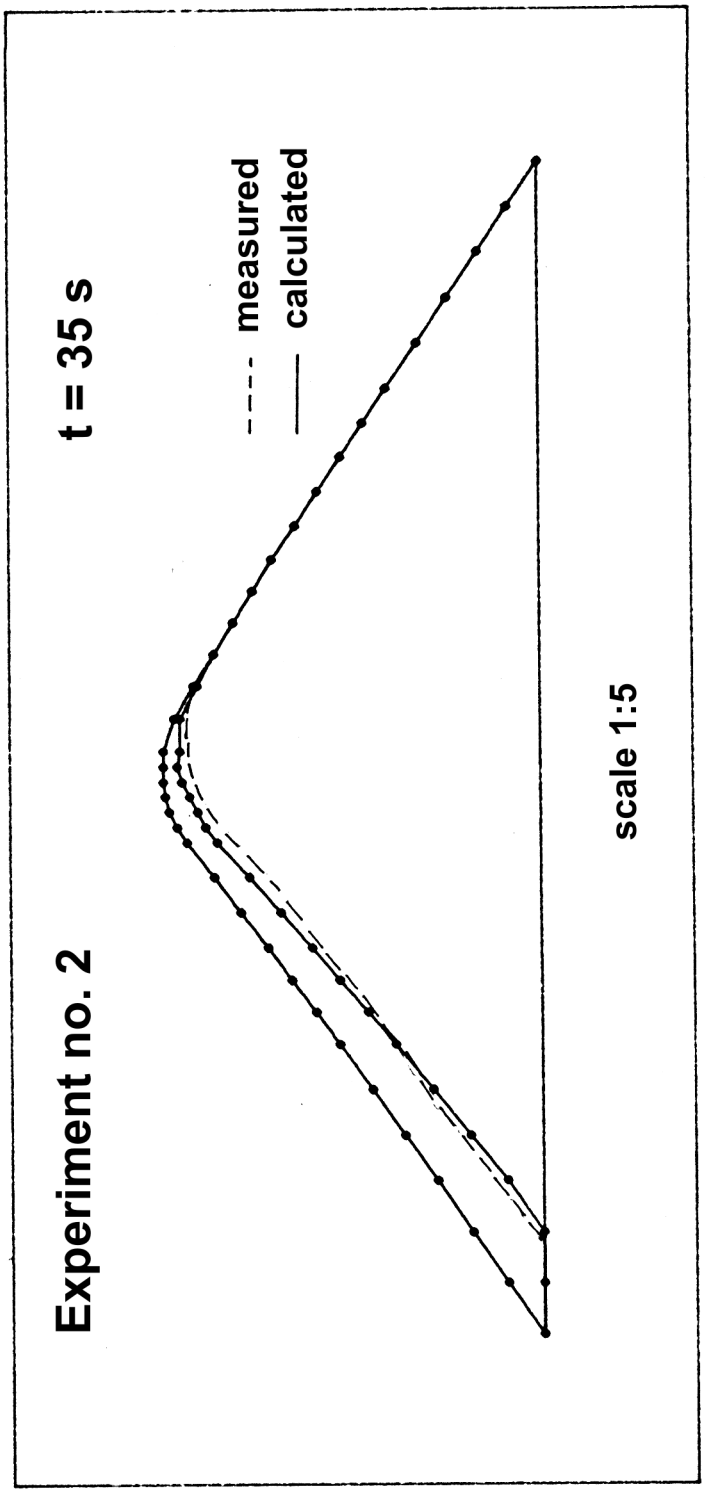
Experiment no. 2
t = 35 s
measured
calculated
scale 1:5

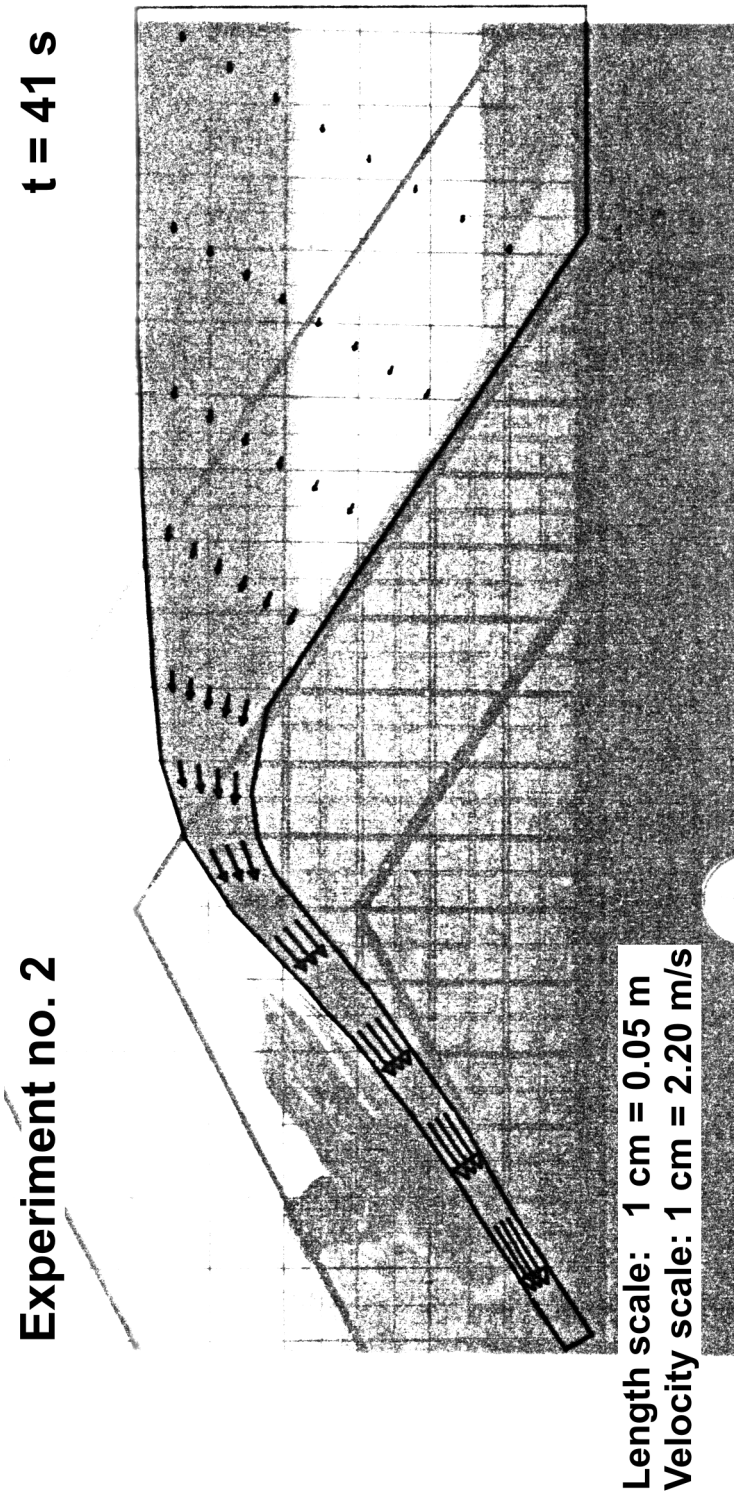
Experiment no. 2
t = 41 s
Length scale: 1 cm = 0.05 m
Velocity scale: 1 cm = 2.20 m/s

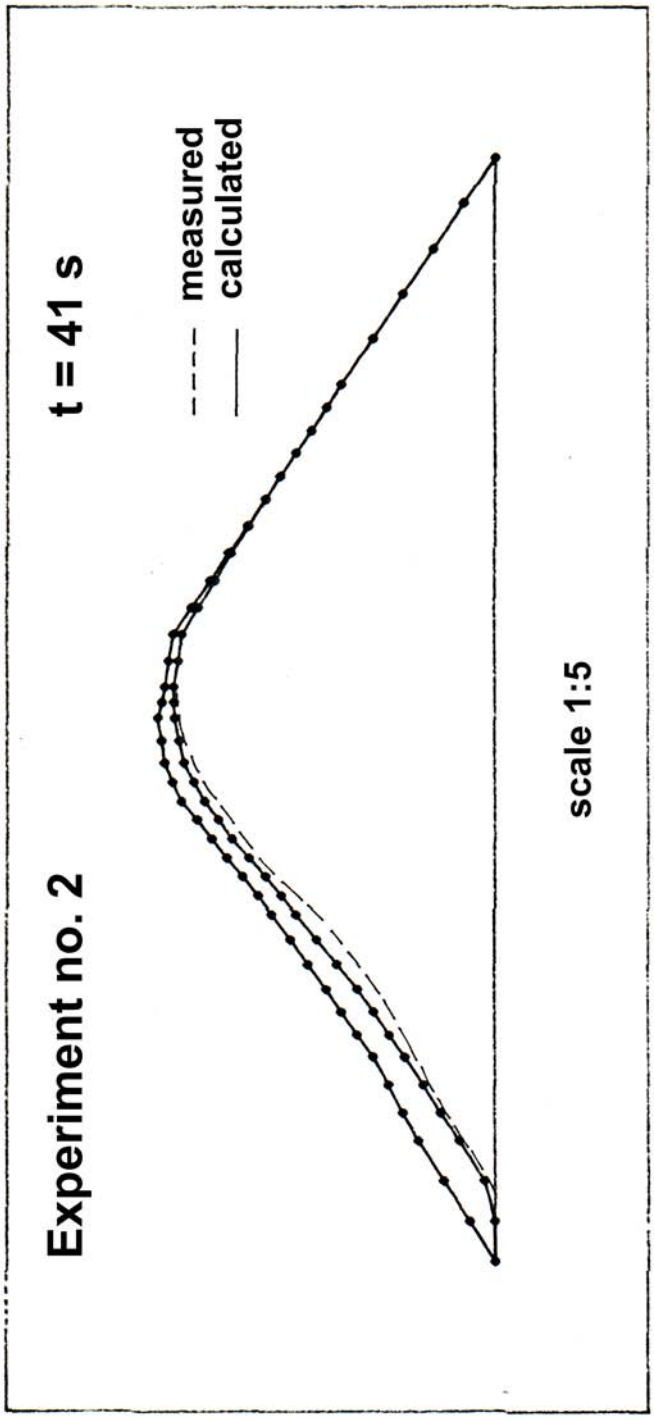
Experiment no. 2
t = 41 s
measured
calculated
scale 1:5

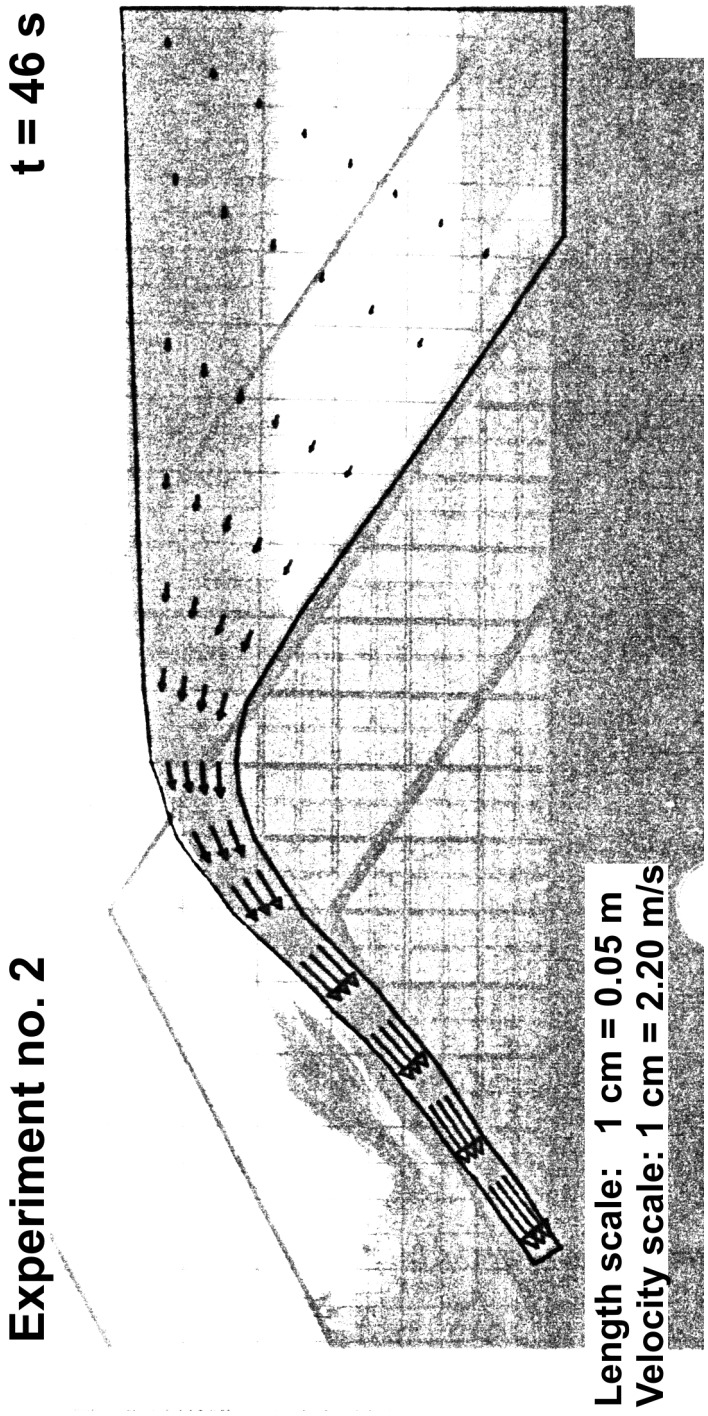
Experiment no. 2
t = 46 s
Length scale: 1 cm = 0.05 m
Velocity scale: 1 cm = 2.20 m/s

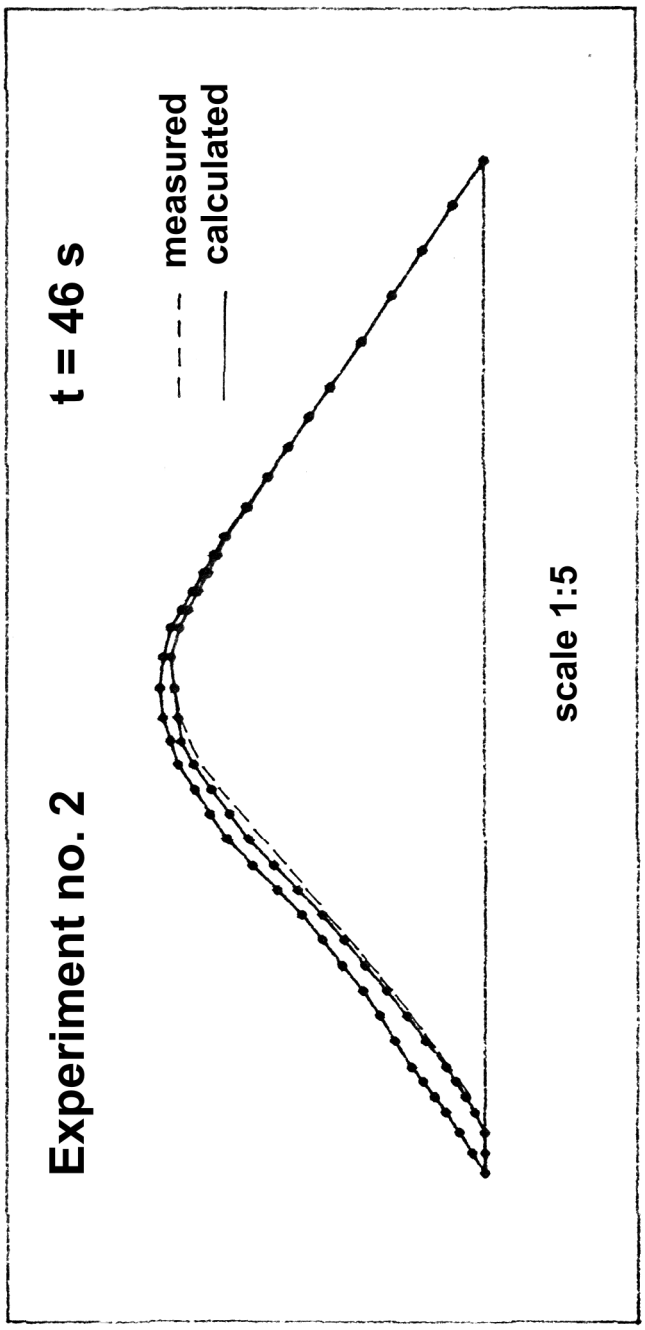
Experiment no. 2
t = 46 s
measured
calculated
scale 1:5

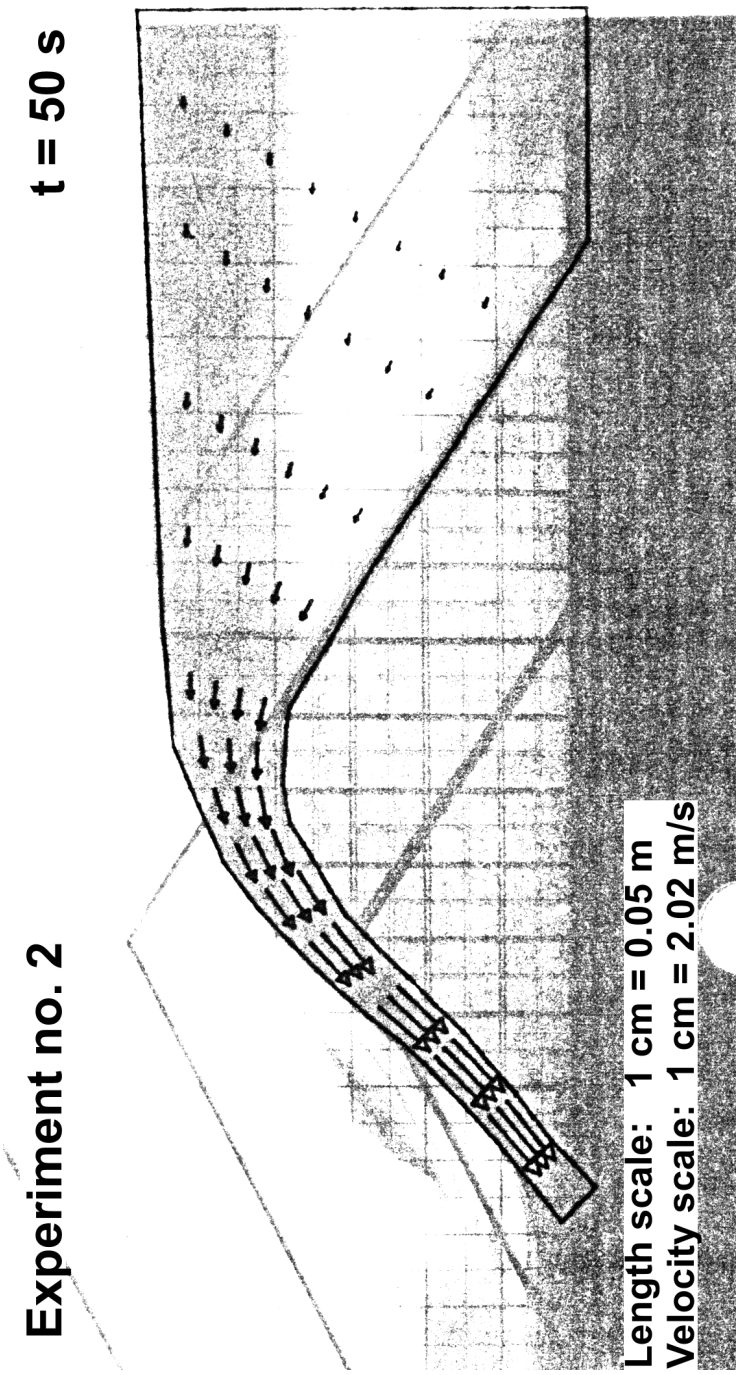
Experiment no. 2
t = 50 s
Length scale: 1 cm = 0.05 m
Velocity scale: 1 cm = 2.02 m/s

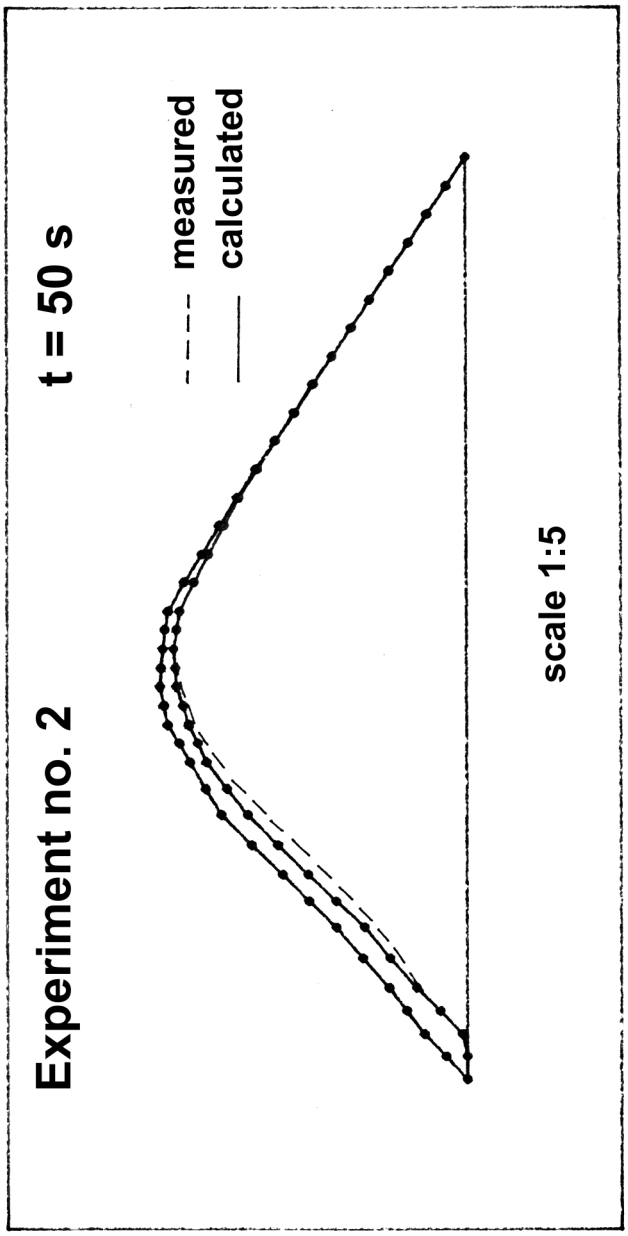
Experiment no. 2
t = 50 s
measured
calculated
scale 1:5

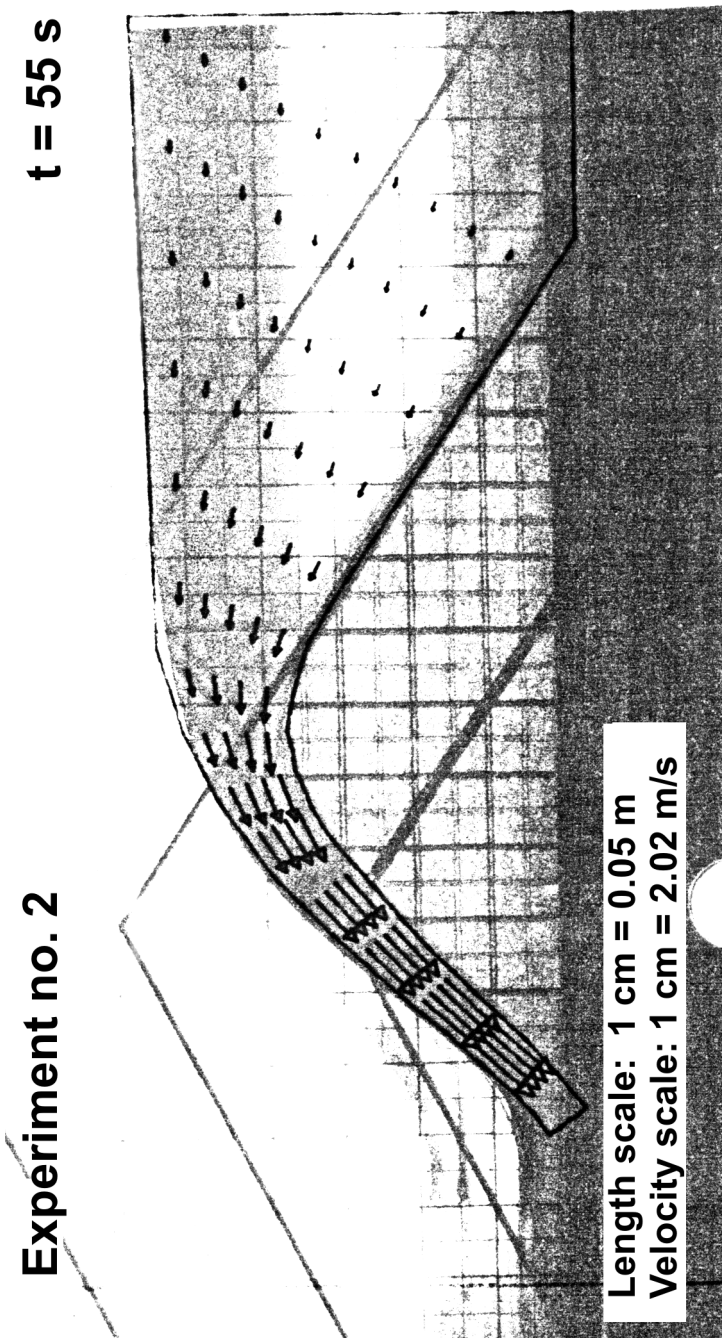
Experiment no. 2
t = 55 s
Length scale: 1 cm = 0.05 m
Velocity scale: 1 cm = 2.02 m/s

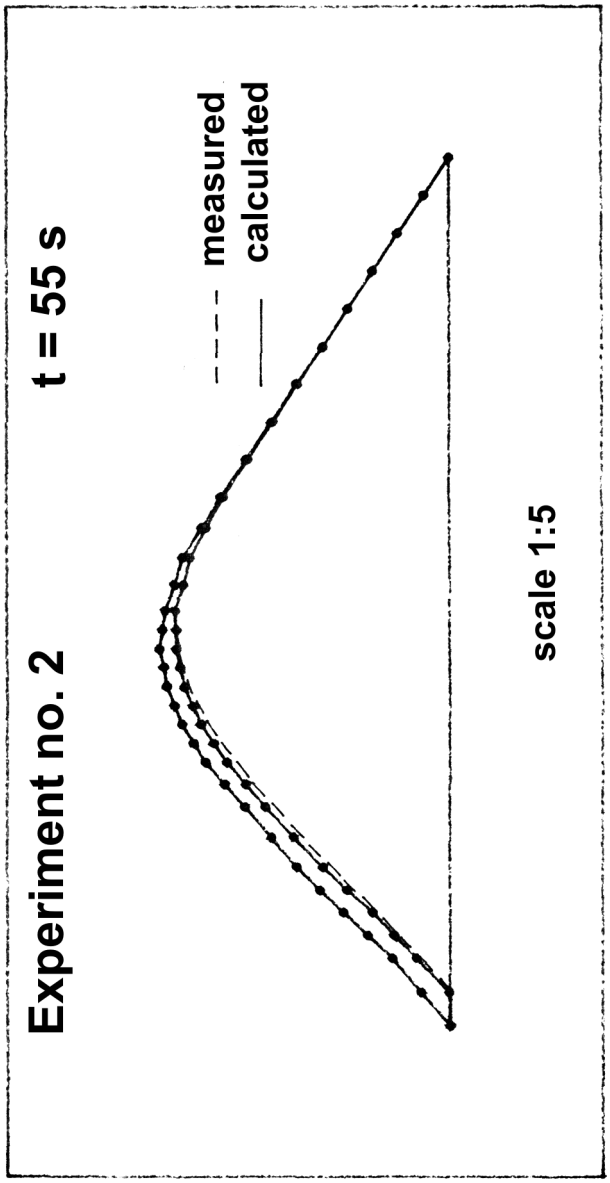
Experiment no. 2
t = 55 s
measured
calculated
scale 1:5

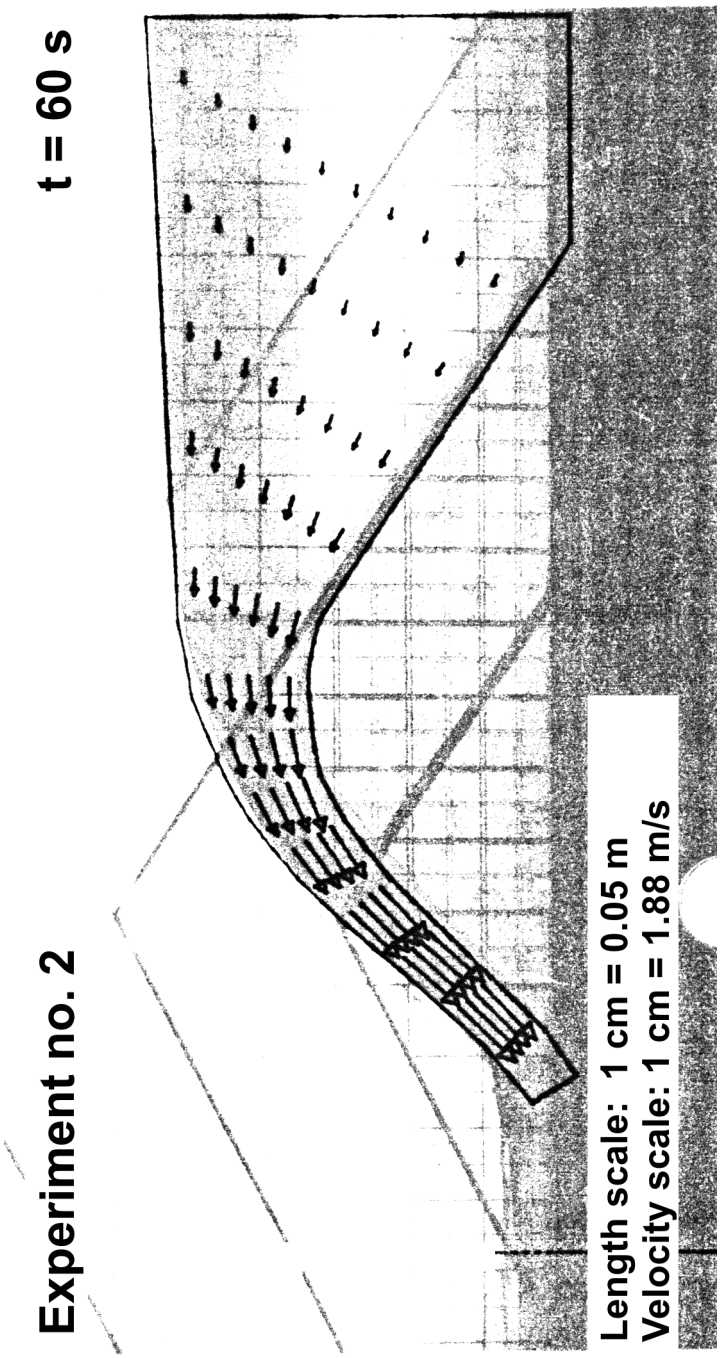
Experiment no. 2
t = 60 s
Length scale: 1 cm = 0.05 m
Velocity scale: 1 cm = 1.88 m/s

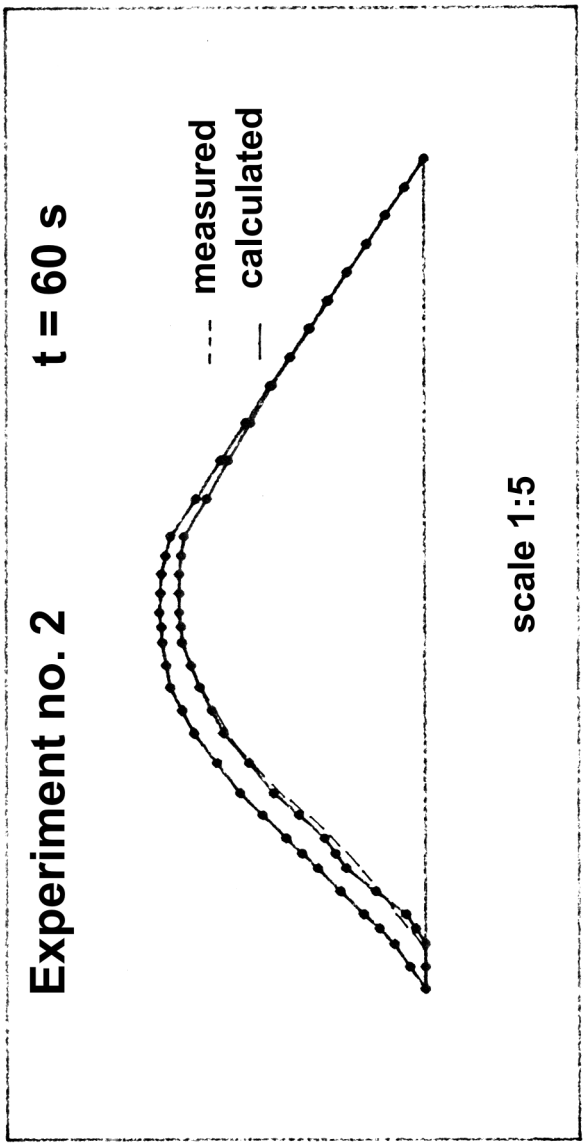
Experiment no. 2
t = 60 s
--- measured
— calculated
scale 1:5

6

Conclusions

On the basis of research in this dissertation, the following conclusions can be drawn:

1. The erosion of earth structures (dams, levees, embankments) exposed to overflowing is a very complex phenomenon. Although numerous physical factors influencing erosion of cohesive materials cannot be fully accounted for analytically, a mathematical model, implemented in a reliable numerical procedure, is proposed in this dissertation, provided two basic conditions are satisfied: (a) the problem is two-dimensional (in the vertical plane), so that the erosion needs to be calculated only in the vertical direction, and (b) the structure is built of homogeneous, moderately cohesive material.

2. The proposed mathematical model enables estimation of: (a) hydraulic characteristics of the accelerated, curvilinear free-surface flow, and (b) quantity of eroded material over time, and (c) the erosion countours, or the deformed shape of the cross-section of the earth structure during the erosion process.

3. An unsteady process is approximated by a succession of steady states, assuming that dependent variables are constant within computational time intervals (quasi-steady regime). A two-step calculation procedure for each time interval is proposed. In the first step the hydraulic characteristics of the stream are calculated. In the second step, erosion contours and the cross-section of the overflown structure is calculated. This is repeated for each time interval, until the structure is completely (or almost completely) washed away by the flowing water.

4. The two-step calculation procedure is implemented in the numerical model which consists of two modules – the first one for calculating the flow field, and the second one, for calculating the change of the solid boundary due to erosion.The two modules are acting independently, the hydraulic

calculation preceeding the calculation of erosion. The time step is problem dependent, and its optimal value is to be determined by trial-and-error.

5. Calculation of the flow field is based on the potential flow theory. Experiance proves that this theory is applicable for weir and spillway type of flows, where inertial effects are dominant in respect to friction.

6. The Boundary Element Method (BEM) is a very convenient method for treatment of free-surface potential flows, as it requires minimum of input data, and no restructuring of the entire computational mesh during iteratitive determination of the free surface.

7. Numerical modeling of the erosion of moderately cohesive materials must be based on empirical relationships. The scale models of earth structures which are used in experimental research must be built of the so-called "equivalent material", the composition of which is chosen according to geometric, hydraulic, and rheologic similarity laws.

8. The laboratory investigations on scale models show that a relationship between the rate of flow and the rate of erosion can be expressed in the form:

$$\frac{Q}{Q_s} = C_1 \, \exp\left(C_2 \cdot \mathrm{Er}\right)$$

where Q and Q_s are the mass discharges of water and material respectively, C_1 and C_2 are empirical constants, and Er is the "erosion number". This parameter is convenient for quantifying the reduction of the structure volume during the erosion process.

9. For particular experimental conditions, the empirical constants have values of $C_1 = 1.6$, and $C_2 = 4.5$. Due to scale effects, the proposed relationship with the given values of constants can be exptrapolated to prototype earth structures not higher than about 4-5 m. This means that the obtained experimental results are valid for relatively small earth structures, such as dams on micro-reservoirs, levees, dikes, emergency spillways, and similar structures.

10. The rate of vertical erosion is constant if earth structures are built of homogenous, modestly cohesive materials, with cohesion up to 10-20 kPa. This range is typical for most small earth structures. Extrapolation of experimental results on field conditions, shows that the total failure time of such structures per unit length would be under 10 min.

11. A more general conclusions would require additional laboratory investigations, preferably with bigger scale models, built of different equivalent materials. Data base for model calibration needs to be considerably extended, before the proposed numerical model gains a wider application in

practice. Some improvement of the convergence of the free surface calculation may be possible. Combining the B.E.M. with the boundary layer modeling is also one possible direction for further improvement.

12. The importance of numerical models such as the one proposed in this dissertation, lies in their capability to predict the failure mode, the maximum discharge, and the total failure time of overflown earth structures. These results represent the basic input data for calculation of flood zones, as well as for risk and damage assessment in the flooded region.

Literature

[1] Bay, E.M., Miller D.L.. *"Inflow Design Flood for Hyrum Dam-Utah-Flood Studies for Existing Reservoirs"*, Bureau of Reclamation, 1965.

Dam-Break

[2] Benoist, G., *"Analyse schematique de la rupture progressive d'un barrage en terre"*, Direction des etudes et recherches, E43/76/15, Chatou, 1976.

[3] Brown, R.J.,*"A simulation of the Hydraulic Events During and Following the Teton Dam Failure"*,Proceedings of Dam-Break Flood Routing Model Workshop Held in Bethesda, Maryland, Oct. 1977, Water Resources Council, Washington D.C, 1977.

[4] Cecilio, C.B., *"Criteria for Routing the Dam-Break Flood"*, Proceedings of Dam-Break Flood Routing Model Workshop Held in Bethesda, Maryland, Oct. 1977, Water Resources Council, Washington D.C, 1977.

[5] Cristofano, E.A., *"Method of Computing Erosion Rate for Failure of Earthfill Dams"*, Bureau of Reclamation, Engineering and Research Center, Denver, Colorado, 1965.

[6] Fread, D.L., *"The Development and Testing of a Dam-Break Flood Forecasting Model"* - Proceedings of Dam-Break Flood Routing Model Workshop Held in Bethesda, Maryland, Oct. 1977, Water Resources Council, Washington D.C, 1977.

[7] Gruetter F., Schnitter, N.J, *"Analytical Risk Assessment for Dams"*, XIV International Congress on Large Dams, Rio de Janeiro, 1982.

[8] Hydrologic Engineering Center, Water Resources Support Center, US Army Corps of Engineers: DAMBRK - The NWS Dam-Break Flood Forcasting Model, 1984.

[9] Mac Donald, C.T., Langridge - Monopolis, J., *"Breaching Characteristics of Dam Failures"*, Journal of the Hydraulics Division, ASCE, Vol. 110, No.5. May 1984.

[10] Programme for alarming and early warning of public in areas potentially endangered by dam-break incidents (Program za izradu elaborata o obaveštavanju i uzbunjivanju stanovništva na području ugroženom od rušenja brana/nasipa), Official Gazette of Republic of Serbia No. 39 (Službeni glasnik SRS, br. 39), 1972 (in Serbian).

[11] Sametz, Z. *"Beitrag zur Frage der Flutwellenbildung bei Progressiven Dammbruchen Infolge Uberstromung"*, Doctoral dissertation, Technical University Gratz, Austria, 1981.

[12] Thiriot, C., *"Modele mathematique approche de 1'erosion de digues ou barrages en terre soumis a submersion"*, XV Congress IAHR, Vol.2., Sao Paolo, 1975.

[13] Dam-break incidents and gained experiences (Udesi na branama i stečena iskustva), ICOLD/Yugoslav Committee for Large Dams, (ICOLD/Jugoslovenski komitet za visbke brane), Beograd, 1975 (in Serbian).

[14] Jovanovič M., *"Hydraulic analysis of progressive failure of earth dams"* (Hidraulicka analiza postepenog rusenja nasutih brana), VIII. Conference of the Yugoslav Association for Hydraulic Resarch (VIII Savetovanje JDHI), Portoroz, Yugoslavia, 1982 (in Serbian).

Free-surface potential flows

[15] All, K.H.M., *"Flow over Rounded Spillways"*, Journal of the Hydraulics Division, ASCE, Vol. 98. No.HY2, Feb. 1972.

[16] Cassidy, J.J., *"Irrotational Flow over Spillways of Finite Height"*, Journal of the Engineering Mechanics Division, ASCE, Vol.91, No.EM6, Dec. 1965.

[17] Garg, S.P., *"Distribution of Head at a Rectangular Conduit Outlet"*, Journal of the Hydraulics Division, ASCE, Vol.92., NoHY4, July 1966.

[18] Henderson, F.M., *"Flow at the Toe of a Spillway - part I: The Open-Toe Spillway"*, La Houille Blanche, No.6, Nov. 1962.

[19] Henderson, F.M., Tierney, D.G., *"Flow at the Toe of a Spillway - part II: The Solid-Toe Spillway"*, La Houille Blanche, No.1, Jan. - Febr., 1963.

[20] Jeppson, R.W., *"Inverse Formulation and Finite Difference Solution for Flow from a Circular Orifice"*, Journal of Fluid Mechanics, Vol. 40, part 1, 1970.

[21] Larock, B.E., *"A Theory for Free Outflow beneath Radial Gates"*, Journal of Fluid Mechanics, Vol. 41, part 4, 1970.

[22] Moayeri, M.S., Strelkoff, T.S., *"Potential Flow at a Two-Dimensional Conduit Outlet"*, Journal of the Hydraulics Division, ASCE, Vol. 99, No.HY4, Sept. 1973.

[23] Moayeri, M.S., *"Flow in Open Channels with Smooth Curved Boundaries"*, Journal of the Hydraulics Division, ASCE, Vol. 99, No.Hy12, Dec. 1973.

[24] Ray, S.K., *"Note sur la profondeur d'eau à I'extremite d'un deversoir horizontal à chute libre"*, La Houille Blanche, Nov. - Dec. 1949.

[25] Strelkoff, T.S., Moayeri, M.S., *"Pattern of Potential Flow in a Free Overfall"*, Journal of the Hydraulics Division, ASCE, Vol.96, No.HY4, April 1970.

[26] Watters, G.Z., Street, R.L., *"Two-Dimensional Flow over Sills in Open Channels"*, Journal of the Hydraulics Division, ASCE, Vol.90, No.HY4, July 1964.

The Finite Element and the Boundary Element Methods for free-surface potential flows

[27] Baker, A.J., Finite Element Computational Fluid Mechanics , McGraw-Hill, 1985.

[28] Brebbia, C.A., Spanos, K.A. , *"Application of the Finite Element Method to Steady Irrotational Flow"*, Rev. Roum. Sci. Tech. - Mec. Appl. Tome 18, No.3, Bucarest, 1973.

[29] Brebbia, C.A., The Boundary Element Method for Engineers, Pentech Press, 1978.

[30] Chan, S.T., Larock, B.E., *"Fluid Flows from Axisymmetric Orifices and Valves"*, Journal of the Hydraulics Division, ASCE, Vol. 99, No.Hyl, Jan. 1973.

[31] Chan, S.T., Larock, B.E.,*"Free-Surface Ideal Fluid Flows by Finite Elements"*, Journal of the Hydraulics Division, ASCE, Vol. 99, No.HY6, June 1973.

[32] Cheng, A.H.D., Liggett, J.A., Liu, P.L.F., *"Boundary Calculations of Sluice and Spillway Flows"*, Journal of the Hydraulics Division, ASCE, Vol. 107, No.HY10, Oct. 1981.

[33] Diersch, J.J., Schinner, A., Busch, K.F., *"Analysis of Flows with Initially Unknown Discharge"*, Journal of the Hydraulics Division, ASCE, Vol. 103, No.HY3, March, 1977.

[34] Diersch, H.J., Martin, H., *"The Numerical Treatment of Free Surface Flows by Finite Elements"*, Finite Elements in Water Resources, Proceedings of the II. International Conference, Imperial College London, Pentech Press, 1978.

[35] Finn, W.D., Varoglu, E., *"Variational Formulation of Free Surface Gravity Flow Including Gated Flow Using Adaptive Finite Elements"*, Computational Techniques in Transient and Turbulent Flow, Vol. 2, Ed. Taylor & Morgan, Pineridge Press, 1981.

[36] Isaacs, L.T., *"Numerical Solution for Flow under Sluice Gates"*, Journal of the Hydraulics Division, ASCE, Vol. 103, No.HY5, May, 1977.

[37] Jovanovic, M. *"Application of the Boundary Element Method for the Solution of Spillway Flows"*, BETECH, Rio de Janeiro, 1987.

[38] Lennon, G.P., Liu, P.L-F., Liggett, J.A., *"Boundary Integral Solutions of Water Wave Problems"*, Journal of the Hydraulics Division, ASCE, Vol. 108. No.HY8, Aug. 1982.

[39] Liggett, J.A., *"Location of Free Surface in Porous Media"*, Journal of the Hydraulics Divion. ASCE, Vol. 103, No.HY4, April, 1977.

[40] Liu, P.L-F, Liggett, J.A., *"Boundary Solutions to Two Problems in Porous Media"*, Journal of the Hydraulics Divion, ASCE, Vol. 105, No.HY3, March 1979.

[41] Liggett, J.A." Liu, P.L-F, The Boundary Integral Equation Method for Porous Media Flow, George Alien & Unwin, London, 1983.

[42] Radojkovic, M., Pecaric, J., Klem, N., *"Application of the Boundary Element Method in Hydraulic Engineering"* (Primena metode graničnih elemenata u hidrotehnici), Scientific Project, Faculty of Civil Engineering, University of Belgrade (Naučno-istraživačka tema Gradjevinskog fakulteta Beograd), 1983 (in Serbian).

[43] Salmon, J.R., Liu, P.L-F, Liggett, J.A., *"Integral Equation Method for Linear Water Waves"*, Journal of the Hydraulics Division, ASCE, Vol. 106, No.HY12., Dec. 1980.

[44] Topics in Boundary Element Research, ed. Brebbia, C.A., Vol. I, II. Springer-Verlag, Berlin, 1984.

[45] Washizu, N.T., Ikegawa, M., *"Application of the Finite Element Method to Some Free Surface Fluid Problems"*, Finite Elements in Water Resources; Proceedings of the I. International Conference, Princeton University, Pentech Press, 1976.

[46] Waters, J.J., Nelson. J.M., *"A program for Solving Potential Problems on a Desktop Computer"*, Adv.Eng. Software, Vol. 2, No.2, 1980.

Erosion of coherent materials

[47] Arulanandan, K., *"Fundamental Aspects of Erosion of Cohesive Soils"*, Journal of the Hydraulics Division, ASCE, Vol. 10!., No.HY5, May 1975.

[48] Cailler, S., Minerologie d'argiles, Masson, 1963.

[49] Cormault, P., *"Determination experimentale du debut solide d'erosion de sediments fins cohesifs"*, XIV Congres AIHR, Vol. 4, Paris, 1971.

[50] Dunglas, J., Fayoux, D., *"Destruction des barrages en terre par submersion. Essais sur modeles reduits"*, Journees Nationales: "Le Comportement des sols avant la rupture", Ministere de 1'equipement et du logement , Laboratoires des Ponts et Chaussees, Paris, 1972.

[51] Erosion of Cohesive Sediments - Report of the Task Cimmittee on Erosion of Cohesive Materials, Journal of the Hydraulics Division, ASCE, Vol.94, No.HYr, July 1968.

[52] Kamphuis, W.J., Hall, K.R., *"Cohesive Material Erosion by Unidirectional Current"*, Journal of the Hydraulics Division, ASCE, Vol. 109., No.1, Jan. 1983.

[53] Kelly, W.E., Gularte, R.C., *"Erosion Resistance of Cohesive Soils"*, Journal of the Hydraulics Division, ASCE, Vol. 107, No.HY10, Oct. 1981.

[54] Mandel, J., *"Essais sur modeles reduits en mecanique des terrains. Etude des conditions de similitude"*, Centre national d'etudes techniques et de recherches technologiques pour 1'agriculture, les forets et I'equipement rural (CERAFER), 1961.

[55] Mirtskhulava, Ts.E., *"Erosional Stability of Cohesive Soils"*, Journal of Hydraulic Research, Vol.4, No.1, 1966.

[56] Migniot: *"Etude des proprietes physiques de differents sediments tres fins et de leur comportement sous des actions hydrodinamiques"*, La Houille Blanche, No.7. 1968.

[57] Murray, W., *"Erodibility of Coarse Sand-Clayey Silt Mixtures"*, Journal of the Hydraulics Division. ASCE, Vol. 103, No.HY10, Oct. 1977.

[58] Otsubo, K., Muraoka, K., *"Resuspension Rate Function for Cohesive Sediments in Stream"*, Journal of Hydrpscience and Hydraulic Engineering, Kyoto University, Vol. 3, No.3, 1985.

[59] Partheniades, E., Paaswell, R.E.,*"Erodibility of Channels with Cohesive Boundary"*, Journal of the Hydraulics Division, ASCE, Vol. 96., No.HY3, March, 1970.

[60] Parchure, T.M., Mehta, A.J., *"Erosion of Soft Cohesive Sediment Deposits"*, Journal of the Hydraulics Division, ASCE, Vol. 111, No.10, Oct. 1985.

[61] Raudkivi, A.J., Tau, S.K., *"Erosion of Cohesive Soils"*, Journal of Hydraulic Research, Vol. 22, No.4, 1984.

[62] Sediment Transportation Mechanics: Initiation of Motion, Progress Report, Task Committee on Preparation of Sedimentation Manual, Journal of the Hydraulics Division, ASCE, Vol. 92, No.HY2, March, 1966.

[63] Shen, H.W., River Mechanics , Vol. II, Chapter 25: *"Erosion and Deposition of Cohesive Materials"*, Fort Collins, Colorado, 1971.

[64] Swain, A., Palmer, H.D., Tzou, K.T.S., *"An Investigation of the Erosional and Depositional Behavior of Cohesive Sediments"*, XV Congres IAHR; Vol.2, Sao Paolo, 1975.

[65] Weber J-D., *"Les applications de la similitude physique aux problemes de la mecanique des sols"*, Editions Eyrolles, 1971.

Miscallenous

[66] Boulder Canyon Project - Final Reports: Part VI - Hydraulic Investigation Bulletin 4: Model Studies of Imperial Dam, Desilting Works, All-American Canal Structures, U.S. Department of the Interior, Bureau of Reclamation, Denver, 1949.

[67] Bowyer, A., Woodwark, J., A Programmer's Geometry, Butterworths, London, 1983.

[68] Cassidy, J.J., *"Designing Spillway Crests for High-Head Operation"*, Journal of the Hydraulics Division, ASCE, Vol .96, No.HY3, March 1970.

[69] Chow, V.T., Open-Channel Hydraulics, McGraw-Hill, 1959.

[70] Daubert, O., Cahouet, J., *"Approche numerique de la houle per les equations de Navier-Stokes"*, EDF, Direction des etudes et recherches, HE41/84-05, Chatou, 1984.

[71] Daubert, O. Rabiller, C., *"Resolution numerique des equations de Navier-Stokes a surface libre - cas des obstacles"*, EDF, Direction des etudes et recherches, HE41/83-24, Chatou, 1983.

[72] de Vries, M., *"Application of Physical aud Mathematical Models for River Problems"*, Delft Hydraulics Laboratory, publication No. 112, 1973.

[73] Dressler, R.F. *"New Nonlinear Shallow - Flow Equations with Curvature"*, Journal of Hydraulic Research, No.3, 1978.

[74] Dressler, R.F., Yevjevich, V.M., *"Comparison of the Dressler and de Saint-Venant Equations for Shallow Curved Flow"*, XX Congress IAHR, Sept. 5-9. 1983.

[75] Hansen, K.D., France, J.W., *"RCC: A Dam Rehab Solution Unearthed"*, Civil Engineering, ASCE, Sept. 1986.

[76] Harlow, F.H., Welch. J.E., *"Numerical Calculation of Time - Dependent Viscous Incompressible Flow of Fluid with Free Surface"*, Physics of Fluids, Vol. 8, No.12, 1965.

[77] Izbash, S.V., Khaldre, Kh.Yu., *"Hydraulics of River Channel Closure*, Butterworths, London, 1970 (translation from Russian).

[78] Klem, N., *"Experimental analysis of direct methods for linear systems solution"*, Master Thesis (Eksperimentalna analiza direktnih postupaka za resavanje sistema linearnih jednacina, Magistarski rad), Faculty of Civil Engineering, Belgrade (Gradjevinski fakultet, Beogradu), 1979 (in Serbian).

[79] Milovanov, D., *"Reconstruction of levee system in Vojvodina, Serbia"* (Dovrsenje rekonstrukcije odbrambenih linija u Vojvodini), Periodical "Vode Vojvodine", 1974 (in Serbian).

[80] Nonveiller, E., Earth Dams (Nasute brane - Projektiranje i gradjenje), Školska knjiga, Zagreb 1983 (in Serbo-Croat).

[81] Peyret, R., Taylor, T.D., Computational Methods for Fluid Flow, Springer - Verlag, New York, 1983.

[82] Powledge, G.R., Dodge, R.A., *"Overtopping of Small Dams - An Alternative for Dam Safety"*, US Bureau of Reclamationa, 1983.

[83] Reznicek, K., *"Flood Management in Lowlands"* (Odbrana od poplava u ravnicarskim predelima), Doctoral dissertation, Novi Sad, 1978 (in Serbian).

[84] Roache P.J., Computational Fluid Dynamics, Hermosa Publishers, Albuquerque, 1982.

[85] Sivakumaran, N.S., Hosking, R.J., Tingsanchali, T., *"Steady Shallow Flow over a Spillway"*, Journal of Fluid Mechanics, Vol. 111, 1981.

[86] Muškatirović, J., *"Model investigation for the Buk Bijela Discharge Structures"* (Modelska ispitivanja evakuacionih objekata HE Buk Bijela), Institute for Water Resources Development "Jaroslav Černi", Beograd, 1986 (in Serbian).

[87] Babb, A.F., Mih, W.C., *"Selection of Model Test Programs with Reparance to Viscous and Gravity Force Similitude"*, Symposium on Scale Effects in Modelling Hydraulic Structures, Eshingen, 1984.

[88] Vallentine, H.R., Applied Hydrodynamics, Butterworths, London, 1970.